INSTITUTE OF PHOTONIC SCIENCES

ICFO
Institut
de Ciències
Fotòniques

Ultracold gases in non-Abelian synthetic gauge fields

Anna Kubasiak

Ph.D. thesis

Academic supervisors: Prof. Maciej Lewenstein
Prof. Jakub Zakrzewski
Co-supervision: Dr Pietro Massignan

April 2011

Abstract

The focus of this thesis is in the area of Abelian and non-Abelian gauge fields that can be efficiently simulated in ultracold atomic systems. These exotic fields and their impact on fermionic particles is studied in the context of two-dimensional systems mainly in optical lattices, that also are available with current experimental techniques. Behaviour of a particle under the influence of such non-Abelian gauge field is contrasted with the standard case of homogeneous magnetic field. Its spectrum and the transport properties such as quantum Hall effect are investigated. The conditions for the energy bands to form a Hofstadter-butterfly-like gaps in a non-Abelian field are given. We show that as long as the Wilson loop for the field is constant, its non-Abelian character does not destroy the big gaps and hence, allows for the integer quantum Hall effect (IQHE). A family of new butterfly spectra is found and the modified IQHE is calculated with the use of Chern numbers. Further, the spectrum of the system is studied in detail and it is demonstrated that it can exhibit anomalies i.e. Dirac cones. The elementary excitations of a system with such spectrum are massless fermions traveling with a modified speed of light similarly to the Majorana fermions in the graphene described by the Dirac equation. We further show that in the case of synthetic non-Abelian gauge field these cones can be squeezed and the speed of light then depends on the direction. Under the conditions of such squeezing the interactions are considered and the first steps towards the analysis of the Fractional quantum Hall effect (FQHE) in the presence of non-Abelian field are done. The matrix elements of the interaction matrix are analytically calculated.

Preface

Ultracold atomic gases since the first experimental realisation of Bose-Einstein condensation have been in the centre of scientific interest. Rapid development of experimental techniques and theoretical advances involving atomic vapours have been developed during and after that pioneer works. Now, after over 15 years since then, trapping, manipulating and measuring of nearly individual atoms is possible. We can design the experiments with great degree of control over densities, temperatures, polarisation, interaction strength, external potential landscapes and even it is possible to create synthetic fields acting on the atoms. All that makes ultracold atomic gases a good candidate for quantum simulations. Indeed they have been used nowadays already to simulate and test condensed-matter models, difficult to study otherwise. Two-dimensional and quasi two-dimensional systems of atoms in synthetic gauge fields - both Abelian and non-Abelian are of particular interest. Even on the single particle level application of fields leads to such interesting phenomena as fractal energy spectrum or relativistic excitations for atoms in a lattice, as well as integer quantum Hall effect. In the interacting system correlations between the particles lead to topological phases and fractional quantum Hall effect if the temperature is low enough and the impurities are small. In the latter case the elementary excitations are quasi-particles with neither bosonic nor fermionic statistics. They are so-called anyons and also they carry a fraction of electric charge. If these exotic particles were in the same time non-Abelian, i.e. if they could remember the order of exchanges with one another they would be a tool to build a fault-tolerant quantum computer robust to decoherence - one of the biggest challenges of quantum physics nowadays. In this the-

sis I will focus on two-dimensional fermi gas under the influence of both Abelian and non-Abelian synthetic gauge fields. The text is organised as follows:
In **chapter 1** I will explain the meaning of ultracold temperature and related to it the quantum regime and the Fermi energy. I will also define an optical lattice and briefly review the properties of atomic gas in such configuration and present the Hubbard model as the main tool to analyse such system. Chapter 1 finishes with presentation of the quantum simulator, which is the underlaying idea and motivation of this thesis.
Chapter 2 is devoted to present several experiments which aim at realising Abelian and non-Abelian gauge fields for neutral atoms. There is a great interest in this field recently and therefore the progress is fast. Creation of an Abelian field has been already reported and prospects for the non-Abelian are very promising. The Chapter is organised a follows: First a general description of a gauge field is given. Then, since the concept of non-Abelian gauge field in the context of atomic gases is relatively new, a definition is given both in the case of continuum system and the lattice system. After this short introduction the experiments are presented starting from the simplest case of rotating harmonic trap and continuing with other concepts such as Berry phase and phase imprinting. First always the scheme for an Abelian field is presented and later possibilities of its generalisation to non-Abelian case are discussed together with existing difficulties and limitations. Presented experiments are educative examples of the most relevant proposals and it was not the intention to list all of the past and ongoing experiments.
Chapter **3** presents the spectrum of an atom in a external gauge field in a two-dimensional lattice. First a classical example of famous Hofstadter butterfly spectrum for a particle in homogenous magnetic field is explained, then analogous calculation for an atom in a non-Abelian field is shown. The latter result is new and it is contrasted both with the first, standard case as well as later works dealing with one example of non-Abelian field. The comparison of those cases allows for defying a new class of systems with butterfly-like spectrum with big energy gaps. It also allows formulating a criterium for the field to conserve this structure, which is a condi-

tion for the integer quantum Hall effect.
Chapter 4 deals with the transport properties of the two-dimensional fermi gas in a square lattice in a non-Abelian gauge field. After presenting the main principles of the IQHE in homogenous magnetic field, the case of non-Abelian field is studied. Technique of the Chern number allows for efficient numerical calculation of the conductivity of the system depending on the Fermi energy and the parameters of gauge potential. This novel results reveal that when non-Abelian field is present an anomalous quantum Hall effect (AQHE) can take place. Previously AQHE was known to exist in graphene for homogenous gauge field, due to its special geometrical properties. This result is new and allows to draw an analogy between these two systems.
In the **chapter 5** further properties of a square lattice with non-Abelian field is analysed. It is further compared with graphene and its properties. It is found that the spectra of both systems have Dirac anomalies support massless elementary excitations following Dirac equation. In the case of non-Abelian field in a square lattice, however, more control is possible over the parameters of the equation allowing for the Dirac cones squeezing and anisotropy of the "speed of light". For the squeezed system the spectrum consist of asymmetric Landau levels. The new Laughlin-like function is proposed for a polarised Fermi gas as a starting point to investigate the fractional quantum Hall effect in the case of interacting system.
Next **chapter 6** presents a mean-field approach to the same system as in previous chapters but in the presence of the spin imbalance and interaction that pairs fermions into superfluid Cooper pairs. BCS theory for this system is formulated and the conditions for its physicality are tested by self-consistent calculation of the pairing strength. This important issue had not been addressed before in the literature. Next, the spectrum is calculated numerically. The phase transition points between different topological phases are found and the phases are characterised with the Chern numbers as well as with the edge modes. Finally the phase diagram is given where the gauge field parameters and the spin imbalance are the variable.
In**chapter 7** the system with squeezed Landau levels that have been described before in chapter 5 is further studied in order to

include the interactions between atoms. Preliminary results for the exact diagonalisation approach presented. Analytical formulas for the interaction matrix in the case of dipolar interactions are given for the polarised system. This work, however not published, is new and can serve as fist step to the study of FQH effect in the non-Abelian field in the future.

This thesis consists of a review of the research work I have done in the Quantum Optics Theory group in ICFO and Atomic Optics group in Jagiellonian University during the last years. In the year 2006 I have started my PhD studies in Kraków at the Jagiellonian University under the supervision of pfor. Jakub Zakrzewski. Soon afterwards I have also started a collaboration with prof. Maciej Lewenstein from ICFO in Barcelona in Spain. The collaboration was very inspiring and soon turned to be main part of my research and on the basis of a cotutelle agreement I moved to Barcelona and started my PhD studies under the supervision of prof. M. Lewenstein. Despite the fact that the cotutelle study program was technically complicated, because I had to travel between Poland and Spain, I had a great support both from prof. J. Zakrzewski as well as prof. M. Lewenstein in organising this collaboration. During last five years I have worked with several people and each of the original results obtained and each publication was a team work. At the beginning I worked with prof. Nuria Barberan and Arnau Riera from University of Barcelona. However our results have not been published, they helped me greatly in understanding of the fractional quantum Hall effect and Landau levels structure. In 2008 I met Nathan Goldman from whom I learned a lot and with whom we worked together for several years with great results. Later, while working on the Dirac physics in non-Abelian fields we started also collaboration with prof. M.-A. Delgado and Alejandro Bermudez from Madrid University. Working with them was a real pleasure and honour. In the end of 2009 I have started working on the interacting systems. One line of this research was mean field treatment and formulating a BCS theory for non-Abelian fields. Dr. Pietro Massignan was my guide through this subject and his help and patience were invaluable. We have worked together until the end of my PhD studies and he became my co-supervisor.

List of original publications

The publications that are the basis for this thesis:

- Proceedings of ICAP-2006 (Innsbruck), *Travelling to exotic places with ultracold atoms*,authors: M. Lewenstein, A. Kubasiak, J. Larson, C. Menotti, G. Morigi, K. Osterloh, A. Sanpera.

- *Ultracold atomic gases in non-Abelian gauge potentials: The case of constant Wilson loop*
  N. Goldman, A. Kubasiak, P. Gaspard, and M. Lewenstein, Phys. Rev. A. **79**, 023624 (2009).

- *Non-Abelian Optical Lattices: Anomalous Quantum Hall Effect and Dirac Fermions*
  N. Goldman, A. Kubasiak, A. Bermudez, P. Gaspard, M. Lewenstein, and M. A. Martin-Delgado, Phys. Rev. Lett. **103**, 035301 (2009).

- *Topological superfluids on a lattice with non-Abelian gauge fields*
  A. Kubasiak, P. Massignan, M. Lewenstein, Europhys. Lett. **92**, 46004 (2010).

I am also a co-author of one publication that is related to the subject:

- *Topological phase transitions in the non-Abelian honeycomb lattice*
  A. Bermudez, N. Goldman, A. Kubasiak, M. Lewenstein, M.A. Martin-Delgado, New J. Phys. **12**, 033041 (2010).

The mathematical sciences particularly exhibit order, symmetry, and limitation; and these are the greatest forms of the beautiful. – Aristoteles

Contents

Chapter 1

Motivation

1.1 Ultracold atoms

At the first sight the world is classical just as described by Galileo and Newton. What we observe and experience in everyday life, what shapes our intuition are classical phenomena. One has to look much more carefully and at much smaller scales to notice that this intuitive picture is not exact. In fact it takes a lot of effort to observe quantum effects even in a laboratory. Even a gas of particles as small as atoms in usual conditions, as room temperature, follows the classical picture of hard balls colliding elastically with one another. As first pointed out by de Broglie each object can be seen as a particle and also as a wave of matter with the wavelength λ_{dB}. The fact that this wave character is hard to observe for most of the macroscopic objects is due to extremely small value of the Planck constant $h \approx 6.6 \times 10^{-34}[\frac{J}{s}]$ that enters in the formula for λ_{dB}:

$$\lambda_{dB} = \frac{h}{\sqrt{2\pi m k_B T}}. \tag{1.1}$$

Here m is the mass, $k_B \approx 1.4 \times 10^{-23}[\frac{m^2 kg}{s^2 K}]$ the Boltzmann constant and T the temperature. From the expression above it is clear that the heavier is the object and the higher the temperature, the shorter is the wavelength and so the scale at which the quantum effects are important. For the atomic gases the quantum limit can be reached when the interparticle spacing is comparable to λ_{dB}. It

is straightforward to see that for particles as heavy as atoms this corresponds to ultracold temperatures or very high densities:

$$T_{dB} = \frac{h^2}{2\pi m k_B} n^{2/3}, \tag{1.2}$$

where n is the density[1]. Taking typical values of the density ($10^{18} - 10^{21}$atoms per m^3) and mass for atoms, we arrive at the temperature below $1\mu K$. However, for such densities the atomic gas is unstable, the three body collisions are frequent enough to cause crystallisation. Therefore diluting of the gases typically to 10^{13} atoms per m^3 is needed in order to have a stable system and even lower temperatures are required to reach the quantum limit. Several techniques of slowing down and trapping atoms have been developed since last 30 years. The Doppler cooling based on slowing down atoms with the laser light typically lowers the kinetic energy of the particles to values corresponding to the temperature of the order of 1mK. At this temperatures the resonant radiation pressure and field gradients acting on magnetic momenta or induced electric dipole momenta are strong enough to trap efficiently neutral atoms. Otherwise, unlike charged particles in Paul's trap, they could not be confined by such weak forces.

The sub-Doppler laser cooling or laser sideband cooling [1, 2, 3] allow the range of the recoil energy which corresponds to the temperature of several μK and finally the evaporative cooling can be used to reduce the temperature to the order of 500 pK [4]. In recognition of the invention of cooling and trapping atoms with laser forces in 1998 the Nobel Prize was granted to S. Chu, C. Cohen-Tannoudji and W.D. Phillips.

All those advances led finally to the culmination point, that was the milestone triggering the immense interest in the field: the first experimental verification of Albert Einstein's prediction that

[1]For electrons that are over 8000 times lighter than protons, the quantum regime can be reached even at room temperature. A simple model of the valence electrons in crystal structure of a metallic solid is a free electron gas with typical densities of $5 \times 10^{28} m^{-3}$. This results in the quantum regime already at the temperature $T^{dB} \approx 7.4 \times 10^4 K$. For this reason metals can not be described with classical model.

weakly interacting bosonic atoms cooled to low-enough temperature form a new, exotic state of matter - pure quantum one, so called Bose-Einstein condensate (BEC) [6]. For an experimental realisation of the BEC in 1995 E.A Cornell, C.E. Wieman and W. Ketterle [5, 7] have been awarded by the Nobel Prize in 2001 and an avalanche of experiments followed the first pioneers [8]. Up to today the BEC has been realized in most of the alkali gases typically with ^{7} Li, ^{23}Na, ^{39}K, ^{41}K, ^{85}Rb, ^{87}Rb, and ^{133}Cs. The development of the sympathetic cooling, which is suitable also for fermions enabled creation of degenerate Fermi gas. In this way the realization of BEC opened the way to studying fermionic quantum regime in experiment and many experiments similar to those with bosons have been done with fermions too [9]. Since the realization of BEC ultracold atomic gases are one of the hottest topic both in theoretical and experimental physics. Among the reasons that make them attractive, the key point probably is that they offer us insight into real quantum regime, still being relatively easy to understand and accessible to engineer in experiment. The nature of the atomic-scale phenomena, however complex, in many cases can be well captured by simple models.

A great advantage in understanding the nature of ultracold bosonic gases and the BEC was, that the transition occurs in diluted atomic vapours. The interparticle spacing $n^{-1/3}$ is in the typical experimental setting of the order of $\lambda_{dB} \sim 1\mu m$, while the range of Van der Waals potential $V_{WdV}(\mathbf{r})$ decaying as $-\frac{C_6}{r^6}$ is only $R_{VdW} \sim 1nm$. In such a configuration the details of the potential do not play essential role. Moreover, the three body collisions are very unlikely. Each particle of the atomic cloud can be then described by Gross-Pitaevski equation, which is non-linear Schrödinger equation with mean-field-like term sumarising the interactions:

$$\left(-\frac{\hbar^2}{2m}\nabla^2 + V(\mathbf{r}) + \frac{4\pi\hbar^2 a}{m}|\psi(\mathbf{r})|^2\right)\psi(\mathbf{r}) = \mu\psi(\mathbf{r}). \tag{1.3}$$

Here

$$\frac{4\pi\hbar^2 a}{m}|\psi(\mathbf{r})|^2 = \frac{4\pi\hbar^2 a}{m}n \tag{1.4}$$

is the mean field term, μ a chemical potential and a is scattering length given by low energy properties of the gas.

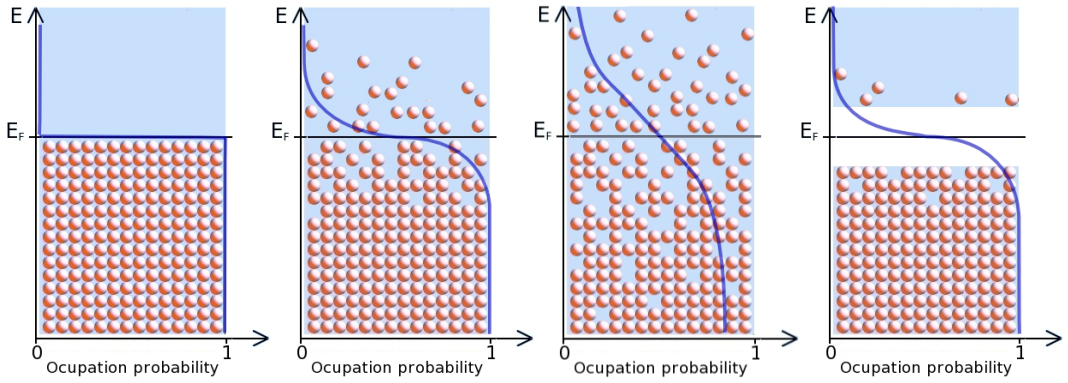

Figure 1.1: Fermi energy and occupation distribution with a) $T = 0$, b) $T << T_F$ - ultracold degenerate fermi gas, c) $T \approx T_F$, d) the same as b) but for a gapped system whose Fermi energy lays in the gap. For gapped systems if the temperature is low enough to forbid excitations above the energy gap, all of the atoms will remain below E_F even for $T > 0$. Here a few excitations are possible. In all cases I assume that all of the energy levels are 14 times degenerate and that the Fermi energy lies exactly above 15-th level.

Unlike bosons, fermions do not have coherent behaviour thus its description can not be reduced to one-body wave function. In addition, for one component fermi gas, the s-wave collisions are prohibited by the Pauli principle and the scattering length is equal 0. This dramatic difference between fermionic and bosonic atoms, that in practice can be even isotops of the same chemical element is yet another manifestation of reaching the quantum regime. Fermionic systems can be characterized by quantity called Fermi energy. It is the highest populated energy level in the system at $T = 0$. At absolute zero temperature all energy levels below E_F are occupied and all levels above are empty so the occupation probability of the energy levels drops at E_F like a step function. As the temperature grows the atoms from the highest occupied levels can jump above T_F by the thermal fluctuations and the sharp edges of the occupation function softens. The temperature at which atoms from the lowest states can be excited above E_F is called the Fermi temperature T_F and above this limit the system can not be considered

degenerate anymore. This limit coincides with the previously mentioned temperature T_{dB} of the transition from classical to quantum regime when $\lambda_{dB} \approx n^{-1/3}$. The idea of the Fermi energy and the change of the energy levels occupation is a very important concept and is illustrated in Fig. 1.1.

Similarly to the bosonic ultracold quantum gas, the degenerate fermionic gases have been realized in very diluted systems where collisions are rare because of the relatively large distances between particles. In addition for the symmetry reasons, low energetic, "spinless" fermions can not interact via s-wave collisions. However, recently there has been remarkable effort made to enhance the interactions both for bosonic, as well as fermionic systems. For fermions even little interaction is enough to form weakly bound Bardeen-Cooper-Schrieffer pairs (BCS) pairs that condense into a superfluid phase. If the bounding force becomes stronger the pairs shrink to bi-atomic molecules and finally a molecular BEC of composed bosons is created. These phenomena were first predicted in condensed matter physics where one does not have any possibility to tune the interactions on demand. Because of this for a long time the transition between BSC pairs and the BCS regime was only a theoretical prediction. Thanks to the discovery of Feshbach resonance in atomic gases it was first time made possible to observe it in detail. Feshbach resonance is a powerful technique that allows to change the scattering length of atoms a by applying an external magnetic field to the system [10, 11]. This way a can be relatively easily tuned in experiment over big range of values. Even the change of the sign of a is possible so that one can switch between both attractive and repulsive forces in both strong and weak interacting regime. Moreover, most of the atomic systems are suitable for application of Feshbach resonance method. Nowadays it has been used commonly in many experiments, for example to observe the above mentioned crossover regime between BCS pairs and BEC [13].

An alternative way to reach highly interaction regime with ultracold atoms is offered by optical lattices. By increasing the intensity of laser beams forming the periodic potential, one can reduce tunnelling between sites and make the interactions dominate the dynamics. Both bosons and fermions can be loaded into lattices,

manipulated and measured with unprecedented controllability. Optical lattices will play central role in this thesis, therefore in the following section I give short introduction about them.

1.2 Optical lattices and Hubbard model

An optical lattice is an array of optical potentials similar to that in atomic optical trap. In a typical configuration the potentials are created by interfering counter propagating laser beams, where the lattice spacing equals half of the laser wavelength. There are also methods for obtaining period larger than half of laser light wavelength by interfering beams with the angle less than 180°. For example if three pairs of orthogonal laser beams of the widths w_x, w_y, w_z in x, y, z directions respectively are used, the resulting potential has the form:

$$V(x,y,z) = -V_x e^{\frac{y^2+z^2}{w_x^2}} \sin^2(kx) - V_y e^{\frac{x^2+z^2}{w_y^2}} \sin^2(ky) - V_y e^{\frac{x^2+y^2}{w_z^2}} \sin^2(kz), \tag{1.5}$$

where V_x, V_y, V_z are potential depths in the three directions, and $k = \frac{2\pi}{\lambda}$ is the wave vector of the laser light. The above example is a square lattice in three dimensions. One may be also interested in creating other geometries similarly to different types of Braevais lattices. The final shape of the optical potential depends on the number of lasers used and their configuration. One can create triangular, honeycomb, kagome lattices and the choice is not limited only to this list. By superimposing the lattices of different spacings, one can create so called superlattices or introduce disorder in the system in a controlled way. Recently, also the holographic optical lattices have been introduce to create complicated optical lattices in a simple way.

Above, for simplicity I assumed that all three laser pairs have the same wavelength λ. If all of them have also the same intensities, then they form three dimensional lattice of equally spaced lattice sites as illustrated in Fig. 1.2b. Instead, by choosing strongly anisotropic parameters of the confinement, the optical potential can be made quasi 2 or 1 dimensional. If for example V_z is much smaller than V_x and V_y then the particles can move freely in z-

direction, and the optical lattice will consist of a two dimensional lattice of elongated atomic clouds as shown in Fig. 1.2a. Changing the dimensionality of the material can have a great influence on its properties. In the last years there has been increasing interest in low dimensional systems for this reason. The famous Hall effects - both integer and fractional are examples of qualitative change in the physics of two and quasi-two- dimensional systems. It is also known from Mermin-Wagner theorem that continuous symmetries cannot be spontaneously broken at finite temperature for any dimension $d \leq 2$. Any long range order must be destroyed by thermal fluctuations and hence low dimensional systems can not have any ordered phase such as crystal, ferromagnet, or BEC at finite temperatures. For exactly $d = 2$, however, topological properties of the system can result in quasi-long range ordered phase. The transition between disordered phase and quasi-ordered one, where the correlations decay algebraically, is the famous Kosterlitz-Thouless transition [12]. In 2D systems the topology plays essential role and this make them so interesting. All systems considered in this thesis are two dimensional.

Atom in optical lattice

If an atom is inserted in an oscillating electromagnetic wave of light, its shape is deformed. The light field moves the electronic cloud surrounding the nucleus and induces the dipole moment whose direction and strength depends on the polarisability of the atom. Polarisability is a function of the light wavelength so that even for the same atom one can find different wavelengths inducing opposite dipole moments. An internal state can also influence the polarisability so that two same atoms but with different internal states, can be affected by the same light field in different ways. This phenomenon can be used for creating state dependent optical lattices and will be discussed later in the chapter on the artificial gauge field creation. Once the dipole moment is induced in the atom, the light interact with it, causing a shift in the potential energy, called the ac-Stark shift. This effect is used to create a conservative trapping potential for neutral atoms. By shining a spatially modulated

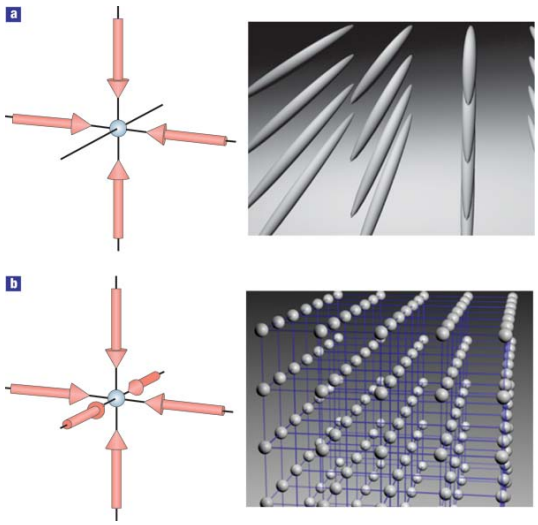

Figure 1.2: **a**, For a 2D optical lattice, the atoms are confined to an array of tightly confining 1D potential tubes. **b**, In the 3D case, the optical lattice can be approximated by a 3D simple cubic array of tightly confining harmonic oscillator potentials at each lattice site. Picture taken from [14]

laser beam onto an atomic cloud, various energy landscapes can be formed, since the potential energy is proportional to the local light intensity [15, 16].

Atoms in optical lattices can move between the potential minima in two ways: The states belonging to the energy bands, whose kinetic energy is higher than the potential barrier are delocalised. If a particle is described by such wave function, it can move freely in the lattice. The atoms from the low energy bands have wave functions localised around the potential minima and their energy is too low to move between the lattice sites in a classical way. These atoms, can still change position, and in this sense delocalise, by tunnelling from one minimum to another. In the limit of strong lattice potential the only mechanism of moving between sites is tunnelling. In this case it is convenient to express the Hamiltonian in terms of well localised functions. In the first approximation one can limit the expansion of the field operators only to the lowest energy band and then the so-called Wannier functions expansion is the standard choice. The Wannier functions $\mathcal{W}(\mathbf{r}-\mathbf{R}_i)$ are localised around $\mathbf{R}_i$ point and are linear combination of Bloch functions $\psi_{\mathbf{k}}(\mathbf{r})e^{-i\mathbf{k}\mathbf{R}_i}$. The creation operator for Wannier state of an atom localised in lattice site i, whose internal degree of freedom (e.g. spin) is σ is defined as:

$$\mathcal{W}_\sigma(\mathbf{r}-\mathbf{R}_i) = \sum_{\mathbf{k}} \psi_{\mathbf{k}}(\mathbf{r})e^{-i\mathbf{k}\mathbf{R}_i}\chi(\sigma) \equiv \langle \mathbf{r}|c^\dagger_{\mathrm{i}\sigma}|0\rangle. \qquad (1.6)$$

$|0\rangle$ is the vacuum state with on particles present: $c_{\mathrm{i}\sigma}|0\rangle = 0$ for any i, σ. The operators have common commutation or anti-commutiaton relations depending on whether atoms are bosonic or fermionic:

$$\begin{aligned} c_{\mathrm{i}\sigma}c_{\mathrm{i}'\sigma'} \pm c_{\mathrm{i}'\sigma'}c_{\mathrm{i}\sigma} &= 0 \\ c_{\mathrm{i}\sigma}c^\dagger_{\mathrm{i}'\sigma'} \pm c^\dagger_{\mathrm{i}'\sigma'}c_{\mathrm{i}\sigma} &= \delta_{i,i'}\delta_{\sigma,\sigma'} \forall i, i', \sigma, \sigma', \end{aligned}$$

where "+" and "-" refer to fermions and bosons respectively. The reason why the atoms can tunnel through a potential barrier higher than their kinetic energy is that the wave functions localised in the two neighbouring lattice sites have non-vanishing overlap. The tunnelling amplitude and the on-site interaction term can be then

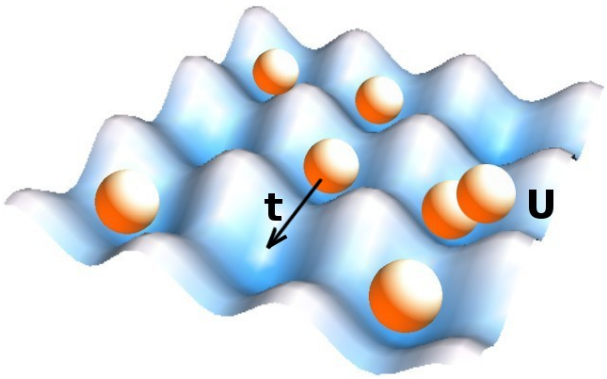

Figure 1.3: Sketch of two-dimensional optical lattice with atoms in potential minima.

calculated as:

$$t_{i,i'} = \int d\mathbf{r} \mathcal{W}^{\dagger}_{\sigma'}(\mathbf{r} - \mathbf{R}_{i'}) H^{single-body}(\mathbf{r}) \mathcal{W}_{\sigma}(\mathbf{r} - \mathbf{R}_i). \tag{1.7}$$

$$U = \int d\mathbf{r}_1 d\mathbf{r}_2 \mathcal{W}^{\dagger}_{\sigma^1}(\mathbf{r}_1) \mathcal{W}^{\dagger}_{\sigma^2}(\mathbf{r}_2) V(\mathbf{r}_1, \mathbf{r}_2) \mathcal{W}_{\sigma^1}(\mathbf{r}_1) \mathcal{W}_{\sigma^2}(\mathbf{r}_2). \tag{1.8}$$

Finally the full Hamiltonian reads:

$$\mathcal{H}^H = - \sum_{<i,j>,\sigma\sigma'} t_{i,j,\sigma,\sigma'} \left(c^{\dagger}_{i\sigma} c_{j,\sigma} + h.c. \right) + U \sum_i n_{i\uparrow} n_{i\downarrow} - \mu \sum_i n_i \tag{1.9}$$

Where $< i, j >$ are all nearest neibourghs in the lattice, $c_{i\sigma}$ annihilates one particle with spin σ at the lattice site i, and n_i is the number of particles at the lattice site i. The last term is chemical potential for fermionic system. In the above formula it is assumed that any long-range interactions are negligible and only the nearest-neibourghs tunnellings contribute to the Hamiltonian and interactions only inside one lattice site.

This Hamiltonian is known as Hubbard model. The Hubbard Hamiltonian was first introduced in condensed matter physics as a toy model describing the dynamics of electrons in the crystal structure. In the case of condensed matter physics this Hamiltonian

gives only a rough approximation of the real behaviour of the system. Moreover, this model, despite its simplicity has not been fully understood yet. For example it is believed that it can be helpful in solving some open problems like finding high temperature superconductivity, or understanding Anderson localisation. For optical lattices, that are almost perfectly isolated from external noises and nearly impurity free, the description with the Hamiltonian (1.9) can be considered exact. For the first proposals of the use of the ultracold atoms in the context of Hubbard model, see ref. [17].

Performing experiments with ultracold atoms can provide us with valuable answers to condensed matter questions. Moreover, testing Hubbard model with optical lattices is far more easy, because of the unprecedented control that we have over atomic systems. This potential to reproduce other systems is one of the most powerful applications of cold atoms. The first experimental realisation of Hubbard model in the ultracold atomic system was reported by in.

The above description can be further simplified by neglecting the interaction term. In many cases such reduction is justified, since some interesting phenomena can be successfully explained within single body picture. The Hamiltonian (1.10) that one is left with is known as tight-binding model. I will use it extensively in the part of my thesis where I study one-body physics of atoms in an optical lattice.

$$H^{TB} = -\sum_{<i,j>,\sigma\sigma'} t_{i,j,\sigma,\sigma'} \left(c^{\dagger}_{i\sigma} c_{j,\sigma} + h.c. \right) \tag{1.10}$$

1.3 Quantum simulator

As pointed out already by Richard Feynman in 1982 [18] a classical computer may not be the best tool for simulating quantum systems. In fact the theory predicts that the time needed to give an answer to physical question for any universal classical computer grows exponentially with the size of the system, unless we want to make a classical approximation of local differential equations. This approximation, however, is not always suitable for description of quantum systems. There exist number of approximate methods

such as for example quantum Monte Carlo or density functional theory but each of them can be applied only for some specific class of problems. In fact any gate-based computing technology fails to be good universal tool for simulating quantum physics. Even quantum computers, if they existed, that indeed need just a few coherent bits to solve problems accessible only for the most powerful supercomputers, still would require enormous number of gates to process the information. The error correction and the decoherence in such complicated circuit would be considerable obstacle [19]. Nevertheless, it is clear that the Nature manages to obtain the "results" so there must be some efficient way to do it other than classical computing. This is how the idea of quantum simulator was born. Feynman suggested that an alternative way of treating difficult quantum problems is to mimic the system of interest with some other one, and measure its properties rather than calculate them. A quantum simulator would have to be then a well understood quantum system that is versatile enough to imitate possibly widest class of Hamiltonians, yet easy to control and measure. This is where the ultracold atoms come into play. Along the years we have learned how to cool, trap, control and measure atomic vapours to an unprecedented degree. We are able to tune its dimensions, temperature, the interaction strength, create external potentials and choose the particle statistics. This plasticity gives us a perfect playground for simulating and studying rich variety of physical phenomena.

Nowadays the simulations made with ultracold atoms are rather being realised with dedicated systems that are not fully universal quantum simulators. They are rather designed to emulate one specific model of interest. Still they give valuable insight in the physics of the system under study and can provide us with answers to open questions.

Chapter 2

Synthetic gauge fields

A gauge theory is any field theory, in which the Hamiltonian is invariant under a group of local transformations. The gauge refers to the redundant degrees of freedom used to describe the field in the Hamiltonian that can be changed, leaving the physics of the system unchanged. The first and simplest example of a gauge theory is classical electrodynamics where the field enters the Hamiltonian as potentials $\mathbf{A}$ and ϕ. These quantities do not have direct physical interpretation. The observable are the electric and magnetic fields $(\mathbf{E}, \mathbf{B})$ given by the derivatives of the potential:

$$\begin{aligned} \mathbf{E}(\mathbf{x}, t) &= -\nabla\phi - \frac{1}{c}\frac{\partial \mathbf{A}}{\partial t} \\ \mathbf{B}(\mathbf{x}, t) &= \nabla \times \mathbf{A} \end{aligned}$$

For this reason one has a freedom of choice of potential as long as the resulting field stays the same.

$$\begin{aligned} \phi &\rightarrow \phi' = \phi - \frac{1}{c}\frac{\partial \Lambda}{\partial t} \\ \mathbf{A} &\rightarrow \mathbf{A}' = \mathbf{A} + \nabla\Lambda \end{aligned}$$

In addition, both in classical gauge field theories and in their quantum formulations, one has to substitute the standard derivatives ∂_μ by co-variant operators D_μ that include the fields. This fact will be illustrated in the following section on the example of the electromagnetic field in the quantum system. Electromagnetic field

has phase rotation $U(1)$ symmetry, which is the simplest Abelian case. It is, however, possible to consider fields given by $N \times N$ matrices, for which the symmetry transformations can belong to more non-trivial, non-Abelian groups, *e.g.* $SU(N)$ as in the case of weak and strong interactions. For the discrete systems a slightly more sophisticated definition of non-Abelian field will be given in the next section.

2.1 Gauge invariance in quantum mechanics

The Schrödinger equation for a particle with charge q in an electromagnetic field, given by the vector potential $\mathbf{A}$ and the scalar potential ϕ is,

$$\left[\frac{1}{2m}\left(-i\nabla - q\mathbf{A}\right)^2 + q\phi\right]\psi(\mathbf{x},t) = i\frac{\partial\psi(\mathbf{x},t)}{\partial t}, \tag{2.1}$$

obtained by the substitution $\mathbf{p} \to -i\nabla$ as is usual for the quantum mechanical momentum operator. For simplicity we put $\hbar = 1$. There is still freedom in the choice of the form of $\mathbf{A}$ and ϕ. We could choose

$$\begin{aligned} \mathbf{A} &\to \mathbf{A}' \equiv \mathbf{A} + \nabla\Lambda, \\ \phi &\to \phi' \equiv \phi - \frac{\partial\Lambda}{\partial t}, \end{aligned}$$

and from the classical theory of electromagnetism we know that the Maxwell equations would not change under this transformation. There is, however, a change in the Schrödinger equation (2.1). The wavefunction solving it is not invariant. It transforms according to:

$$\psi(\mathbf{x},t) \to \psi'(\mathbf{x},t) \equiv e^{iq\Lambda(\mathbf{x},t)}\psi(\mathbf{x},t).$$

This is not in a contradiction with its physicality since the wavefunction's phase is not an observable while the magnetic and electric fields are. Now, in the terms of this transformed wavefunction, the Schrödinger equation has the same form i.e. it is covariant:

$$\left[\frac{1}{2m}\left(-i\nabla - q\mathbf{A}'\right)^2 + q\phi'\right]\psi'(\mathbf{x},t) = i\frac{\partial\psi'(\mathbf{x},t)}{\partial t}. \tag{2.2}$$

A question can be asked, if the two wavefunctions describe the same physics. The probability density for ψ and for ψ' are of course the same. For the invariance of the probability current, we need to change its definition from

$$j = \psi^\dagger(\nabla\psi) - (\nabla\psi)\psi^\dagger \tag{2.3}$$

to

$$j = \psi^\dagger[(\nabla - iq\mathbf{A})\psi] - [(\nabla - iq\mathbf{A})\psi]\psi^\dagger. \tag{2.4}$$

So we can see that the operator ∇ must be substituted by $\nabla - iq\mathbf{A}$. In fact all derivatives must be modified in order to get fully covariant equation:

$$\nabla \rightarrow \nabla - iq\mathbf{A} \tag{2.5}$$

$$\frac{\partial}{\partial t} \rightarrow \frac{\partial}{\partial t} + iq\phi \tag{2.6}$$

The new differential operators:

$$\mathbf{D} = \nabla - iq\mathbf{A} \quad , \quad D^0 = \frac{\partial}{\partial t} + iq\phi \tag{2.7}$$

can be written in a Lorentz covariant form:

$$D^\mu = \partial^\mu + iqA^\mu \tag{2.8}$$

where

$$\begin{aligned} \partial^\mu &\equiv (\frac{\partial}{\partial t}, \frac{\partial}{\partial x_i}) \\ A^\mu &\equiv (iq\phi, -iqA_i), \quad i = 1..3 \end{aligned} \tag{2.9}$$

This allows us to write:

$$-iD'^\mu\psi' = e^{iq\Lambda}(-iD^\mu\psi) \tag{2.10}$$

and the Schrödinger equation involving the operator ∂^μ can be made gauge invariant under the transformations:

$$\begin{aligned} A^\mu \rightarrow A'^\mu &= A^\mu - \partial^\mu\Lambda \\ \psi \rightarrow \psi' &= e^{iq\Lambda}\psi \end{aligned}$$

provided that the minimal coupling is also made:

$$\partial^\mu \rightarrow D^\mu = \partial^\mu + iqA^\mu \tag{2.11}$$

From the derivation above we can see the remarkable property of quantum systems: the requirement of local gauge invariance determines the form of the interactions with gauge fields.

2.2 Definition of non-Abelian fields

A non-Abelian field is a field given by a vector potential $\mathbf{A} = (A_x, A_y, A_z)$ whose components are non-commuting operators:

$$\exists(i,j) : [A_i, A_j] \neq 0 \tag{2.12}$$

For lattice systems a non-Abelian field has a more subtle definition and requires introduction of the, so called, Wilson loop operator. The latter case will be discussed later in this section.

For the magnetic field $\mathbf{B}= (B_x, B_y, B_z)$ always $[B_x, B_y] = [B_y, B_z] = [B_z, B_x] = 0$, and so this field is called Abelian. In order to have a non-Abelian field, we need its components to be non-commuting matrices. Physically it means that a particle moving in such field must be described by at least a two-component wave function, on which the matrices can act. The internal degree of freedom can corresponds to a spin, pseudo-spin, a colour, hyperfine state or any other local property. In the following the pseudo-spin notation will be used and for simplicity we will focus on the case of 2×2 matrices and 2-component wave functions.

$$|\Psi\rangle = (\Psi_\uparrow, \Psi_\downarrow)^T$$

$$\begin{pmatrix} A_{i,11} & A_{i,12} \\ A_{i,21} & A_{i,22} \end{pmatrix} \begin{bmatrix} \Psi_\uparrow \\ \Psi_\downarrow \end{bmatrix} = \begin{bmatrix} \Psi'_\uparrow \\ \Psi'_\downarrow \end{bmatrix} \quad i = x, y, z \tag{2.13}$$

An example of a non-Abelian field arises naturally in the context of condensed-matter physics. A spin-orbit (SO) coupling Hamiltonian

can be rewritten in a form of a specific example of a non-Abelian gauge field. A general SO Hamiltonian contains kinetic, Rashba citerashba and Dresselhaus [21] terms:

$$\begin{aligned} H^{SO} &= \frac{p_x^2+p_y^2}{2m} + \alpha(\sigma_y p_x - \sigma_x p_y) + \beta(\sigma_x p_x - \sigma_y p_y) \\ &= \frac{1}{2m}\{[p_x - m(\alpha\sigma_y - \beta\sigma_x)]^2 + [p_y - m(\beta\sigma_y - \alpha\sigma_x)]^2\} \\ &\equiv \frac{1}{2m}\{[p_x - \frac{e}{c}A_x]^2 + [p_y - \frac{e}{c}A_y]^2\} \end{aligned} \tag{2.14}$$

$$A_x \equiv \frac{mc}{e}(\alpha\sigma_y - \beta\sigma_x)$$
$$A_y \equiv \frac{mc}{e}(\beta\sigma_y - \alpha\sigma_x).$$

Since $[A_x, A_y] \neq 0$ the latter derivation explicitly shows that the SO coupling may be recast in the form of a non-Abelian field. Here in the second equality a constant term has been neglected since it has no relevant physical meaning.

Lattice case

As described in the previous chapter, an atom in an optical lattice can be described in terms of a Hubbard Hamiltonian (1.9). For deep enough optical potential, this reduces to tight-binding model (1.10) where the interparticle interactions are neglected. Following the Peierls substitution, if additional gauge vector potential $\mathbf{A}$ is present, the tunnelling amplitudes between the i and j lattice sites become operators given by:

$$t_{ij} \longrightarrow U_{ij} \equiv t\mathbf{e}^{i\int_i^j \mathbf{A}(\mathbf{r})\mathbf{dl}}. \tag{2.15}$$

In general case the tunnelling amplitude t can also depend on the lattice site i but here for simplicity and because in all interesting cases the homogeneous and isotropic tunnelling is assumed, we set it to a constant. If the vector potential components are numbers, this results in extra phase factor in the wave function of the particle moving in the field, which leads to the standard Aharonov-Bohm effect. If, however, they are matrices, acting on some internal degree

of freedom σ of the particle, the operators U_{ij} become matrices as well. The Hamiltonian changes accordingly:

$$H = -\sum_{<i,j>}\sum_{\sigma\sigma'} c^{\dagger}_{i,\sigma} U_{ij} c_{j,\sigma'} + h.c. \tag{2.16}$$

where σ, σ' are matrix indices. In the general case $\mathbf{A}$ components can be non-commutative matrices, so the resulting physical field is given by equations:

$$\begin{aligned} B_i &= \tfrac{1}{2}\epsilon_{ikl} F_{kl}, \\ F_{kl} &= \partial_k A_l - \partial_l A_k - \frac{i}{\hbar}[A_k, A_l]. \end{aligned} \tag{2.17}$$

When a particle tunnels around a plaquette of the lattice, following a closed loop trajectory, its wave function undergoes a transformation given by the product of all corresponding operators U_{ij}. The product operator is called Wilson loop operator W. A gauge field acting on a particle moving in a lattice, is called non-Abelian if and only if its Wilson operator can not be reduced to the unity matrix. This condition is fulfilled if

$$|\mathrm{Tr} W| \neq \nu, \tag{2.18}$$

where ν is the number of the components in the wavevector. In all of the examples considered in this thesis, fields are given by vector potentials whose components are 2×2 matrices, and so for them $\nu = 2$. An example in a square lattice is illustrated in fig. 2.2. In this case the Wilson loop operator is given by formula:

$$W = U_{ij} U_{jk} U_{kl} U_{li}. \tag{2.19}$$

A detailed derivation of the Hamiltonian, as well as the calculation of the Wilson loop operator and spectrum for $\mathbf{A}_i \in \mathrm{SU}(2)$ group in a system of atoms in 2D square lattice, can be found in chapter 5.

2.3 Simulation of fields

As described in previous chapter, atoms offer us unusual flexibility and control. We are able to tune the dimensionality of the system,

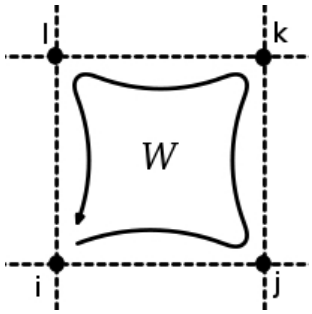

Figure 2.1: The Wilson loop $W = U_{ij}U_{jk}U_{kl}U_{li}$ for a square lattice.

lower its temperature nearly to $0K$ to reach the quantum limit, mimic crystal structure with them and even change their interparticle interactions at wish. All those properties make them a good candidate for a quantum simulator. The missing piece to make ultra cold atoms capable of reproducing nearly any Hamiltonian we want are interactions with external fields. Indeed, atoms being neutral, do not respond to magnetic nor electric field like electrons. Nonetheless we can force them to behave as charged particles in an electromagnetic-type field if we create proper conditions. There is no real external field in the system, effectively however, the dynamics of the particles is described by Hamiltonian containing a field-like term. In order to illustrate the idea of synthetic fields in the following I will review shortly some of the proposals of their experimental realisation.

2.3.1 Rotating 2D gases in harmonic trap

The first example will be a system that simulates the dynamics of a charged particle whose motion is limited to a 2D surface and with a constant magnetic field $\vec{B}$ perpendicular to the surface acting on it. Simulating this field one can reproduce for example such interesting and important phenomena as Hall effects and the Landau level structure of the spectrum, known from two dimensional electronic systems in a magnetic field. It is known that there exist an interesting similarity between the Lorentz and the Coriolis forces. In fact their form is exactly the same from the mathematical point

of view. In the rotating frame of reference the Hamiltonian H^{rot} describing an atom in a 2 dimensional harmonic trap rotating with the frequency $\mathbf{\Omega} = (0, 0, \Omega)$ reads:

$$H^{rot} \equiv H - \Omega L_z \quad = \quad \frac{1}{2M}\mathbf{p}^2 + \frac{1}{2}M\omega^2 r^2 - \mathbf{\Omega} \cdot (\mathbf{r} \times \mathbf{p}). \quad (2.20)$$

After performing simple algebra the same Hamiltonian can be written as

$$H^{rot} = \frac{1}{2M}(\mathbf{p} - M\mathbf{\Omega} \times \mathbf{r})^2 + \frac{1}{2}M(\omega^2 - \Omega^2)r^2. \quad (2.21)$$

Now recalling that the action of the magnetic field $\mathbf{B} \equiv \nabla \times \mathbf{A}$ and the scalar potential ϕ operators in quantum mechanics are given by the minimal coupling:

$$\nabla \to \nabla - \mathrm{i}\frac{q}{c}\mathbf{A} \qquad \text{and} \qquad \partial_t \to \partial_t + i\frac{q}{\hbar}\phi, \quad (2.22)$$

one can identify $\frac{mc}{q}\mathbf{\Omega} \times \mathbf{r}$ as a vector potential $\mathbf{A}$. In this way, if we move the description of the system to the rotating frame, we have an effective field acting on the particles. The last term in equation (2.21): $\frac{1}{2}m(\omega^2 - \Omega^2)r^2$ contains a new trapping frequency $\tilde{\omega} \equiv (\omega^2 - \Omega^2)$. It is clear that as the rotating of the trap increases, the effective trapping frequency decreases. In the limit when $\omega \approx \Omega$ the system becomes unstable. Because of this fact very high precision or an extra trapping potential is necessary in the experimental realisation of that scheme. The energy levels are enumerated now by two numbers: n - the Landau Level index in the units of $2\hbar\Omega$ and $m - n$ - the angular momentum in the units of $\hbar\omega$:

$$E = 2\hbar\omega(n + \frac{1}{2}) + \hbar(\omega - \Omega)(m - n) \quad (2.23)$$

For the rotation frequency approaching the trapping frequency $\frac{\Omega}{\omega} \approx 1$ the energy eigenvalues are nearly degenerate and depend very weakly on the angular momentum. They resemble Landau levels of

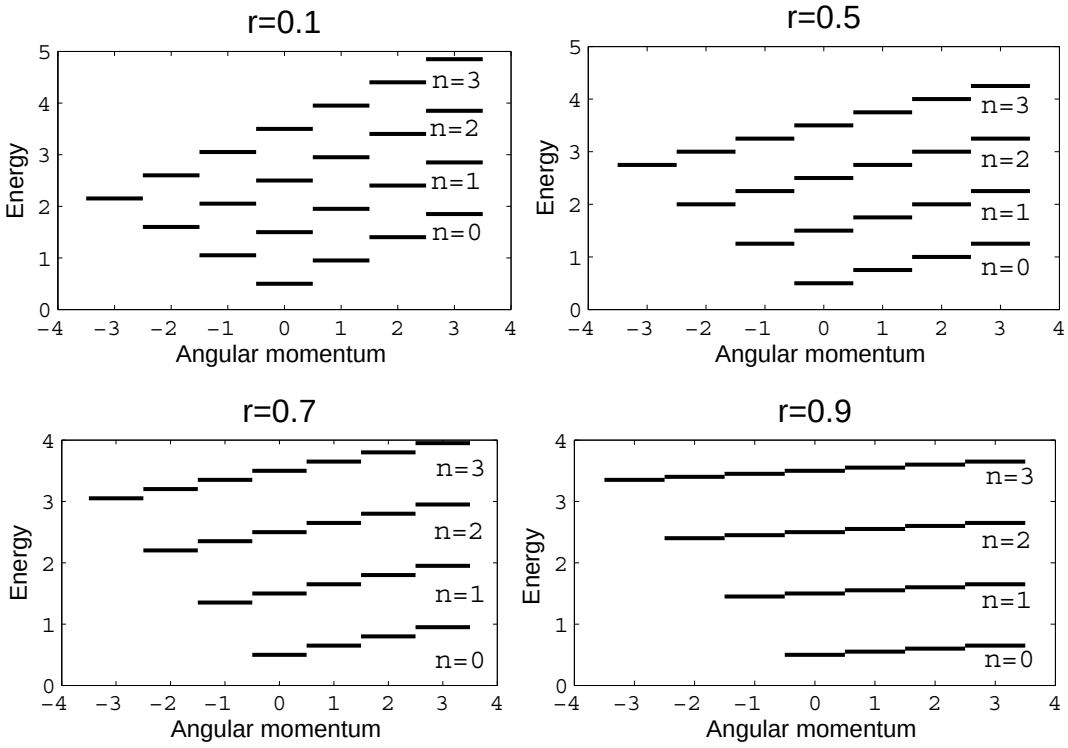

Figure 2.2: The energy levels for rotating harmonic trap. The parameter $r \equiv \frac{\Omega}{\omega}$ measures the ratio between rotation speed Ω and the trapping frequency ω. The energy is given in the units of $2\hbar\Omega$ and the angular momentum is equals to $n - m$ in the units of $\hbar\omega$.

a charged particle in a strong magnetic field (see the last plot in the Fig. 2.3.1). This idea of creating synthetic fields that would act on neutral atoms, as if they were charged inspired many experiments [22, 23, 24]. Even though rotation mimics only one class of field - a homogeneous, magnetic field perpendicular to the $x - y$ plane, it is a very important example. For increasing rotation the system is strongly correlated, forming different nontrivial states [26, 27], and in the regime of critical frequencies it is expected to become the Laughlin liquid [28]. One of the most exciting possibilities is the the simulation of fractional quantum Hall effect for interacting fast rotating gases, and in consequence, observation of its excitations: both Abelian and non-Abelian anyons [29].

2.3.2 Simulation of Aharonov Bohm effect with the Berry phase

The rotation of harmonic trap is the simplest way to mimic magnetism with ultracold atoms. It has, however, disadvantages. The rotation of the trap needed to reproduce Landau levels in the spectrum structure is very fast and in the interesting limit $\Omega \approx \omega$ the system becomes unstable due to centrifugal force balancing the trapping. Moreover, if the trapping potential does not have rotational symmetry, the problem becomes hard to handle analytically. One can avoid those problems using more sophisticated method of geometric phase.

The Berry phase is the simplest example of a geometrical phase and is the one that can be used to create an artificial magnetic field as shown by Berry [30]. The effective magnetic field can be created for a neutral particle with a magnetic momentum μ moving slowly in a real inhomogeneous magnetic field $\mathbf{B}(\mathbf{r})$. The atoms centre of mass motion will not be affected by the presence of $\mathbf{B}(\mathbf{r})$, but the eigenvalues and eigenstates of the system are space dependent. If the particle is prepared at the initial time t_i in one of the eigenstates $|\mathbf{n}_0(\mathbf{r}_i)\rangle$ of the local Hamiltonian $-\mu\mathbf{B}(\mathbf{r})$ and its motion is slow enough, the particle will adiabatically follow the eigenstate. At the final point of the trajectory the particle will still be in state $|\mathbf{n}_0(\mathbf{r})\rangle$ but also will acquire a phase factor containing a geometric

component. If the trajectory is a loop, at the final point the particle comes back to its initial state up to a phase factor. This is then equivalent to the famous Aharonov-Bohm effect for a charged particle in an effective magnetic field. This effective field depends on the gradients of the original $\mathbf{B}(\mathbf{r})$. In the following it will be illustrated, how the effective vector potential appears in more general case. We will assume that the system consists of a neutral particle whose centre of mass m is moving in a space with some possible external potential $V(\mathbf{r})$ present. Additionally the particle has some degree of freedom described by space dependent Hamiltonian $H_0(\mathbf{r})$. The full Hamiltonian then reads:

$$H = \frac{\mathbf{p}^2}{2m} + V(\mathbf{r}) + H_0(\mathbf{r}, t). \tag{2.24}$$

H_0 can for example be equal to before mentioned $-\mu\mathbf{B}(\mathbf{r})$, if the internal degree of freedom is the magnetic momentum. It can also represent the light field coupling to atoms and the eigenstates of H_0 are, so-called, dressed states. Then in general H_0 can be time dependent. assuming that the light field is stationary and use the rotating wave approximation (RWA) this time dependence can be eliminated. Denoting the eigenvectors and eigenvalues of this local Hamiltonian by:

$$H_0(\mathbf{r})|\chi_n(\mathbf{r})\rangle = \epsilon_n(\mathbf{r})|\chi_n(\mathbf{r})\rangle, \tag{2.25}$$

the full solution of the problem with the full Hamiltonian can be written as a series:

$$|\psi(\mathbf{r}, t)\rangle = \sum_n \psi_n(\mathbf{r}, t)|\chi_n(\mathbf{r})\rangle \tag{2.26}$$

At this point an assumption should be made about the system under consideration: Among the energy levels of H_0 there must be a level ϵ_0 decoupled from the rest. This does not necessarily have to be the lowest energy level. Here for simplicity ϵ_0 is taken as an example.If the particle is prepared in the initial state $|\Psi(\mathbf{r}, t = 0)\rangle = \psi_0(\mathbf{r}, t)|\chi_0(\mathbf{r})\rangle$ and if it is moving slowly enough, then its state will always follow adiabatically the same eigenstate. The action of

the momentum operator $\mathbf{p}$ on this state is:

$$\begin{aligned} \mathbf{p}|\Psi(\mathbf{r},t)\rangle &= -i\hbar\nabla\left[\psi_0(\mathbf{r},t)|\chi_0(\mathbf{r})\rangle\right] \\ &= -i\hbar|\chi_0(\mathbf{r})\rangle\nabla\psi_0(\mathbf{r},t) - i\hbar|\nabla\chi_0(\mathbf{r})\rangle\psi_0(\mathbf{r},t) \\ &= ... \end{aligned} \tag{2.27}$$

and after using the completeness and orthonormality of the $|\chi_n(\mathbf{r})\rangle$ basisthe above formula gives:

$$... = |\chi_0(\mathbf{r})\rangle\left(-i\hbar\nabla - i\hbar\langle\chi_0(\mathbf{r})|\nabla\chi_0(\mathbf{r})\rangle\right)\psi_0(\mathbf{r},t)$$

Now, recalling that the local Hamiltonian $H_0(\mathbf{r})$ is position dependent, we see that both of the terms are non-zero. In addition the term $\langle\chi_0(\mathbf{r})|\nabla\chi_0(\mathbf{r})\rangle$ is imaginary and can then be identify as the effective vector potential . Finally one gets:

$$\mathbf{p}|\Psi(\mathbf{r},t)\rangle = |\chi_0(\mathbf{r})\rangle\left(\mathbf{p} - \mathbf{A}(\mathbf{r})\right)\psi_0(\mathbf{r},t), \tag{2.28}$$

where

$$\mathbf{A}(\mathbf{r}) \equiv i\hbar\langle\chi_0(\mathbf{r})|\nabla\chi_0(\mathbf{r})\rangle. \tag{2.29}$$

The equations (2.27) and (2.28) resemble the minimal coupling of the vector potential to the momentum. This gives an Abelian magnetic field $\mathbf{B} = \nabla \times \mathbf{A}$, that one can obtain under experimental control, because it depends on the gradients of the internal eigenstates of the particle. After taking second power of the momentum operator one also a scalar term that can be interpreted as the scalar potential ϕ

$$\phi = -\frac{\hbar^2}{2m}\sum_{j=2}^{N}\langle\chi_1(\mathbf{r})\nabla\chi_j(\mathbf{r})\rangle\langle\chi_j(\mathbf{r})\nabla\chi_1(\mathbf{r})\rangle. \tag{2.30}$$

Both $\mathbf{A}$ and ϕ appear due to space dependency of eigenstates $\chi_i(\mathbf{r})$. There are several proposals of using above method in the experiments with ultracold atoms by using the atom-light coupling. I will now review some practical implementations schemes following the excellent review of the subject by J. Dalibard et. al. [40].

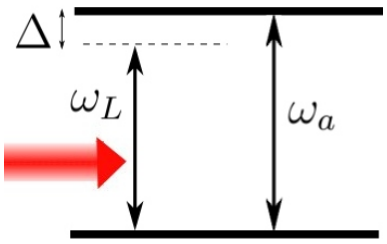

Figure 2.3: The schematic representation of two-level system. The laser light has frequency ω_L, which differs from the atomic resonant frequency ω_a by Δ. Both energy levels are long-lived and any coupling to other energy levels is neglected.

Implementation: Two-level atom

First, the simplest implementation following the example of two-level system from the ref. [41] - an atom in a non-homogeneous laser field will be presented. Presence of a harmonic trapping potential $V(\mathbf{r})$ is also assumed, which in the z direction limits the atoms centre of mass motion to $x-y$ plane only. The atom has two internal energy levels: $|g\rangle$ and $|e\rangle$ separated by the energy gap corresponding to frequency ω_a. They are eigenstates of the internal Hamiltonian in the absence of the coupling laser light. The two energy levels must have a long lifetimes, so that we can neglect the spontaneous emission and other losses in the problem at least in the interesting time-scale. There are several known atoms (Ca, Sr, Yb) whose energy levels structure allows the lifetimes above one second, which is sufficient for our purpose. The laser light is detuned from the atomic resonance by $\Delta \equiv \omega_L - \omega_A$, which is small see Fig 2.3. The full Hamiltonian for the atom in the light field in the rotating wave approximation reads [31]:

$$H = \frac{\mathbf{p}}{2M} + V(\mathbf{r}) + H_c, \tag{2.31}$$

where $V(\mathbf{r})$ is the trapping potential in $x-y$ plane and H_c is the atom-light coupling:

$$V(x,y) = \frac{1}{2M}(\omega_x^2 x^2 + \omega_y^2 y^2) \tag{2.32}$$

$$H_c = \frac{\hbar}{2}\begin{pmatrix} \Delta(\mathbf{r}) & \Omega(\mathbf{r}) \\ \Omega^*(\mathbf{r}) & \Delta(\mathbf{r}) \end{pmatrix}. \tag{2.33}$$

Here Ω is the Rabi frequency and corresponds to the strength of the atom-light interaction. The light is a Gaussian wave travelling in the x direction. We can set $\Omega(\mathbf{r}) = \tilde{\Omega}(y)e^{ikx}$, where $\tilde{\Omega}$ is real and positive. The eigenvectors of the interaction Hamiltonian are:

$$|\chi_1\rangle = \begin{pmatrix} \cos\frac{\Delta}{2} \\ \\ e^{ikx}\sin\frac{\Delta}{2} \end{pmatrix} \tag{2.34}$$

$$|\chi_2\rangle = \begin{pmatrix} -e^{-ikx}\sin\frac{\Delta}{2} \\ \\ \cos\frac{\Delta}{2} \end{pmatrix}. \tag{2.35}$$

Now, from the eq. (2.29) it is easy to see that the effective vector potential can be created if $\nabla\Delta \neq 0$ or/and $\nabla\Omega \neq 0$. The non-vanishing gradient of Δ means that the detuning of a laser light is varying in space, while the case with non-zero gradient of the Rabi frequency means that the laser light intensity is non-constant. The first experimental realisation of the artificial magnetic fields by Lin et. al. [35] used a configuration with a gradient of the detuning for alkali atoms. The scheme with two levels has, however, a big limitation, which is the requirement of long radiative lifetime of the excited state. It has been further developed and generalised to more sophisticated configurations that allow the use of wider class of atoms.

Generalisations of the two-level atom

One of the first improved methods to overcome the problem of short lifetimes of excited state was creation of the, so called, dark

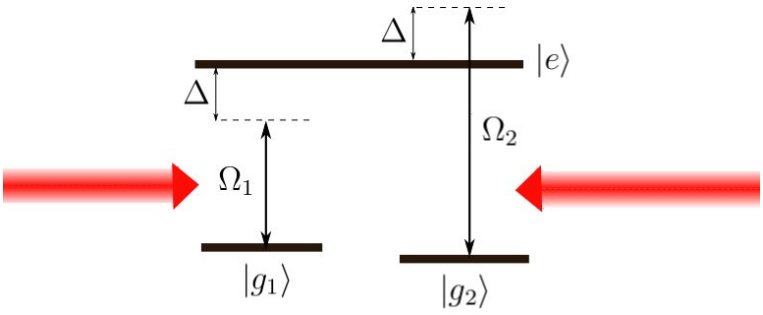

Figure 2.4: Energy levels in so called Λ system. There are two (quasi)degenerate ground levels and one excited level. This energy level structure supports the dark state that depends on the parameters Ω_1, Ω_2.

states that exist in the systems with degenerate or quasi-degenerate ground level. In such system among eigenvectors of the coupling Hamiltonian, there exist at least one state that is a superposition of the degenerate ground states only. This sate $|D\rangle$ is called the dark state, because it is decoupled from the excited state and from the interaction with the light. It is robust with respect to decoherence, and its lifetime is practically infinite. The simplest and historically the first implementation of the idea is a case with two ground states $|g_1\rangle, |g_2\rangle$ and one excited state $|e\rangle$ [44, 33] i.e. so called Λ-system, because of the shape of its energy levels, which is depicted in the Fig. 2.4. The two lasers are symmetrically detuned from the transitions between $|g_1\rangle, |g_2\rangle$ respectively and $|e\rangle$.

In analogy to the two-level example, the atom-light coupling Hamiltonian for this configuration can be written in the basis of the states $\{|g_1\rangle, |g_2\rangle, |e\rangle\}$ as:

$$H_c = \begin{pmatrix} -2\Delta & \Omega_1^* & 0 \\ \Omega_1 & 0 & \Omega_2 \\ 0 & \Omega_2^* & 2\Delta \end{pmatrix}. \tag{2.36}$$

Here again the Rabi frequencies Ω_i are space dependent and complex because they include the varying phase of the light. The detuning of the two-photon Raman transition from the resonant

frequency is denoted as 2Δ. In the case when the detuning is negligible, there exist one dark state:

$$|D\rangle = \frac{1}{\sqrt{|\Omega_1|^2 + |\Omega_2^2|}} \left(\Omega_2|g_1\rangle + \Omega_1|g_2\rangle\right), \tag{2.37}$$

and two other, so called, bright eigenstates $|B\rangle$ that couple the excited energy level:

$$|B_\pm\rangle = \frac{1}{\sqrt{2}} \left(\frac{1}{\sqrt{|\Omega_1|^2 + |\Omega_2^2|}} \left(\Omega_1^*|g_1\rangle + \Omega_2^*|g_2\rangle\right) \pm |e\rangle \right). \tag{2.38}$$

Now, the full atomic wave function is decomposed in the basis of $|D\rangle, |B\pm\rangle$

$$|\Psi(\mathbf{r})\rangle = \sum_{i=B\pm,D} \psi_i(\mathbf{r})|i\rangle \tag{2.39}$$

We assume also that the dynamics of the system is sufficiently slow, so that if we prepare an atom in the initial state $|D\rangle$ then the above sum will contain the D- term only all the time and this way it will be protected from the spontaneous emission all the time as well:

$$|\Psi(\mathbf{r})\rangle \approx \psi(\mathbf{r})|D(\mathbf{r})\rangle. \tag{2.40}$$

Using once more eq. (2.29) we can get the Schrödinger equation for $\Psi(\mathbf{r})$:

$$\mathrm{i}\partial_t\psi = \left(\frac{(\mathbf{p} - \mathbf{A})^2}{2M} + V + \phi \right) \psi(\mathbf{r}), \tag{2.41}$$

where $\mathbf{A}$ and ϕ are the effective potentials

$$\begin{aligned} \mathbf{A} &\equiv \langle D|\nabla D\rangle, \\ \phi &\equiv \frac{1}{2M} \left(|\langle B_-|\nabla D\rangle|^2 + |\langle B_+|D\rangle|^2 \right). \end{aligned}$$

and V is the trapping potential that can be present in the system as well. After performing some algebra one finds that the synthetic field created in the system is:

$$\mathbf{B} = \frac{\nabla(\phi_1 - \phi_2) \times \nabla \frac{|\Omega_1|}{|\Omega_2|}}{\left(1 + \frac{|\Omega_1|}{|\Omega_2|}\right)^2}, \tag{2.42}$$

where ϕ_i are the phases of the frequencies $\Omega_i = \tilde{\Omega}_i(\rho)e^{i\phi_i}$, and ρ is the radial coordinate in the $x-y$ plane. The field $\mathbf{B}$ is non-vanishing if both the gradients of the relative phase $\nabla(\phi_1 - \phi_2)$ and the ratio of intensities $\nabla\frac{|\Omega_1|}{|\Omega_2|}$ are nonzero and linearly independent. There has been proposed three types of experimental setups to achieve this condition.

- The proposal by Juzeliūnas et. al. [32], which uses the laser beams with orbital angular momentum. The fig. 2.5 represents this setup. The two laser beams carry the orbital angular momenta l_1 and l_2. The phases ϕ_i then can be written as $\phi_i = l_i\phi$ where ϕ is now the azimuthal angle around the z axis. In the plot only one of the beams have non-vanishing orbital angular momentum. This method is, however, not suitable for creating high magnetic fields because the effective field flux through the system is of the order of $l_2 - l_1$, which is typically of the order of 10 in the units of the Plank constant $\hbar$.

- The second proposal that does not requires the light with angular momentum, [33] uses two counter propagating Gaussian shaped laser beams. Thank to counter propagation the gradient of the relative phase is nonzero. The centres of the beams are shifted with respect of one another as represented in fig. 2.6. In this way the ratio of the intensities varies in space. This proposal has been further developed in 2009 by Günter et.al. to a configuration that allows more flexibility in the laser polarisations [34] where the authors use two laser beams that are perpendicular to one another and shifted with the respect to the centre of the atomic cloud. The light is far detuned from the resonance in order to reduce the spontaneous emission and only the electronic angular momentum is relevant quantum number since the hyperfine splitting is much smaller than the detuning. This method has an advantage over the previous one that it allows creation of high magnetic field in relatively large regions of space, still taking advantage of the minimal spontaneous emission.

- Most recently in the experiment by the Y.J. Lin et. al. the

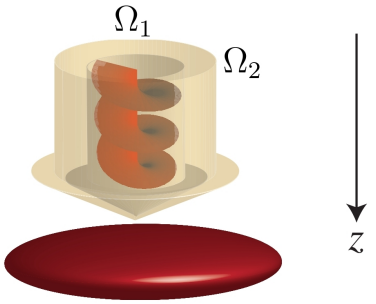

Figure 2.5: Two Gaussian beams with the Rabi frequencies Ω_1, Ω_2 prepared in Gaussian Leguerre modes with angular momentum l_1, l_2. Here only one of the laser beams has non-zero orbital angular momentum and l_2 is zero. The beams are tuned to the transition to the excited state $|E\rangle$ respectively from $|g_1\rangle$ and $|g_2\rangle$ with the detunings Δ and $-\Delta$. Both the ratio between the intensities of the Rabi frequencies as well as the gradient of the phase difference. In effect, the atom prepared in the dark state $|D\rangle$ "feels" an effective magnetic field along the z-axis. Picture taken from [40].

Figure 2.6: Two counter propagating laser beams as in the proposal from the ref. [33]. The figure is taken from the cited reference.

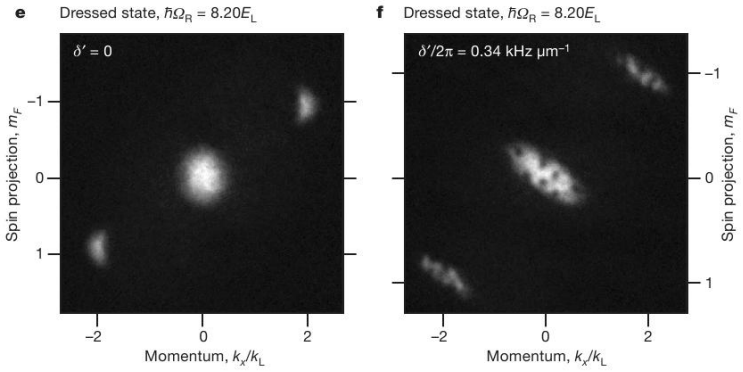

Figure 2.7: The vortices formation in the experiment by Lin et.al. [25]. In the left figure, the detuninig gradient is zero and there are no vortices. In the right figure, the gradient is turned on. The vortices being a sign of the synthetic magnetic field presence are formed. The fig. taken from the reference above.

nonzero magnetic field is created with the use of space dependent detuning of the light [25]. In their proposal the authors used the Raman transition between the hyperfine levels ($F = 1$) in a gas of ^{87}Rb. The Zeeman sublevels $m_F = 0, \pm 1$ were splitted by magnetic field and the two laser beams transfer the atoms between them via Raman transitions. The detuning in these transitions was regulated by non-homogeneous real-magnetic field. In effect the neutral atoms felt the effective magnetic field. One can see the vortex formaton in the case where the detuning gradient was present in the experiment in fig. 2.7

The non-Abelian generalisation

Recently there are being developed proposals to extend above method to simulate non-Abelian effective gauge fields. For this to be possible one needs a degenerate subspace of the Hilbert space of the internal Hamiltonian H_0 that is at least two-dimensional, with the orthonormal basis: $\{|\chi_0^1\rangle, |\chi_0^2\rangle, ...|\chi_0^q\rangle\}, q > 1$, such that $\forall_i H_0|\chi_0^i\rangle = \epsilon_0|\chi_0^i\rangle$ and such, that it is decoupled from the rest of the states, so

there must be an energy gap between ϵ_0 and the rest of the spectrum. If now the initial state of the particle is prepared in any linear combination of the degenerate states, it will remain a linear combination of those states with different coefficients after the particle moves,

$$\begin{aligned} |\Psi_i(\mathbf{r},t)\rangle &= \psi_i(\mathbf{r},t)\sum_{j=1..q} C_j|\chi_0^j\rangle \\ \downarrow & \\ |\Psi_f(\mathbf{r},t)\rangle &= \psi_f(\mathbf{r},t)\sum_{j=1..q} \widetilde{C}_j|\chi_0^j\rangle \end{aligned}$$

We can then think of it as a q-component wave function that transforms while moving from one point to another with the transformation given by a unitary operator instead of just a phase factor. This defines the effective matrix vector potential acting on the particle while it is moving from $\mathbf{r}_i$ to $\mathbf{r}_f$ [36]:

$$U_{if} \equiv e^{i\int_{\mathbf{r}_i}^{\mathbf{r}_f}\mathbf{A}(\mathbf{r})\mathbf{dl}} \tag{2.43}$$

2.3.3 Synthetic gauge field in an optical lattice

Optical lattices are one of the most promising setups for creating wide class of artificial gauge fields. In the seminal paper by D. Jaksch and P. Zoller [38] from 2003 the authors design an experiment, in which one can simulate the Aharonov-Bohm effect on a two dimensional square lattice. If the particle moving in the lattice potential was charged any external magnetic field would couple to the momentum resulting in extra phase factor in the hopping operator. A particle tunnelling from site to site would acquire a phase the same as predicted by Aharonov-Bohm theory in continuum. This effect can be simulated by laser assisted tunnellings between lattice sites, as the atom-light interaction can also induce a phase factor of the atoms wave function. In the following a general concept of the experiment will be presented following ref. [39].

The starting point is the tight-binding Hamiltonian for 2D square

lattice (1.10).

$$H = -t \sum_{m,n} c^{\dagger}_{m,n} U^{\dagger}_{x} c_{m-1,n} + c^{\dagger}_{m,n} c_{m,n-1} + h.c., \tag{2.44}$$

where m, n enumerate the lattices sites respectively in x and y direction. The atoms trapped in this lattice can be in two states, which are denoted $|g\rangle$ and $|e\rangle$. The periodic potential created by the laser beams in the y direction traps both types of the atoms in the intensity minim-as. It is possible to find such wavelength of the light that the polarisabilities of both states $|g\rangle, |e\rangle$ are exactly the same. This wavelength is called magic wavelength λ_m. On the other hand, in the x direction the laser is tuned to anti-magic wavelength λ_{am}, that produces reversed optical potential for the two atomic types. This way, the state $|g\rangle$ is trapped in the intensity minima while $|e\rangle$ in its maxima. The effective state-dependent lattice has period of $d_y = \lambda_m/2$ in y direction and $d_x = \lambda_{am}/4$ in x direction:

$$V(y) = V_m \cos^2\left(\frac{\pi y}{d_y}\right) \tag{2.45}$$

$$V(x) = \pm V_{am} \cos^2\left(\frac{\pi y}{2d_y}\right), \tag{2.46}$$

with the "+" sign for $|e\rangle$ state and "-" for $|g\rangle$ state. The nearest neighbouring sites in the lattice in the x-direction are then alternating minima and maxima of the laser light intensity. The jumps between them impose a change in the internal state of the atom (see fig. 2.8). The laser intensities must be carefully adjusted so that the tunnellings in y direction are significant and that the hopping along x direction without the state change are negligible. This can be achieved by tilting the lattice in the x-direction so that the jumps due to the kinetic energy in this direction are forbidden. The two states $|g\rangle$, $|e\rangle$ must also be chosen with care so that they are both long-lived. The ground state $^1S_0$ and the excited state $^3P_0$ of Ytterbium can serve as an example of the system that provide such configuration. There are, however, more possibilities and a detailed description of this matter one can find in the literature cited above.

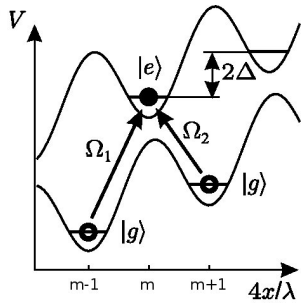

Figure 2.8: Trapping potential in the x-direction. Adjacent sites are set off by an energy Δ because of the acceleration or a static inhomogeneous electric field. The laser Ω_1 is resonant for transitions $|g\rangle \longrightarrow |e\rangle$ and Ω_2 is resonant with transitions $|e\rangle \longrightarrow |g\rangle$, due to the offset of the lattice sites. Because of the spatial dependence of $\Omega_{1,2}$ atoms hopping around one plaquette get phase shifts of $2\pi\alpha = \phi m + 0 + \phi m + 0$ where $\phi = 2\pi\alpha$ and $\alpha = q\lambda_{am}/4\pi$, where q is the laser wavevector.The figure has been taken from the ref. [38]

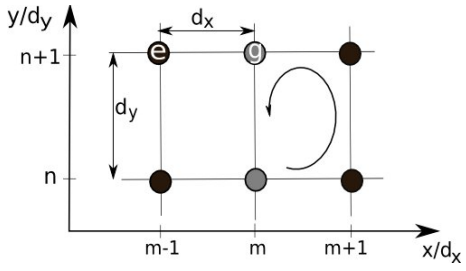

Figure 2.9: The scheme of state dependent lattice. The grey dots denote the ground state sublattice and the black ones the excited ones. the tunnelling in y direction does not contribute to the overall phase factor and the hopping in the x direction is laser assisted by an beam coupling the ground and the excited state. $d_x = \frac{\lambda_{am}}{4}$ and $d_y = \frac{\lambda_m}{2}$. This laser beam lies in $y - z$ plane and contribute to the phase factor. This way the phase factor depends on y coordinate. The overall phase after an atom moves around one lattice plaquette equals $\phi = 2\pi\alpha$ where α is tuneable and depends on the configuration of the coupling laser.

The transition between $|e\rangle$ and $|g\rangle$ along x direction is laser assisted and the coupling laser light of the wave length λ_c propagates in $y-z$ plane. The atom-light interaction results in the tunneling operator U_x present in the corresponding term in the Hamiltonian (2.44). This extra phase factor depends on the y coordinate of the lattice site: for $(n,m) \longrightarrow (n+1,m)$ transition

$$U_x(|g_{n,m}\rangle \longrightarrow |e_{n+1,m}\rangle) = e^{ik_c r_g} = e^{im2\pi\alpha}, \tag{2.47}$$

where k_c is the wave vector of the coupling laser, r_g is the position of the tunnelling atom in the state $|g\rangle$ and $\alpha = \frac{\lambda_m}{2\lambda_c}$. The phase acquired by a particle moving along a loop around one lattice plaquette equals $\phi = 2\pi\alpha$, which corresponds to a magnetic flux $\Phi_B = \frac{\alpha}{\Phi_0} = \frac{\alpha hc}{e}$ of the effective magnetic field. The parameter α can be tuned over wide range of amplitudes, and allows simulating very strong magnetic fields.

Rotating optical microtraps

Another very promising line of experiments that may provide a tool to create synthetic gauge fields for neutral atoms is using the rotation combined with the optical lattice. Up to now they probably offer the most efficient way to create strong artificial magnetic fields needed to reach both the integer and the fractional quantum Hall effects. An array of rotating microtraps can be created either with the array of laser beams or lenses that create optical microtraps [37].

The non-Abelian generalisation

The above described lattice realisation of artificial potentials has been further generalised to simulate non-Abelian fields by K. Osterloh *et al* ([48]). This is done by filling the lattice with atoms that have an internal degree of freedom that can be treated as a "colour". By creating an effective gauge field that affects that internal degree of freedom, one is in general able to simulate an external gauge field belonging to non-Abelian $U(n), SU(n)$, or even $GL(n)$ group. In that case the tunnelling amplitudes are replaced by corresponding $n \times n$ matrices and the Wilson loop is nontrivial. In

the proposal of Osterloh et. al. they used two different hyperfine states as "colours" for simulation of $U(2) = U(1) \times SU(2)$ fields. In their scheme each atom in the lattice can be in one of two ground states: $|g_i\rangle, i = 1, 2$ or two excited states: $|e_i\rangle, i = 1, 2$, where the index i indicates the colour. The hopping due to kinetic energy in both directions is prohibited by tilting the lattice. The tunnelings are possible only thanks to laser assisted tunneling in both directions. In the x direction the hopping is given by unitary matrix U_x that is identical for both ground and excited states. The atoms tunnel from their ground states to a ground state and the same with the excited ones. They, however, change their internal state - the tunnelling is accompanied by colour switching. The lasers in the y- direction are not changing the internal state of the atom, but only taking it from the ground to excited state and back. The light frequencies are denoted Ω_{1i}, Ω_{2i} for the transfer $|g_i\rangle \longrightarrow |e_i\rangle$ and back respectively. As may be read from the fig. 2.10b, those two frequencies are different due to the lattice tilting. Because of the state-dependent lattice and special choice of the lasers not only the state of the atom changes from $|e\rangle$ to $|g\rangle$ and back, but also the internal state can alter while hopping. This is equivalent to having a matrix operators U_x, U_y mixing the internal degrees of freedom while tunnelling from one lattice site to another. The tunnelling operators in the x and y directions are then given by non-trivial matrices that, in general case, do not commute and can have the Wilson loop operator not reducible to unity matrix, depending on specific choice of the experimental setup.

In general there is a lot of freedom in choosing the parameters of the tunnelling matrices. The authors chose the configuration where Ω_is are depending on x-coordinate (a running wave in the x direction), and because of this they obtained non-trivial Wilson loop (i.e. $\mathrm{Tr}W \neq 2$) for their system. This setup will be further analysed in the chapter 3 where also other choice of the gauge field is discussed.

The knowledge of synthetic gauge fields has been developing rapidly during last years. The list of the proposals of synthetic fields realisations given above is far from being complete. One of the interesting methods proposed recently is to immerse a lattice of trapped atoms A in a rotating BEC of different atoms - type B. The bosons

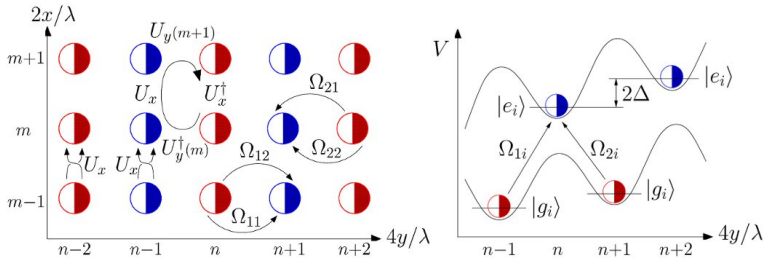

Figure 2.10: see [48]. a)Optical lattice setup for U(2) gauge fields: Red and blue open semi-circles (closed semi-circles) denote atoms in states $|g_1\rangle$ and $|g_2\rangle$, respectively ($|e_1\rangle$ and $|e_2\rangle$). Left) Hopping in the x-direction is laser assisted and allows for unitary exchange of colours. Hopping along the y-direction is also laser assisted and gives colour dependent phase factors while tunnelling. b) Trapping potential in y-direction. Consecutive sites are set off by an energy Δ. The lasers Ω_{1i} are resonant for transitions $|g_{1i}\rangle \leftrightarrow |e_{2i}\rangle$, while Ω_{2i} are resonant for transitions between $|e_{1i}\rangle \leftrightarrow |g_{2i}\rangle$ due to the offset of the lattice sites.

B collide with A-atoms, causing phonon-like excitations, changing their dynamics. This effect can be employed to simulate an effective potential felt by A-atoms [42]. The scheme showing the lattice hopping, as well as the energy levels structure is presented in fig. 2.10

Interestingly enough, employing above methods gives us such control over the effective field that we can design it in almost any form. We are no longer limited to considering the objects known from observations, but can realise novel ones and make them behave in a desired way. One good example can be breaking the Maxwell laws of electrodynamics with a magnetic monopole, that can be realised in synthetic fields [43]. The non-Abelian fields are not completely new objects in physics, since they have been studied for long time in the context of high energy research, but the possibility to choose their form and strength definitively is.

Chapter 3

Atoms in external gauge fields in lattices

As described in Chapters 1 and 2, ultracold atoms can be used as quantum simulators for a wide variety of phenomena. With the use of technologies allowing for interaction manipulation and synthetic field creation we can engineer the systems to an unprecedented degree. One of the most promising setups for creation of synthetic gauge fields are optical lattices. They are also important from the point of view of the simulation of condensed-matter systems. Let us in this chapter review the basic properties characterising of fermionic particles in square lattice and in external gauge fields. In this chapter I will follow the historical order in presenting the results. First in section 3.1 we will present the original work by D. R. Hofstadter [45] about the influence of the classical magnetic field on the charged particles in a square lattice, discussed by the author in the context of electrons in a crystal structure. We will discover that the spectrum of this system has unusual and beautiful form of a fractal. It has however not yet been observed due to huge magnetic fields needed. It is probable that the first experimental observation will be done with the use of cold atoms since there are proposals how to simulate fields strong enough for this purpose. Next, in the section 3.2 we will discuss a modification of previous case proposed first by K. Osterloh et. al. [48]. We will study the same system in the presence of non-Abelian gauge fields possible to realise with ultracold atoms. The spectrum of this system will

no longer have the structure of the butterfly. The big energy gaps will be destroyed. The authors conclude that the spectrum changes due to the introduction of the non-Abelian field. However, we will present another example of a system that will prove that even in the case of Abelian field the gaps can be destroyed. Our conclusion is that the decisive factor in the shape of the spectrum is not the non-Abelianity of the gauge field but rather the constant or non-constant character of the Wilson loop. In the section 3.3 we will confirm that even in the non-Abelian case one can have butterfly-like spectrum provided that the condition of constant Wilson loop is fulfiled.

3.1 Spectrum for Abelian fields: Hofstadter butterfly

In this chapter we will consider a system of non-interacting fermionic atoms trapped in a two-dimensional square optical lattice of unit length a which for the simplicity we take as the unit of length. In the system an external gauge field given by the vector potential $\mathbf{A}$ is present. The sites of the lattice are at $(x = m, y = n)$ where m, n are integer numbers. If one wishes to simulate such system with ultracold atoms, the non-interacting limit can be reached by the use of Feshbach resonances or simply at low densities [1]. If the optical potential is strong, so that the tight-binding approximation holds then the Schrödinger equation for a single particle subjected to an artificial gauge potential is given by the minimal coupling and reads:

$$\begin{aligned} &- t \left(U_x \, \psi_{m+1,n} + U_x^\dagger \, \psi_{m-1,n} \right. \\ &+ \left(U_y \, \psi_{m,n+1} + U_y^\dagger \, \psi_{m,n-1} = E \, \psi_{m,n} \, , \right. \end{aligned} \tag{3.1}$$

where U_x (resp. U_y) is the tunnelling phase in the x (resp. y) direction and t is the tunnelling amplitude. For the simplicity in the following we have chosen the amplitudes in both directions to

[1] The case of square lattice is the simplest and was used in original works by R. Hofstadter. However, one can consider other geometries in similar context.

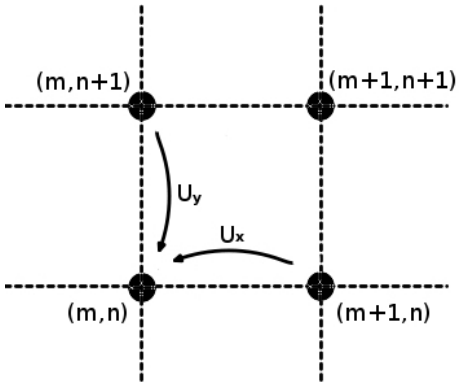

Figure 3.1: Atoms hopping from one site to the other gain extra phase due to the presence of gauge field. The phases are given by complex numbers U_x, U_y.

be equal and we also choose t as the energy unit and set $\hbar = c = e = 1$, except otherwise stated. The tunnelling phases (Fig. 3.1) are related to the gauge potential according to

$$U_x = e^{i\int_m^{m+1} \mathbf{A}\cdot\mathbf{dl}} \tag{3.2}$$

$$U_y = e^{i\int_n^{n+1} \mathbf{A}\cdot\mathbf{dl}}. \tag{3.3}$$

This formula is valid for any type of gauge field - Abelian and non-Abelian. Now we want to consider a homogeneous magnetic field $\mathbf{B}$ perpendicular to the $x-y$ plane of the optical lattice. This field is represented by a vector potential which is however not uniquely defined, as we have a choice of the gauge. We choose the so called Landau gauge:

$$\mathbf{A}(\mathbf{r}) = B(0, x, 0) = (0, 2\pi\Phi m, 0). \tag{3.4}$$

Which gives a constant magnetic field in the z- direction:

$$\mathbf{B}(\mathbf{r}) = 2\pi\Phi(0, 0, 1) \tag{3.5}$$

It is worth noting at this point that the magnetic flux through unit plaquette of the lattice is equal to Φ and it is expressed in the units

of $\Phi_0 =$ which is the flux quantum. With this choice our tunnelling phases are:

$$\begin{aligned} U_x &= 1 \\ U_y &= e^{i2\pi\Phi m} \end{aligned}$$

The Wilson loop for this system is equal

$$\mathcal{W} = |\mathrm{Tr}\ e^{-i2\pi\Phi m} e^{i2\pi\Phi(m+1)}| = 1, \tag{3.6}$$

Which for the system of atoms with no internal degrees of freedom indicates an Abelian gauge field.

Since y- coordinate does not enter in the expression (3.1), the system is still periodic in this direction and the problem can be reduced to effective one-dimension by a partial Fourier transform. We substitute

$$\Psi(m,n) = e^{i\mathbf{k}_y n} g(m) \tag{3.7}$$

and we get the famous Harper equation [46]:

$$g(m+1) - g(m-1) + 2\cos(2\pi\Phi - \mathbf{k}_y) = Eg(m). \tag{3.8}$$

The parameter Φ is equal to the number of the magnetic flux quanta penetrating single lattice cell. In the following we will be interested in the regime $\Phi \approx 1$. For a typical crystal structure, where the distances between atoms are of order of $10^{-10}m$ this translates to enormous magnetic field amplitude of the order of $B \approx 10^5 T$. Equation (3.8) can be rewritten in a recursive matrix form:

$$\begin{pmatrix} g(m+1) \\ g(m) \end{pmatrix} = \underbrace{\begin{pmatrix} E - 2\cos(2\pi\Phi - \mathbf{k}_y) & -1 \\ 1 & 0 \end{pmatrix}}_{\hat{A}_m(k_y).} \begin{pmatrix} g(m) \\ g(m-1) \end{pmatrix} \tag{3.9}$$

Matrix $\hat{A}_m$ is so called transfer matrix and it is a function of Φ and $\mathbf{k}_y$. The interesting phenomena occurs when Φ is a rational number $\frac{p}{q}$ with p and q co-prime numbers. We assume then that this is the

case. It implies that the matrix $\hat{A}_m$ is periodic in m with period q. Later in this chapter we will mention the case when the flux per lattice plaquette is an irrational number. For the present case the long product of matrices taking us from $g(0)$ to $g(m)$ where we take $m = Nq$ must consist of repeating blocks of the first q matrices:

$$\hat{A}_{Nq}\hat{A}_{Nq-1}...\hat{A}_1 = \underbrace{\hat{A}_q\hat{A}_{q-1}...\hat{A}_1}_{1}\underbrace{\hat{A}_q\hat{A}_{q-1}...\hat{A}_1}_{2}.....\underbrace{\hat{A}_q\hat{A}_{q-1}...\hat{A}_1}_{N} = \hat{Q}^N \tag{3.10}$$

with $Q(k_y)$ defined as the block of q consecutive $\hat{A}_m(k_y)$ matrices:

$$\hat{Q}(k_y) \equiv \hat{A}_{Nq}(k_y)\hat{A}_{Nq-1}(k_y)...\hat{A}_1(k_y). \tag{3.11}$$

The problem can be further simplified by noting that all eigenfunctions must be bounded for all lattice sites m and $Q(k_y)$ must be periodic in m. This constrains the $\hat{Q}(k_y)$ matrix. Both of the eigenvalues of $\hat{Q}(k_y)$ must have unite magnitude which transaltes to the condition of the trace of $\hat{Q}(k_y)$:

$$|Tr\hat{Q}(k_y)| \leq 2. \tag{3.12}$$

In fact we are interested in all these values of E for which we are able to find at least one value of k_y fulfilling the above condition. It can be shown [47] that since k_y enters the expression as a phase the only way it affects $Tr\hat{Q}$ is by creating oscillations around its mean value. We find:

$$Tr\hat{Q}(k_y) = Tr\hat{Q}(k_y = \frac{\pi}{2q}) + 2f(k_y), \tag{3.13}$$

and $f(k_y)$ is an oscillating function with the amplitude 1. Taking this all into account one can write a new condition for physicality:

$$|Tr\hat{Q}(k_y = \frac{\pi}{2q})| \leq 4. \tag{3.14}$$

Solving this equation with respect to E gives the spectrum plotted in Fig. 3.2. At a closer look at the picture, one can see that the pattern of the energy bands has a fractal character. As shown in the inset of figure, parts of it have the same structure as the whole.

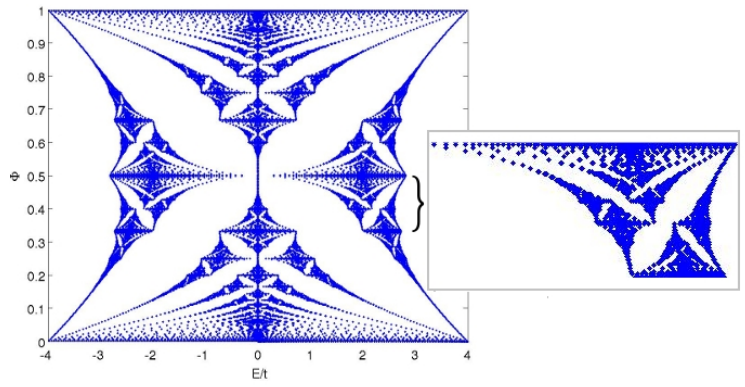

Figure 3.2: The spectrum for a single particle in constant magnetic field in a square lattice known as Hofstadter butterfly after its discoverer. Eigenenergies in the units of t (horizontal axis) are plotted against $\Phi = \frac{p}{q}$ (vertical axis). $\Phi \in [0, 1]$, since the spectrum for $\Phi + N$ equals the spectrum for Φ for any $N \in \mathbb{Z}$.

The trace of $\hat{Q}(k_y)$ is always a polynomial of degree q in E. Since generally it has q roots, the condition (3.14) will be fulfilled for q different regions of E, which means q allowed energy bands. Indeed, if we look at the Fig. 3.2, we can confirm, that for $\Phi = \frac{1}{2}$ we have two bands (they are connected in the middle), for $\Phi = \frac{1}{3}$ we have three, for $\Phi = \frac{1}{5}$ five etc. It may seem suspicious at the first sight that the number of bands is so sensitive to the small changes in the magnetic flux Φ. It can be shown however [45], that if we have two values of magnetic flux $\Phi' = \Phi + \epsilon$, as $\epsilon \longrightarrow 0$ the energies of corresponding bands also converge to same value. A question remains about the irrational values of Φ. The original work by R.D. Hofstadter argues that analogically to the unique and finite decomposition of each rational number $\Phi = \frac{p}{q}$

$$\Phi = \frac{1}{N_1 + \frac{1}{N_2 + \frac{1}{\ddots}}}, \tag{3.15}$$

the energy bands for the rational field fluxes can be decomosed into finite number of subbands. On the contrary, if the flux is irrational, the decomposition never finishes and the spectrum consists

of infinite number of infinitesimally small energy bands that form a Cantor set, whose Lebesgue measure is zero. On the other hand, since irrational numbers are dense (i.e. between any two rational numbers one can find irrational ones) the measure of the spectrum is a discontinuous function for rational numbers and continuous for irrational ones. This paradox leaves the question about physicality of the Hofstadter butterfly open. In the reality however in any experimental setup there exist fluctuations and uncertainty, that blures the spectrum. Thus the peculiar mathematical properties are never to be observed. For more careful analysis of this beautiful spectrum, its symmetries and properties the reader is referred to the original work in the ref. [45] the PhD thesis of the author.

3.2 Spectrum for non-Abelian fields: Hofstadter-Osterloh moth

In chapter 2 it has been shown that cold atoms offer us possibility of creating artificial fields of non-Abelian character. If such field is introduced instead or next to the Abelian field described above, the butterfly-like spectrum is modified. First analysis of such configuration was proposed by K. Osterloh et. al. in 2005 [48] where they studied on specific case of a non-Abelian gauge field. From his study one may draw a conclusion that the structure of butterfly with well developed gaps in the spectrum is destroyed by non-Abelian field. However as will be demonstrated later, this is not always the case.

The gauge field considered in the ref. [48] consists both of the Abelian $\mathbf{A}^A$ and non-Abelian $\mathbf{A}^{NA}$ parts and the same as in the previous example it is constant in the $y(n)$-direction. The atoms moving in the lattice have two internal degree of freedom and their wave functions are represented by two component vector. The two component we denote as $\uparrow, \downarrow$ but they do not have to be spins. In fact in the experimental realisation scheme proposed in the ref.[48] the authors use hiperfine states as internal degree of freedom.

$$\Psi = \begin{pmatrix} \Psi_\uparrow \\ \Psi_\downarrow \end{pmatrix}$$

In result the gauge field is represented by 2×2 matrices with three independent parameters $\alpha_{1,2}, \Phi$:

$$\mathbf{A}(m) = \left(\frac{\pi}{2} \begin{pmatrix} -1 & e^{i\Phi} \\ e^{-i\Phi} & -1 \end{pmatrix}, 2\pi m \begin{pmatrix} \alpha_1 & 0 \\ 0 & \alpha_2 \end{pmatrix}, 0 \right). \quad (3.16)$$

Which yields

$$\begin{aligned} U_x &= \begin{pmatrix} 0 & e^{i\Phi} \\ e^{-i\Phi} & 0 \end{pmatrix} \\ U_y(m) &= \begin{pmatrix} e^{i2\pi m\alpha_1} & 0 \\ 0 & e^{i2\pi m\alpha_2} \end{pmatrix} \end{aligned}$$

The non-Abelian part of the vector potential $\mathbf{A}$ reads

$$\mathbf{A}^{NA} = \tfrac{\pi}{2}(\cos\Phi\sigma_x - \sin\Phi\sigma_y, m\tfrac{\alpha_1-\alpha_2}{2}\sigma_z).$$

It is clear that since the coordinate m enters this expression, the field calculated as (2.17)

$$B_i = \tfrac{1}{2}\epsilon_{ikl}(\partial_k A_l - \partial_l A_k - i[A_k, A_l]) \quad (3.17)$$

will contain a term with the B_i depending on m.

$$B_z = \frac{\alpha_1 + \alpha_2}{2}\mathbb{I} + \frac{\alpha_1 - \alpha_2}{\sigma \quad _z} + m\frac{\alpha_1 - \alpha_2}{(}\cos\Phi\sigma_y - \sin\Phi\sigma_x) \quad (3.18)$$

In the lattice this translates to non-constant Wilson loop. Indeed one can easily check that except some specific cases when $\alpha_1 - \alpha_2 \in \mathbb{Z}$ the Wilson loop of this system will depend on the position and moreover the system will be non-Abelian. For $\Phi = 0$ the Wilson loop $\mathcal{W}$ is equal:

$$\begin{aligned} \mathrm{Tr}\mathcal{W} &= \mathrm{Tr}U_y(m+1)U_x U_y^\dagger(m)U_x^\dagger \\ &= \mathrm{Tr}\begin{pmatrix} e^{i2\pi m(\alpha_1-\alpha_2)} & 0 \\ 0 & e^{-i2\pi m(\alpha_1-\alpha_2)} \end{pmatrix} \\ &= 2\cos(2\pi m(\alpha_1 - \alpha_2)). \end{aligned} \quad (3.19)$$

This fact is important because the systems with constant Wilson loop are qualitatively different than ones for which $\mathcal{W}$ varies in

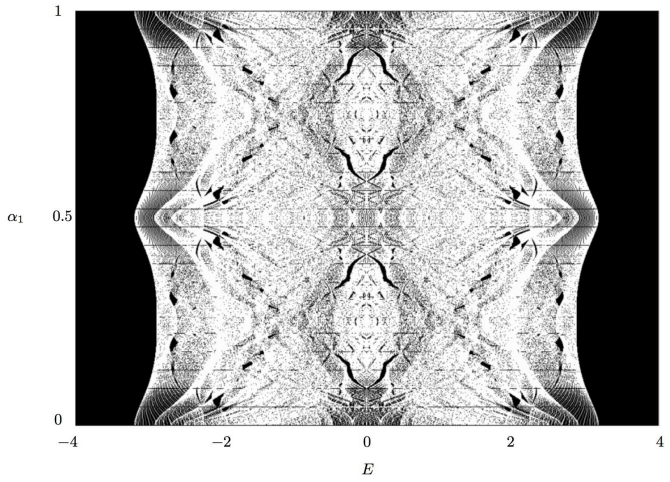

Figure 3.3: Spectrum $E(\alpha_1)$ for $\Phi = 0$, $\alpha_2 = 31/701$. Gaps are shown in black. The Hofstadter butterfly corresponds to $\alpha_1 = \alpha_2(= 31/701)$ *i.e.* the Abelian case, where its larger gaps are put forward through thin black lines

space. In the present case the butterfly-like spectrum is destroyed. As illustrated in the Fig. 3.3. There are no big gaps and the picture looks more like a moth than a butterfly. The figure has been taken from the ref. [49] where the authors also prove that anisotropies in the lattice can destroy the butterfly structure. More details the reader will find in the cited article. As will be evident from the calculations in the chapter 4 this lack of big energy gaps has important consequences, as the quantisation of the Hall conductivity depends on them.

At this point it should be stressed that the Non-Abelian character of the field in the system is not a necessary condition for destroying the big gaps. One can find easily examples of Abelian fields that have the same effect on the spectrum. It is in fact enough to take any field that is not constant in space. If we take for example

$$\mathbf{A} = (0, Bx^2, 0) \tag{3.20}$$

which results in the magnetic field that increases with x, one gets spectrum as shown in Fig. 3.4.

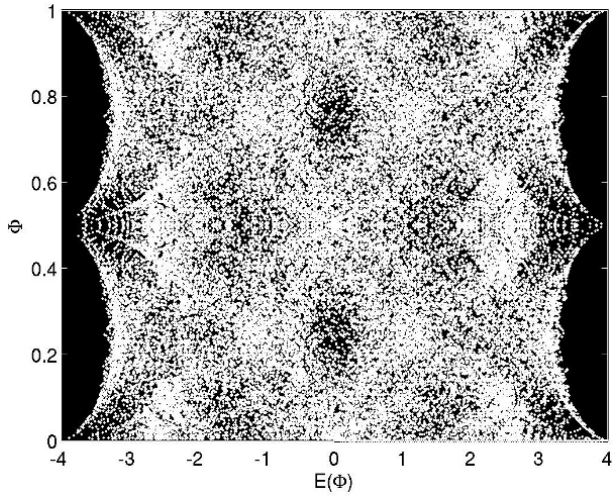

Figure 3.4: Spectrum $E(\phi)$ for an Abelian field, with non-constant Wilson loop for $\mathbf{A} = (0, 2\pi\Phi m^2)$.

3.3 Spectrum for a non-Abelian field: constant Wilson loop

This time we consider a general non-Abelian gauge potential

$$\boldsymbol{A} = \big(\alpha\sigma_y, 2\pi\Phi m + \beta\sigma_x, 0\big), \tag{3.21}$$

where α and β are parameters, $(\sigma_x,\ \sigma_y)$ are Pauli matrices and Φ is the number of (Abelian) magnetic flux quanta per unit cell. This will naturally modify the tunnelling operators U_x, U_y. The tunnelling operators are again represented by 2×2 unitary matrices,

$$\begin{aligned} U_x &= \cos\alpha + i\sigma_y \sin\alpha, \\ U_y(m) &= e^{i2\pi\Phi m}(\cos\beta + i\sigma_x \sin\beta), \end{aligned} \tag{3.22}$$

which act on the two-component wave function $\psi_{m,n}$. The single-particle Hamiltonian is invariant under translations defined by the operators $T_x^q\,\psi_{m,n} = \psi_{m+q,n}$ and $T_y\,\psi_{m,n} = \psi_{m,n+1}$ under the condition that $\Phi = \frac{p}{q}$, where p and q are integers. Consequently, the system is restricted to a $q \times 1$ super-cell and one can express the

wave function as $\psi_{m,n} = e^{ik_x m} e^{ik_y n} u_m$, with u_m a q-periodic function. The wave vector $\boldsymbol{k}$ belongs to the first Brillouin zone, a 2-torus defined as $k_x \in [0, \frac{2\pi}{q}]$ and $k_y \in [0, 2\pi]$. The Schrödinger equation (3.1) then reduces to a generalised Harper equation

$$E\, u_m = \begin{pmatrix} \cos\alpha & \sin\alpha \\ -\sin\alpha & \cos\alpha \end{pmatrix} u_{m+1} e^{ik_x} + \begin{pmatrix} \cos\alpha & -\sin\alpha \\ \sin\alpha & \cos\alpha \end{pmatrix} u_{m-1} e^{-ik_x}$$

$$+ 2 \begin{pmatrix} \cos(2\pi\Phi m + k_y)\cos\beta & -\sin(2\pi\Phi m + k_y)\sin\beta \\ -\sin(2\pi\Phi m + k_y)\sin\beta & \cos(2\pi\Phi m + k_y)\cos\beta \end{pmatrix} u_m. \tag{3.23}$$

Wilson loop

In the presence of the gauge potential Eq. (3.21), atoms performing a loop around a plaquette undergo the unitary transformation:

$$\mathcal{W} = e^{i2\pi\Phi} \left(\begin{array}{c:c} \cos^2\alpha + \cos(2\beta)\sin^2\alpha & \sin(2\alpha)\sin^2\beta \\ +\frac{i}{2}\sin(2\alpha)\sin 2\beta & -i\sin^2\alpha\sin(2\beta) \\ \hdashline \\ -\sin(2\alpha)\sin^2\beta & \cos^2\alpha + \cos(2\beta)\sin^2\alpha \\ -i\sin^2\alpha\sin(2\beta) & -\frac{i}{2}\sin 2\alpha\sin(2\beta) \end{array} \right). \tag{3.24}$$

If one sets $\alpha = d\pi$ or $\beta = d\pi$, where d is an integer, the Wilson operator matrix $\mathcal{W} = \exp(i2\pi\Phi)$ is proportional to the identity (constant and with trace equal 2) and the system behaves similarly to the Hofstadter model [45]. When $\alpha = \beta = (2d+1)\pi/2$, where $d \in \mathbb{Z}$, one finds that $\mathcal{W} = -\exp(i2\pi\Phi)$ and the system is equivalent to the π-flux model in which half a flux quantum is added in each plaquette [50]. In these particular cases where $\mathcal{W} = \pm\, e^{i2\pi\Phi}$, the system is in the Abelian regime. For any other values of the parameters α and β, the matrix $\mathcal{W}$ is a non-trivial $U(2)$ matrix and the system is non-Abelian.
The Wilson loop characterising the system is given by:

$$\begin{aligned} \mathrm{Tr}\mathcal{W} &= \mathrm{Tr}\, U_x U_y(m+1) U_x^\dagger U_y^\dagger(m) \\ &= 2\, e^{i2\pi\Phi} \left(\cos^2\alpha + \cos 2\beta \sin^2\alpha\right) \end{aligned} \tag{3.25}$$

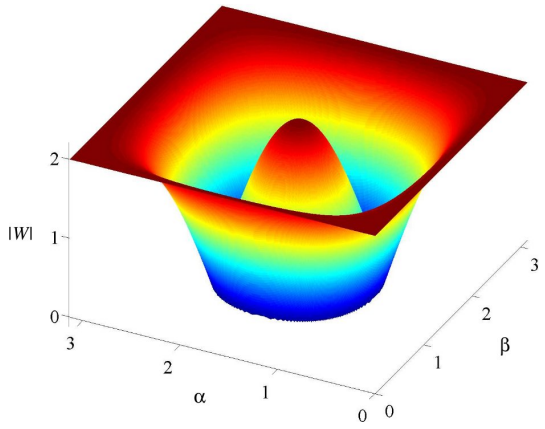

Figure 3.5: Wilson loop's magnitude $|\mathcal{W}|$ as a function of the parameters α, β. The system is equivalent to the Abelian Hofstadter model along the lines $\alpha = d\pi$ or $\beta = d\pi$, where $d \in \mathbb{Z}$ and is equivalent to the Abelian π-flux model at singular points, $\alpha = \beta = (2d+1)\pi/2$. For any other values of the parameters α and β, the system is non-Abelian.

It is straightforward to verify that the system is non-Abelian when $|W| \neq 2$ (It is then not proportional to unity matrix), and that $\mathcal{W}(\alpha, \beta) = \mathcal{W}(\beta, \alpha)$. In Fig. 3.5, we show the Wilson loop's magnitude $|\mathcal{W}|$ as a function of the parameters, $|\mathcal{W}| = |\mathcal{W}(\alpha, \beta)|$, we can easily identify the regions corresponding to the Abelian ($|\mathcal{W}| = 2$) and to the non-Abelian regimes ($|\mathcal{W}| \neq 2$). We note that the Abelian π-flux regime is reached at a singular point, $\alpha = \beta = (2d+1)\pi/2$, where $d \in \mathbb{Z}$.

We also point out that the statement according to which the non-Abelian regime is reached when $[U_x, U_y] \neq 0$, and which can be found in the literature [48, 52], is incorrect: for the situation where $\alpha = \beta = (2d+1)\pi/2$, one finds that $[U_x, U_y] = 2i\, e^{2im\pi\Phi}\sigma_z$, while the system is Abelian because of its trivial Wilson loop, $|\mathcal{W}| = |-2e^{2i\pi\Phi}| = 2$. On the contrary to the non-Abelian systems considered in previous works [48, 51, 52], we emphasise that the gauge potential Eq. (3.21) leads to a Wilson loop which does not depend on the spatial coordinates.

Energy spectrum

The energy spectrum can be obtained through direct diagonalisation of Eq. (3.23). In the Abelian regime corresponding to $\alpha = d\pi$ or $\beta = d\pi$, where $d \in \mathbb{Z}$, one finds q doubly-degenerated bands for $\Phi = \frac{p}{q}$. In this particular case, the representation of the spectrum as a function of the flux Φ leads to the fractal Hofstadter "butterfly" (Fig. 3.7a). For the other Abelian case $\alpha = \beta = \frac{\pi}{2}$, the system behaves according to the π-flux lattice: the spectrum $E = E(\Phi)$ depicts a Hofstadter "butterfly" which is contained between $\Phi = [0.5; 1.5]$, i. e. shifted by $\Phi = 0.5$ with respect to the original "butterfly" (Fig. 3.7f).

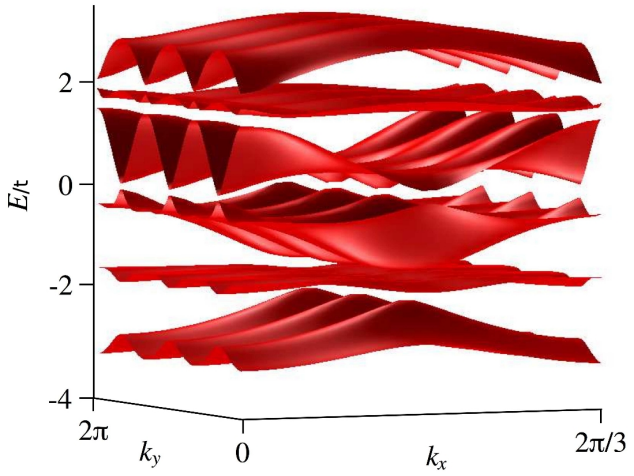

Figure 3.6: Spectrum $E = E(k_x, k_y)$ for $\alpha = \beta = 1$ and $\Phi = \frac{1}{3}$.

In the non-Abelian regime, which is reached for arbitrary values of the parameters (α, β), the spectrum is constituted of $2q$ separated bands as illustrated in Fig. 3.6. For these general situations, the representation of the spectrum as a function of the flux Φ leads to new interesting features. As in the Abelian case, one observes repetitions of similar structures at various scales. However, new patterns arise in the non-Abelian case, as illustrated in Fig. 3.7. There spectra with different values of α, β are compared. It is worth noticing that for arbitrary values of the parameters (α, β),

the spectra show well-developed gaps contrasting with the Hofstadter "moth" which appears in the non-Abelian system proposed in Ref. [48]. We further notice that the spectrum is periodic in Φ with period $T_\Phi = 1$ and is symmetric with respect to $E = 0$ and $\Phi = 0.5$.

Conclusions

Summarising, in this chapter we have proposed how to realize in cold atomic systems a textbook example of non-Abelian gauge potential characterised by a *constant* Wilson loop. Our main result is that despite the coupling between the different "flavour" components of the single-particle wave functions, the spectrum exhibits well-developed gaps of order of 0.1-1t. It is in contrast to before predicted behaviour of non-Abelian system.

	Constant $\mathcal{W}$	space dependent $\mathcal{W}$
Abelian $\mathbf{A}$	Butterfly	Moth
Non-Abelian $\mathbf{A}$	Modified Butterfly	Moth

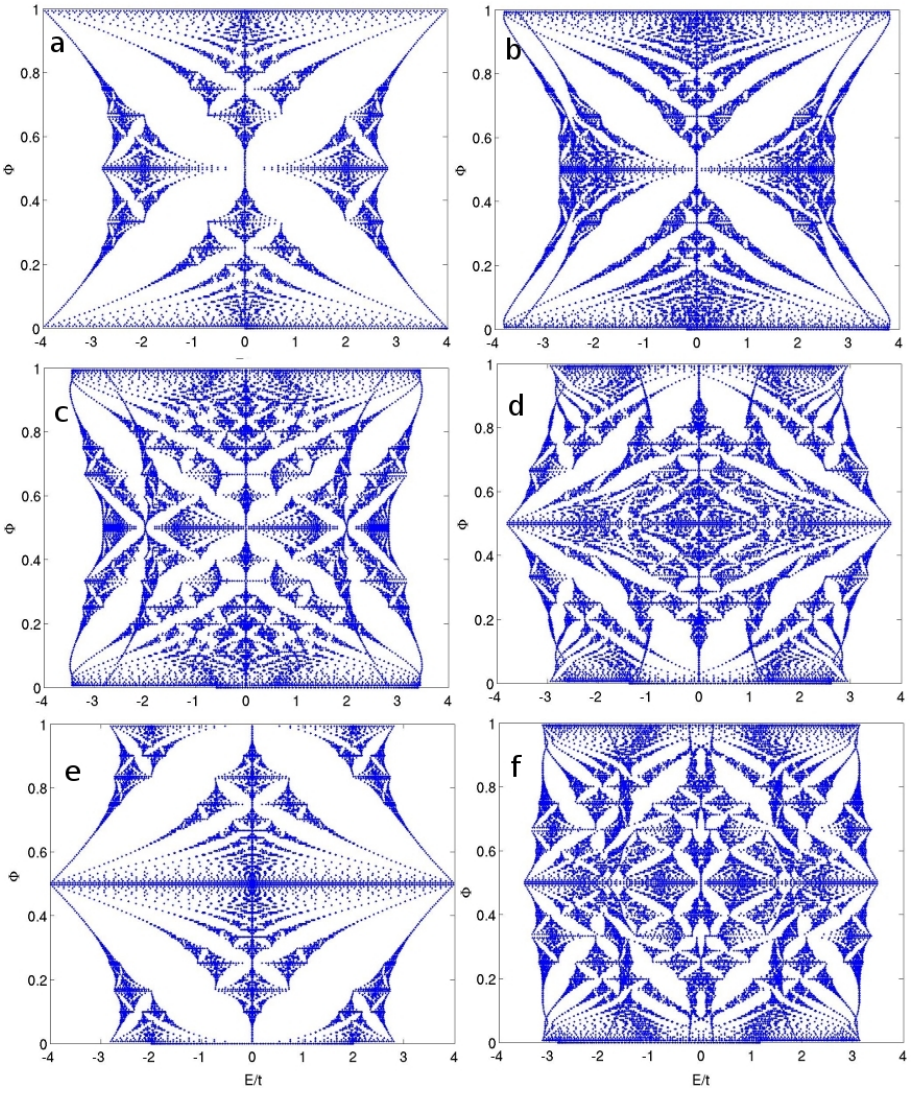

Figure 3.7: Spectra for (α, β) equals a) $(0, 0)$, b) $(\pi/7, \pi/7)$, c)$(\pi/4, \pi/4)$, d)$(\pi/3, \pi/3)$, e) $(\pi/2, \pi/2)$, f) $(1, 2)$

Chapter 4

Integer quantum Hall effect

4.1 Introduction to Hall effects

The classical Hall effect was first discovered in 1879 by Edwin Hall, after whom it is now named. His experimental setup was a planar conductor inserted in a homogenous magnetic field $\mathbf{B}$ perpendicular to the conductor surface, see Fig. 4.1 He observed that a current in the conductor is accompanied by a traverse (Hall) voltage. The Hall voltage is a result of the equilibrium between the Lorentz and the electrostatical forces in the transverse direction: $\mathbf{F} = q\left(\mathbf{E} + \frac{\mathbf{v}}{c} \times \mathbf{B}\right)$ acting of the particles of charge q moving with the velocity $\mathbf{v}$. The electric field E_y is a result of the charge accumulating on the boundaries of the system. The resistivity and conductivity of a conductor are then rather tensors than numbers. For $\mathbf{j} \equiv q\mathbf{v}n$ being the current density vector for the particles of the density n, they are defined by:

$$\mathbf{j} \equiv \hat{\sigma}\mathbf{E}, \tag{4.1}$$

$$\hat{\rho} \equiv \hat{\sigma}^{-1}. \tag{4.2}$$

These formulas are general and hold for any system, also three-dimensional. In two dimensions, in the context of Hall effect, eq. (4.2) gives:

$$\hat{\rho} = \frac{1}{\sigma_{xx}^2 + \sigma_{yy}^2} \begin{pmatrix} \sigma_{yy} & -\sigma_{yx} \\ -\sigma_{xy} & \sigma_{xx} \end{pmatrix}. \tag{4.3}$$

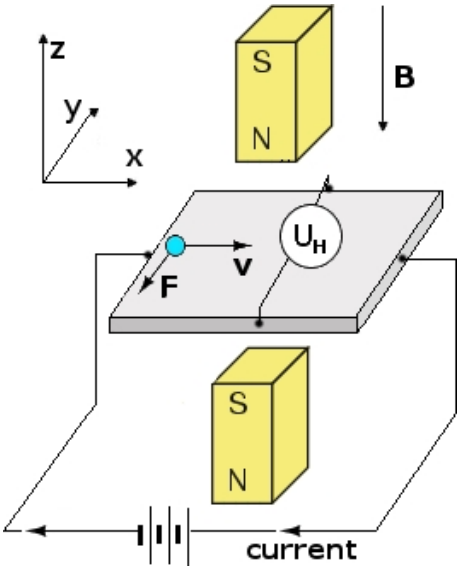

Figure 4.1: The sketch of the experimental realisation of the classical Hall effect

The Hall conductivity and resistivity refer then to the off-diagonal elements of the corresponding tensors: $\sigma_H \equiv \sigma_{xy}$, $\rho_H \equiv \rho_{xy}$. Following the classical picture $\hat{\sigma}_H$ is inversely proportional to the magnetic field amplitude B and proportional to the particles density n and charge q.

$$\sigma_H = \frac{qnc}{B} \tag{4.4}$$

This is true for small magnetic fields. For higher values of B, and for low temperatures, the quantum effects start playing important role and this picture fails. Both conductivity and resistivity develop series of plateaus in their dependence on the magnetic field, instead of a inversely-linear and linear dependences. The quantum of Hall conductivity equals $\frac{q^2}{h}$, and in each plateau the Hall conductivity is given by an integer number of those quanta. This proportionality

coefficient N is a function of the magnetic field strength:

$$\sigma_H = N(B)\frac{q^2}{h} \tag{4.5}$$

$$\rho_H = \sigma_H^{-1} \tag{4.6}$$

$$\rho_{xx,yy} \longrightarrow 0 \tag{4.7}$$

The quantisation of the Hall resistivity and conductivity was first discovered by Klaus von Klitzing in 1980, who received Nobel prize for his discovery five years later. His experimental result demonstrating the plateaus was later confirmed by others and a typical experimental result is presented in Fig. 4.2. Later it has been shown that in very cold and pure samples, one can observe also fractional plateaus. The nature of the fractional quantisation of Hall conductivity is much different than one of the integer quantisation. To distinguish the two effects, the first one is called the Integer quantum Hall effect (IQHE) and the latter, that will be discussed later, the Fractional quantum Hall effect (FQHE).
From the formulas above one can see that the values depend only on the universal constants, and not on any particular experimental setup. Because of this the quantised values of the resistivity are universal. They can be measured with high accuracy and for this reason IQHE is used to set a standard unit of resistivity - the klizing. This is a beautiful example of quantum effects that are exhibited in macroscopic properties of the system.

4.2 The theory of integer quantum Hall effect

The integer quantum Hall effect is a single particle phenomenon. It can be understood following the formalism proposed by L.D. Landau already in 1930. He solved the quantum mechanical problem of energy states of a charged particle in a uniform magnetic field. As already mentioned in the chapter 2 the energy levels of its Hamiltonian coincide with the ones for a particle in harmonic trap. In the symmetric gauge: $A = \frac{B}{2}(-y, x, 0)$ the Hamiltonian describing

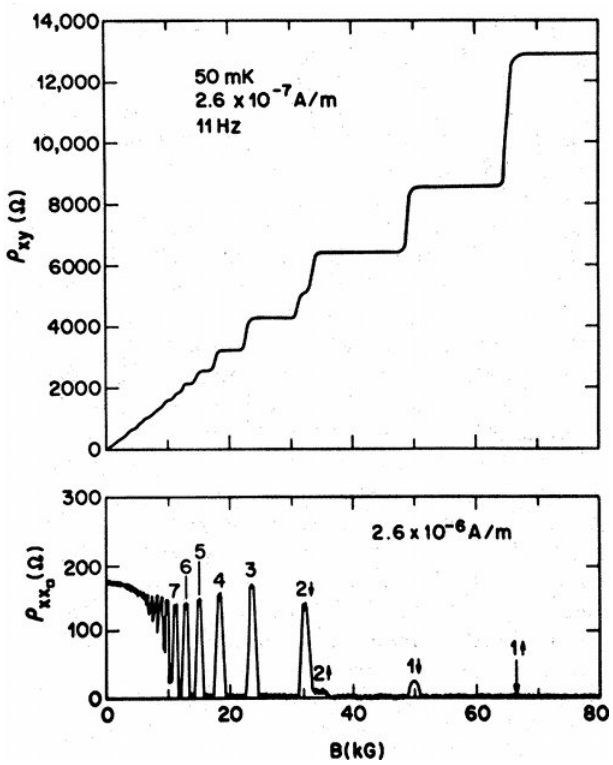

Figure 4.2: The plot taken from [53]. The Hall resistivity (top) and the diagonal resistivity (bottom) plotted against the perpendicular magnetic field amplitude.

the system reads

$$H = \frac{1}{2m}\left[\left(p_x - \frac{eB}{2c}y\right)^2 + \left(p_y + \frac{eB}{2c}x\right)^2\right], \tag{4.8}$$

and the energy states, called Landau levels are labelled by one quantum number n:

$$E_n = \hbar\omega_c\left(n + \frac{1}{2}\right) \tag{4.9}$$

where $\omega_c = \frac{eB}{cm}$ is the cyclotron frequency of the harmonic oscillator. Each of the Landau levels is multiply degenerate. The number of independent orbits in each of them is given by the number of the magnetic flux quanta penetrating the surface of the system. This fact can be demonstrated as follows: The wave function of the ground state, the lowest Landau level $|LLL\rangle$ can be written with the use of the complex variable $z \equiv x + iy \equiv re^{i\phi}$ in the form:

$$\Psi_{n=0,m}(z) \propto z^m e^{-\frac{1}{4l^2}|z|^2} \tag{4.10}$$

where $l^2 = \frac{\hbar c}{eB}$ is the magnetic length and $m \in \mathbb{N}$ is the quantum number labelling the states inside the degenerate subspace. In fact this is nothing else than the angular momentum of the state. One find the spatial size of the states by looking at the place where the wave function's amplitude a has maximum. The location where it is peaked depends on the angular momentum quantum number and equals $r^2 = 2l^2m$. It is then clear that the finite size of the system imposes also limitation on the maximum $r = r_{max}$ and $m = m_{max}$. If R is the size of the system, one has

$$\begin{aligned} R^2 \geq r_{max} &= 2l^2 m_{max} \\ &\text{and} \\ m_{max} &= \left\lfloor \frac{R^2}{2l^2} \right\rfloor = \left\lfloor \frac{R^2 eB}{2\hbar c} \right\rfloor. \end{aligned}$$

Defying the magnetic flux quantum $\phi_0 \equiv \frac{\hbar c 2\pi}{e}$ and noting that the total magnetic flux through the system of radius R equals $\phi_B = \pi R^2 B$ one finds finally:

$$m_{max} = \left\lfloor \frac{\pi R^2 B}{\phi_0} \right\rfloor = \left\lfloor \frac{\phi_B}{\phi_0} \right\rfloor = \#\text{flux quanta}. \tag{4.11}$$

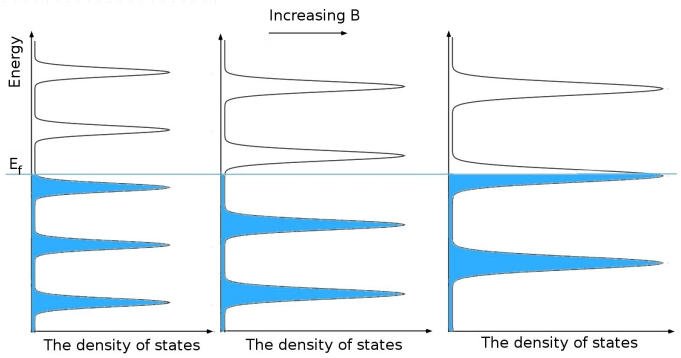

Figure 4.3: The scheme of filled (blue) and empty (white) Landau levels with increasing magnetic field strength. The higher the field, the more degenerate levels and bigger the distances between them.

It is also easy to see that increasing the magnetic field amplitude B, decreases l^2 which results in decrease of the spacings between each maximum as well as an increase of the Landau levels spacing ω_c. This means that the higher the B is, the bigger the spacing of the Landau levels is and the more degenerate they are. This mechanism is summarised in Fig. 4.3 In the figure the levels are not perfectly degenerate - the density of states is broadened by impurities in the system. In the centre of each Landau level there are delocalised states, that are responsible for the conductivity. Moreover, only the levels that are occupied, i.e. that are below the Fermi energy E_f contribute to the conductivity. As E_f increases, or equivalently B decreases, the number of contributing Landau levels increases and in the result the σ as well. It is now clear that for low temperatures, when the Landau Levels are filled one by one, the change is not linear. Each time the Fermi energy crosses centre of a Landau level, the conductivity jumps. The more impurities or thermal fluctuations in the system, the more the plateaus are washed out and the quantisation of the Hall effect is less visible.
This simple picture can explain the main physics of the integer quantum Hall effect. Its perfect and universal quantisation attracted much attention and soon after the first observation, more elegant and sophisticated theories were developed in order to ex-

plain this phenomenon. Starting with the linear response theory, R. Kubo derived a formula for the conductivity tensor expressed with the autocorrelation function of currents. Later for periodic systems, with a discrete Brillouin zone D. J. Thouless et. al. have proven that this can be rewritten in terms of the partial derivatives of the eigenfunctions of the Hamiltonian and, that the topological properties of the expression assure that it is always an integer [60]. They have found a simple formula for the quantisation of the Hall conductivity, where the conductivity is a sum of integer numbers computed separately for each contributing energy band i.e. bands below the Fermi energy level.

$$\sigma_H = \frac{e^2}{h} \sum_{E_\lambda \leq E_f} C_\lambda. \tag{4.12}$$

C_λ is, the so called, Chern number of λ-th Bloch band (sometimes called after the authors of the theory TKNN numbers). Chern numbers are topological invariants and are necessarily integers. For the classical system, with an Abelian magnetic field and for which the Bloch bands do not cross, they are defined as:

$$C_\lambda = \frac{1}{2\pi i} \int_{\mathbb{T}^2} d^2k \mathcal{F}_\lambda(\mathbf{k}), \tag{4.13}$$

where the integral runs over the whole Brillouin zone, here

$$\mathcal{F}_\lambda(\mathbf{k}) = \frac{\partial}{\partial k_x}\mathcal{A}_y(\mathbf{k}) - \frac{\partial}{\partial k_y}\mathcal{A}_x(\mathbf{k}) \tag{4.14}$$

is the so called Berry's curvature and

$$\mathcal{A}^\mu_\lambda(\mathbf{k}) = \langle u_\lambda | \frac{\partial}{\partial k_\mu} | u_\lambda \rangle. \tag{4.15}$$

where $\mu = x, y$ is so called Berry's connection. $|u_\lambda\rangle$ are normalised wave functions of the λ-th Bloch band so that $H(\mathbf{k})|u_\lambda\rangle = E_\lambda(\mathbf{k})|u_\lambda\rangle$. As a consequence, the transverse Hall conductivity of the system evolves by steps corresponding to integer multiples of the inverse of Planck's constant, and is robust against small perturbations. In various works [62, 63, 54] it has been proven that

topology and the gauge invariance theory are the natural contexts in which the physics of quantum Hall effect should be considered. The reader will find a detailed derivation of the above formulas starting with the linear response theory in the literature, for example in [65].

4.3 Integer quantum Hall effect for non-Abelian fields

Following the method of Ref. [52], one can generalise the formulas (4.13 - 4.15) [54] to the case where the gauge field is non-Abelian. In the general case the gauge field can be represented by $N \times N$ matrices acting on wave functions with N dimensional internal degree of freedom:

$$|u_\lambda\rangle = \begin{pmatrix} u_{\lambda 0} \\ u_{\lambda 1} \\ ... \\ u_{\lambda N} \end{pmatrix}. \tag{4.16}$$

The Berry's connection (4.15) become a matrix:

$$(\mathcal{A}^\mu_\lambda)_{ij} = \langle u_{\lambda i} | \partial_{k_\mu} u_{\lambda j} \rangle \qquad i,j = 1,2,..N, \tag{4.17}$$

and the curvature (4.14):

$$\mathcal{F}_\lambda = \left(\partial_{k_x}\mathcal{A}^y_\lambda - \partial_{k_y}\mathcal{A}^x_\lambda + [\mathcal{A}^x_\lambda, \mathcal{A}^y_\lambda]\right), \tag{4.18}$$

and in general case $[\mathcal{A}^x_\lambda, \mathcal{A}^y_\lambda] \neq 0$. Similarly to the Abelian case, the Hall-like conductivity is given by a sum of integer Chern numbers (4.12), but this time the Chern numbers are given by:

$$C_\lambda = \frac{1}{2i\pi}\int_{\mathbb{T}^2} \mathrm{tr}\mathcal{F}_\lambda. \tag{4.19}$$

The final expression for the Hall conductivity reads:

$$\sigma_{xy} = \frac{e^2}{2\pi i h} \sum_{E_\lambda < E_\mathrm{F}} \int_{\mathbb{T}^2} \sum_j \Big(\langle \partial_{k_x} u_{\lambda j} | \partial_{k_y} u_{\lambda j} \rangle - \langle \partial_{k_y} u_{\lambda j} | \partial_{k_x} u_{\lambda j} \rangle + \sum_i (\langle u_{\lambda j} | \partial_{k_x} u_{\lambda i} \rangle \langle u_{\lambda i} | \partial_{k_x} u_{\lambda j} \rangle - \langle u_{\lambda j} | \partial_{k_y} u_{\lambda i} \rangle \langle u_{\lambda i} | \partial_{k_y} u_{\lambda j} \rangle) \Big) d\boldsymbol{k}, \tag{4.20}$$

where $|u_{\lambda j}\rangle$ is the jth component of the wave function corresponding to the band E_λ such that $H(\mathbf{k})|u_{\lambda j}\rangle = E_{\lambda j}(\mathbf{k})|u_\lambda\rangle$, and $\mathbb{T}^2$ refers to the first Brillouin zone of the system. The Fermi energy E_F is supposed to lie within a gap of the spectrum. The transverse conductivity is then given by the contribution of all the states filling the bands $E_\lambda < E_\mathrm{F}$ situated below this gap.

The evaluation of this topological invariant leads to a complete understanding of the IQHE. The aim is then to compute the Chern number associated to each band E_λ of the spectrum. This can be achieved numerically thanks to an efficient method developed by Fukui et al. [56], which can be applied to our specific system. This method is summarised as follows: the Brillouin zone $\mathbb{T}^2$, defined by $k_x \in [0, \frac{2\pi}{q}]$ and $k_y \in [0, 2\pi]$, is discretised into a lattice constituted by points denoted $\boldsymbol{k}_l = (k_{xl}, k_{yl})$. On the square two-dimensional lattice one defines a curvature $\mathcal{F}_\lambda$ expressed as

$$\mathcal{F}_\lambda(\boldsymbol{k}_l) = \ln U_x(\boldsymbol{k}_l) U_y(\boldsymbol{k}_l + \hat{\boldsymbol{x}}) U_x(\boldsymbol{k}_l + \hat{\boldsymbol{y}})^{-1} U_y(\boldsymbol{k}_l)^{-1}, \tag{4.21}$$

where the principal branch of the logarithm with $-\pi < \mathcal{F}_\lambda / i \leq \pi$ is taken, $\hat{\boldsymbol{\mu}}$ is a unit vector in the direction μ, and

$$U_\mu(\boldsymbol{k}_l) = \sum_j \langle u_{\lambda j}(\boldsymbol{k}_l) | u_{\lambda j}(\boldsymbol{k}_l + \hat{\boldsymbol{\mu}}) \rangle / \mathcal{N}_\mu(\boldsymbol{k}_l), \tag{4.22}$$

defines a link variable with a normalisation factor $\mathcal{N}_\mu(\boldsymbol{k}_l)$ such that $|U_\mu(\boldsymbol{k}_l)| = 1$. The Chern number associated to the band E_λ is then defined by

$$C_\lambda = \frac{1}{2\pi i} \sum_l \mathcal{F}_\lambda(\boldsymbol{k}_l). \tag{4.23}$$

This method ensures the integral character of the Chern numbers and holds for non-overlapping bands. In the situations where the spectrum reveals band crossings, a more general definition of the link variables $U_\mu(\boldsymbol{k}_l)$ has been proposed in Ref. [56].

The IQHE can be simulated with ultracold atoms and in this context the transverse Hall conductivity measures the response of the system to a static force, e.g. a lattice acceleration. It takes on quantised values $\sigma_{xy} = \frac{e^2\nu}{h}$ with $\nu \in \mathbb{Z}$, when the Fermi energy E_F lies in a gap [79]. Surprisingly, the quantized conductivity of cold gases can be directly observed through density measurements thanks to the Streda formula [81]. Here we show that non-Abelian effects have dramatic consequences on the IQHE which occurs when an additional Abelian flux Φ_0 is applied. The system under consideration is the same as in chapter 3. The fermionic gas in 2D lattice is subject to the gauge field given by the vector potential (3.21):

$$\boldsymbol{A} = \big(\alpha\sigma_y, 2\pi\Phi m + \beta\sigma_x, 0\big), \tag{4.24}$$

and the Hamiltonian (3.23):

$$\begin{aligned} E\,u_m = &\begin{pmatrix} \cos\alpha & \sin\alpha \\ -\sin\alpha & \cos\alpha \end{pmatrix} u_{m+1}e^{ik_x} + \begin{pmatrix} \cos\alpha & -\sin\alpha \\ \sin\alpha & \cos\alpha \end{pmatrix} u_{m-1}e^{-ik_x} \\ &+ 2\begin{pmatrix} \cos(2\pi\Phi m + k_y)\cos\beta & -\sin(2\pi\Phi m + k_y)\sin\beta \\ -\sin(2\pi\Phi m + k_y)\sin\beta & \cos(2\pi\Phi m + k_y)\cos\beta \end{pmatrix} u_m. \end{aligned} \tag{4.25}$$

We first compute the Chern numbers for a specific case, illustrated in Fig. 3.6 and 4.4. For $\alpha = \beta = 1$ and $\Phi_0 = \frac{1}{3}$, the Chern numbers associated to the six bands are respectively $1; -5; 6; 2; -5; 1$. According to Eq. (4.12), the transverse conductivity's values associated to the 5 gaps are $1; -4; 2; 4; -1$. There are 5 opened gaps since all of the bands are well separated. If we consider another system, with different parameters some of the gaps close and for those bands that touch one has to compute corresponding Chern numbers treating the bands together. An example is shown in the Fig. 4.5. There $\Phi_0 = \frac{1}{5}$ and $\alpha = 1, \beta = 2$. Looking at the Fig. 4.6(a) one can see that indeed there are only 6 steps in the Hall conductivity. The steps are of different width, which

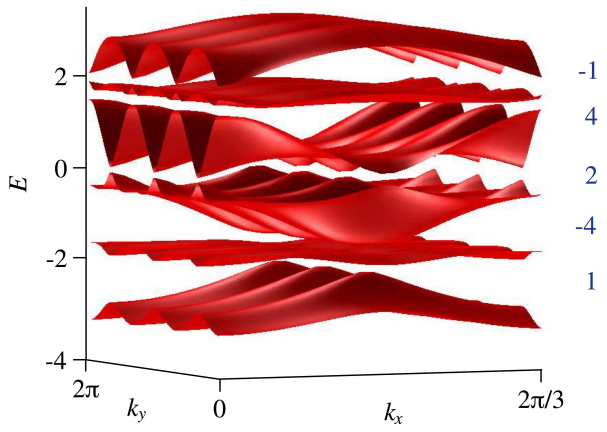

Figure 4.4: The same figure as 3.6 but with computed Chern numbers for each gap.

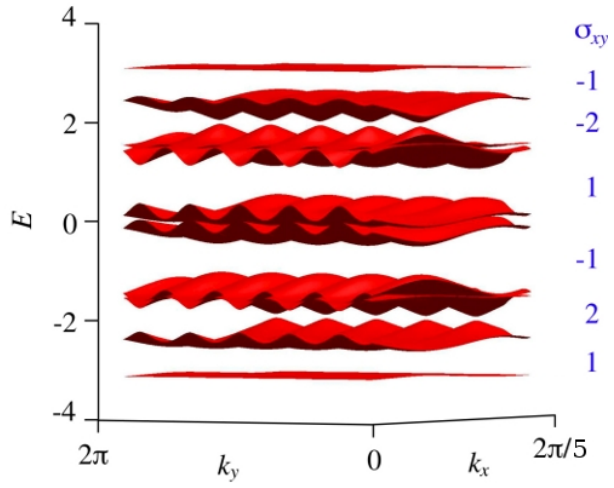

Figure 4.5: The energy bands for $\Phi_0 = \frac{1}{5}$ and $\alpha = 1, \beta = 2$. The Chern numbers are $1; 1; -3; 2; -3; 1; 1$ and the transverse conductivity respectively $1; 2; -1; 1; -2; -1$

reflects the differences in the gaps sizes. The empty spaces between the steps are due to finite widths of the energy bands, where the Hall conductivity is not defined. For other values of Φ_0 with big denominators, one gets more plateaus which is illustrated in Fig. 4.6(b).

The phase diagram describing the IQHE for our model can eventually be drawn. In this diagram we represent the quantised transverse conductivity as a function of the Fermi energy E_{F} and flux Φ_0. Here we illustrate a representative example of such a phase diagram which was obtained for $\alpha = 1$, $\beta = 2$ (cf. Fig. 4.8). This striking figure differs radically from the phase diagrams obtained by Osadchy and Avron in the Abelian case [64]. The figures 4.7 and 4.8 compare the Abelian and non-Abelian cases. Because the Hall plateaus result from constant conductance when the Fermi energy is between the bands, the new pattern of the gaps must modify the quantum Hall effect. Consequently, the measurement of the transverse conductivity in this system should show a specific sequence of robust plateaus, heralding a new type of quantum Hall effect.

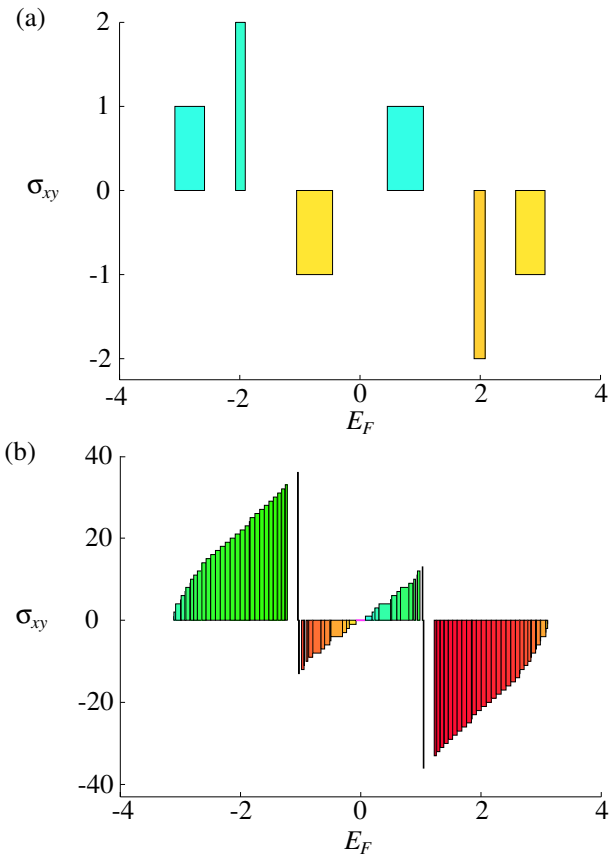

Figure 4.6: Sections through the phase diagram illustrated in Fig. 4.8: $\sigma_{xy} = \sigma_{xy}(E_F)$, at $\Phi = 0.2$ (a) and $\Phi = 0.02$ (b). To each plateau $\sigma_{xy} =$ constant, is associated a coloured rectangle based on the line $\sigma_{xy} = 0$. The colour code and the parameters ($\alpha = 1$, $\beta = 2$) are the same as in Fig. 4.8. When $\Phi = 0.2$ (a), one observes the sequence already represented in Fig. 4.5: the transverse conductivity associated to the six gaps is respectively $\{1; 2; -1; 1; -2; -1\}$. When $\Phi = 0.02$ (b), the quantized conductivity evolves monotonically but suddenly changes sign around the van Hove singularities located at $E \simeq \pm 1$. The Fermi energy is expressed in units of the hopping parameter t and the transverse conductivity is expressed in units of $1/h$.

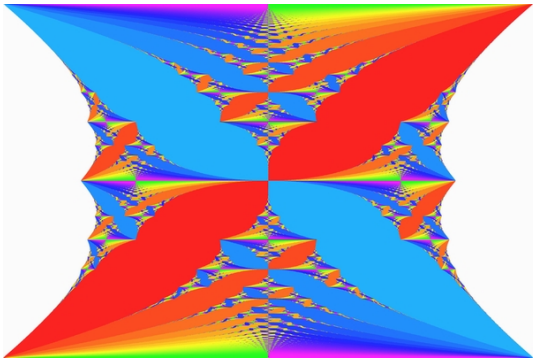

Figure 4.7: The Hofstadter butterfly as a phase diagram for the Abelian case. The figure has been taken from the original paper [64]. Spectrum $E = E(\Phi_0)$ and phase diagram for $\alpha = 0, \beta = 0$ and $\Phi_0 = \frac{p}{q}$ with $p < q < 100$. Warm (resp. cold) colours correspond to positive (resp. negative) values of the quantized conductivity.

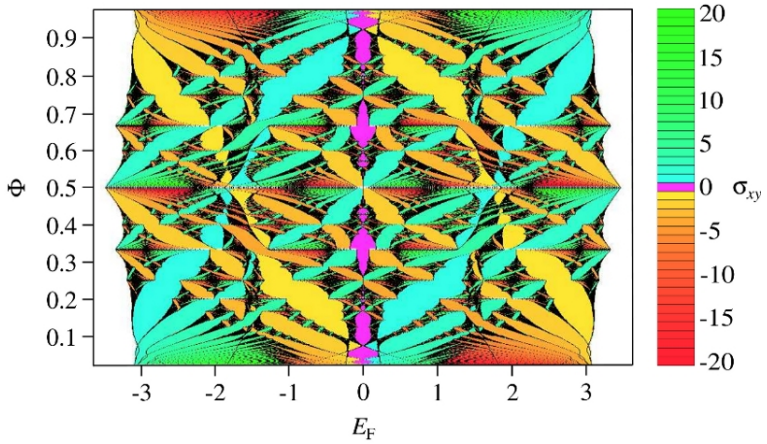

Figure 4.8: Spectrum $E = E(\Phi_0)$ and phase diagram for $\alpha = 1, \beta = 2$ and $\Phi_0 = \frac{p}{q}$ with $p < q < 97$. Warm (resp. cold) colours correspond to positive (resp. negative) values of the quantized conductivity. Purple corresponds to a null transverse conductivity. For $\Phi_0 \ll 1$, the quantized conductivity evolves monotonically but suddenly changes sign around $E \simeq \pm 1$ (see the alternation of cold and warm colours).

Remarkably, the sequence of Hall plateaus is extremely sensitive to the values of the non-Abelian fluxes. The comparison of the IQHE for four cases of different values of α, β are presented in Fig. 4.9. In the Abelian regime $\alpha = \beta = 0$, we observe that the Hall conductivity follows the usual integer QHE $\sigma_{xy} = \frac{2\nu}{h}$, where the factor 2 is due to colour-degeneracy, see Fig. 4.9(a). Conversely, in the π-flux regime ($\alpha = \beta = \pi/2$) illustrated in Fig.4.9(c), we obtain a completely different sequence of Hall plateaus where $\sigma_{xy} = \frac{4}{h}(\nu + \frac{1}{2})$ around $E_{\rm F} = 0$. This sequence is characterised by sudden changes of sign across the point situated at $E = \pm 2$, and by unusual double steps which can be tracked back to underlying low-energy relativistic excitations as will be shown in the chapter 5.

The points where the Hall conductivity has sudden jumps are the same places where the density of energy states diverges. Those special points are called van Hove singularities (VHS). The DOS for our system for the same parameters α, β as in the Fig. 4.9 is illustrated in Fig. 4.10. As one can see, for $\alpha = \beta = \frac{\pi}{2}$ (case (c)) there are two VHS near $E = \pm 2$ which coincide with the points of jumps in σ_{xy} in Fig. 4.9 (c). As the gauge fluxes vary in the vicinity of the π-flux point ($\alpha = \pi/2 + \epsilon$ and $\beta = \pi/2 - \epsilon$), in the DOS one observes a striking behaviour: the two VHS originally situated at $E = \pm 2$ are split into four

$$E_{\rm red}^{\rm VHS} = \pm 2(1 + \cos\beta), \;\; E_{\rm green}^{\rm VHS} = \pm 2(1 + \cos\alpha). \tag{4.26}$$

The system enters the non-Abelian regime and the Hall plateaus are modified (see Fig.4.9(d) for $\epsilon = 0.1$). Indeed most of the degeneracies are lifted and the anomalous double steps around $E_{\rm F} = 0$ are progressively destroyed. Surprisingly enough, anomalous double steps in the plateau sequence reappear at higher energies outside the two points marked with red arrows in the Fig. 4.9(d). It is interesting to note that the anomalous behaviour persists in the high-energy regime. The temperature required to observe these plateaus should be smaller than the spectral gaps, namely $T \sim 10$ nK.

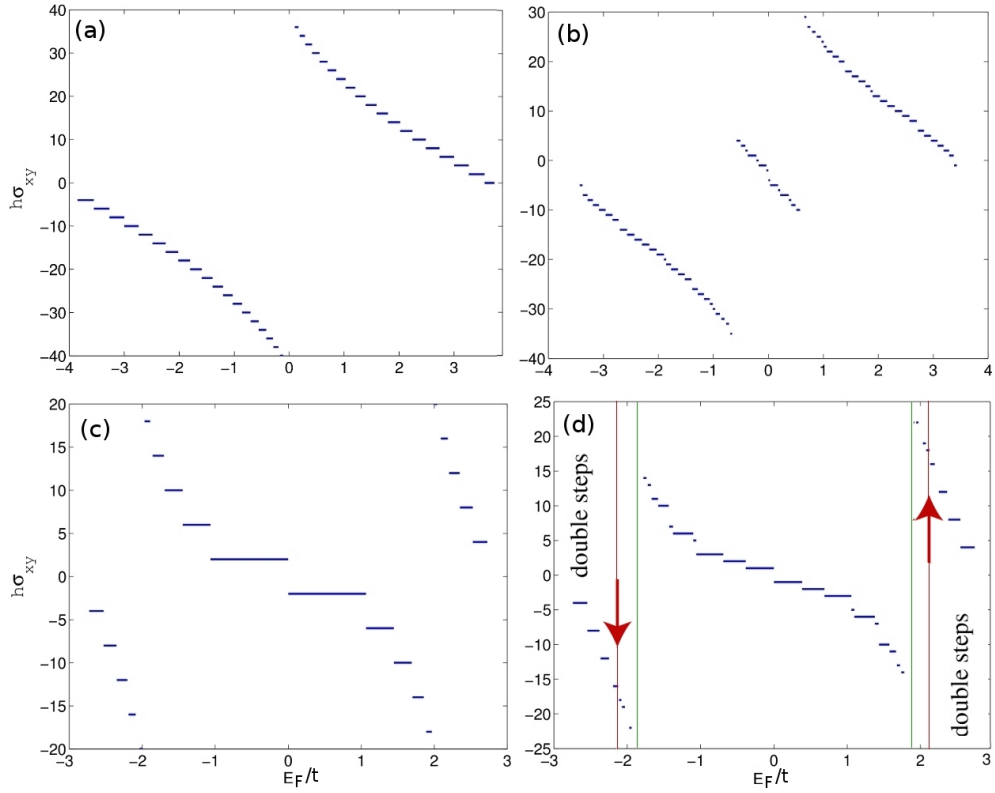

Figure 4.9: The Hall conductivity calculated with the Chern numbers for four cases with $\Phi_0 = 41$. (a) Abelian case i.e. $\alpha = \beta = 0$, the steps are double because of the color-degeneracy, (b) $\alpha = \beta = \pi/4$, (c) $\alpha = \beta = \pi/2$ and (d) an anisotropic case $\alpha = \pi/2 - 0.1, \beta = \pi/2 + 0.1$. In the last graph, the green line marks the points of the sudden jumps in the conductance and the red lines and arrows the points where the anomalous double steps are restored.

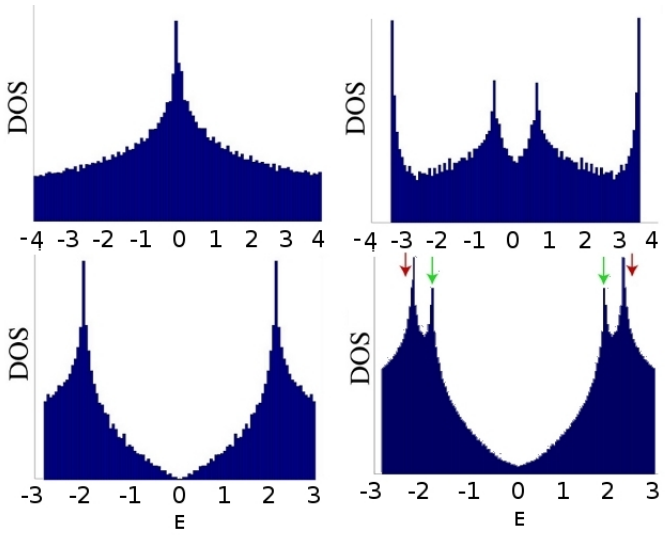

Figure 4.10: The density of states ploted for $\Phi_0 \approx 0$ for the same cases as the IQHE in Fig. 4.9.

4.4 Conclusions

The IQHE survives in the deeply non-Abelian regime and acquires a unique character specific to the non-Abelian nature of the gauge fields. It is characterised by a particular sequence of robust plateaus corresponding to the quantised values of the transverse conductivity. Moreover, the non-Abelian coupling induces controllable van Hove singularities as well as an anomalous Hall effect, similar to the effect induced by the hexagonal geometry in graphene. Experimental observation of this distinctive effect requires to achieve T smaller than the gaps, i.e. of order of 10-50 nK, which is demanding, but not impossible.

Chapter 5

Dirac physics in SU(2) gauge fields

The sequence of double plateaus in the Hall conductivity described in the previous chapter is comparable to the IQHE observed in Si-MOSFET, or the anomalous IQHE observed in graphene [69] in the "low flux" regime $\Phi_0 \ll 1$ corresponding to experimentally available magnetic fields. The quantisation of σ_{xy} for the graphene has been measured in 2005 by K.S. Novoselov et.al. [66] and the experimental results are presented in Fig. 5.1. Graphene is a fascinating material and for groundbreaking experiments regarding its properties Andre Geim and Konstantin Novoselov have been awarded with Nobel Prize in 2010. Moreover, graphene similarily to the square lattice system with non-Abelian gauge field that has been studied in the previous chapter, exhibits van Hove singularities in its DOS (see Figs. 5.2 and 4.10). The unusual quantisation of Hall conductivity in graphene comes from special geometrical properties of the lattice so it has different origin than our system of interest. However, several analogies between these two cases are intriguing. In order to understand better the physics of the anomalous IQHE let us first briefly summarise the graphene's properties.

Graphene

Graphene is a monolayer of carbon crystal structure. The lattice has honeycomb geometry and the elementary lattice cell contains

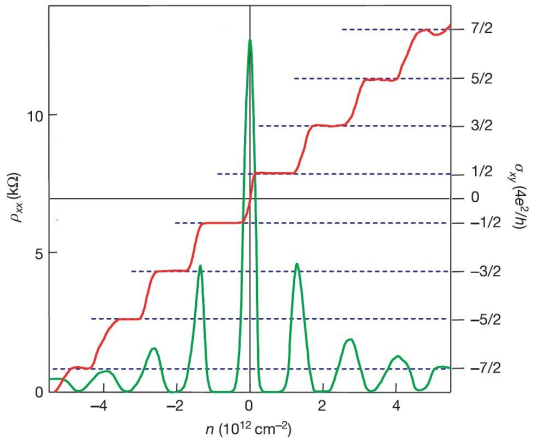

Figure 5.1: The anomalous quantisation of σ_{xy} for graphene plotted against density of charge carriers. The change of the filling factor in the lattice is equivalent to changing of the magnetic field (see chapter 4).

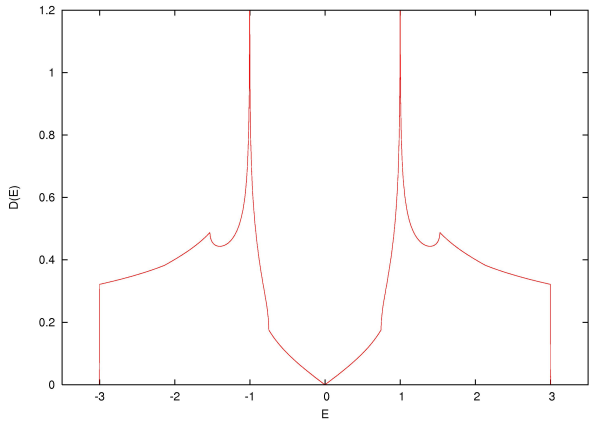

Figure 5.2: The density of states calculated for the honeycomb lattice. There are two van Hove singularities where the DOS diverges.

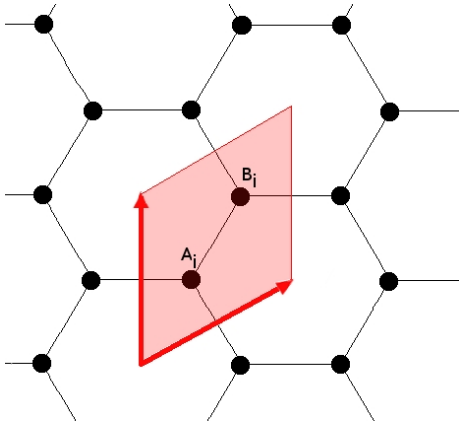

Figure 5.3: The sketch of honeycomb lattice and its unit cell.

two atoms as illustrated in Fig. 5.3. The tight-binding Hamiltonian reads:

$$H = -t \sum_{<i,j>} a_i^\dagger b_j + h.c., \tag{5.1}$$

where $a_i^\dagger, b_i^\dagger (a_i, b_i)$ create (annihilate) a fermion on the i-th site of the A and B site respectively, t is the hopping amplitude and i, j are nearest-neighbour lattice cells. In the presence of the periodic boundary conditions in both directions, the Hamiltonian can be reduced by the Fourier transformation to block-diagonal form with a 2×2 matrix for each lattice cell separately. In the case one finds the energy of two corresponding bands analytically:

$$E_\pm = \pm \sqrt{1 + 4 \cos \frac{\sqrt{3} k_x}{2} \cos \frac{k_y a}{2} + 4 \cos^2 \frac{k_y a}{2}} \tag{5.2}$$

where $a = \sqrt{3} a_{cc}$. and a_{cc} is the distance between two nearest atoms in the lattice. The bands touch in two independent points, at the edges of the Brillouin zone as illustrated in the Fig. 5.4. From the picture one can see that the closing of the gap has shape of two touching cones. These points are called Dirac points because in their vicinity the spectrum is linear. Low energy excitations of fermionic lattice systems are usually governed by the non-relativistic Schrödinger equation. However, this description must

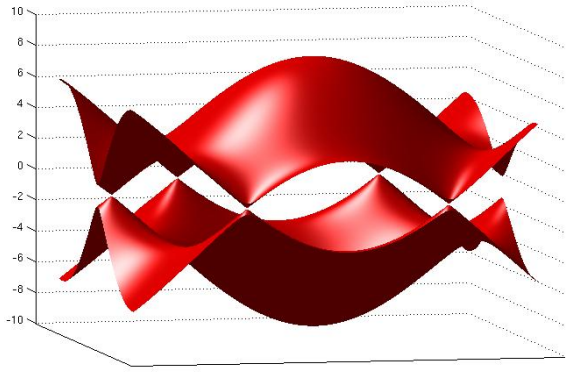

Figure 5.4: The energy bands calculated for the honeycomb lattice. One can see that the bands touch and the spectrum in the vicinity of the touching points is linear. The elementary excitations in such case are described by Dirac equation.

be profoundly altered in the region of linear spectrum. There the quasiparticles become massless relativistic fermions [66, 67, 68, 69, 70].
Such a remarkable behaviour in the case of graphene is induced by the bipartite nature of the honeycomb geometry. It has been also reported that additional uniform [71] or staggered [72, 73] magnetic fields in the square lattice have similar effect. In the following we show that the natural playground for emerging Dirac fermions is provided by multi-component fermionic atoms subjected to artificial non-Abelian gauge fields. We will also show that the physical properties of massless relativistic fermions are completely characterised by the non-Abelian features of the external gauge fields. Furthermore the anisotropy of the underlying Minkowski space-time can be controlled externally, producing an anomalous quantum Hall effect characterised by a squeezed Landau vacuum.

5.1 Purely non-Abelian fields

In order to isolate non-Abelian effects, we first study the regime of vanishing Abelian flux $\Phi = 0$. As before we will consider fermions in 2D square lattice with non-Abelian field given by the vector potential $A = (\alpha\sigma_y, \beta\sigma_x)$. This form of the vector potential for generic values of α, β gives non-trivial constant Wilson loop which is the condition to have non-Abelian behaviour of the system. The Hamiltonian can be written in a convenient way with the use of fermionic field operator $c_\tau(m,n)$:

$$H = -\sum_{<m,n>}\sum_{\tau=1,2} e^{i\int_{m,n}^{m',n'}\mathbf{A}\cdot\mathbf{dl}} c^\dagger_{\tau'}(m',n')c_\tau(m,n) + h.c. \qquad (5.3)$$

In the present case the vector potential is constant which gives $\int_{m,n}^{m',n'}\mathbf{A}\cdot d\mathbf{l} = const$ and the hopping operators are:

$$U_x = e^{i\alpha\sigma_y}, \quad U_y = e^{i\beta\sigma_x}$$

Next, we introduce the Fourier transform of the field operators and so we transform the equation to the momentum space.

$$\begin{aligned} c_\tau(\mathbf{r}) &= \frac{1}{\sqrt{N}}\sum_{\mathbf{k}} e^{i\mathbf{kr}} c_{\tau,\mathbf{k}} \\ c_\tau(\mathbf{r})^\dagger &= \frac{1}{\sqrt{N}}\sum_{\mathbf{k}} e^{-i\mathbf{kr}} c^\dagger_{\tau,\mathbf{k}} \end{aligned}$$

Where we have used the notation with the lattice spacing a taken as a unit lenght, so that $\mathbf{r} = (m,n)$ and $\mathbf{kr} = \mathbf{k}_x m + \mathbf{k}_y n$. Inserting all this into the Hamiltonian and using:

$$\begin{aligned} \frac{1}{N}\sum_{\mathbf{r}} e^{-i\mathbf{r}(\mathbf{k}-\mathbf{k}')} &= \delta(\mathbf{k}-\mathbf{k}') \\ e^{i(\alpha\sigma_x+\beta\sigma_y)} &= \cos(\sqrt{\alpha^2+\beta^2})\mathbf{1} + i\frac{\sin(\sqrt{\alpha^2+\beta^2})}{\sqrt{\alpha^2+\beta^2)}}(\alpha\sigma_x+\beta\sigma_y) \\ \Psi_k &= (c_{1,\mathbf{k}}, c_{2,\mathbf{k}})^T \end{aligned}$$

one finds:

$$\begin{aligned}
\mathcal{H} &= -t \sum_{<\mathbf{r},\mathbf{r}'>} \sum_{\tau,\tau'} \frac{1}{N} \sum_{\mathbf{k},\mathbf{k}'} e^{-(i\mathbf{k}\mathbf{r}-\mathbf{k}'\mathbf{r}')} c^{\dagger}_{\tau',\mathbf{k}'} c_{\tau,\mathbf{k}} + h.c. \\
&= -t \sum_{\mathbf{r}} \sum_{\tau,\tau'} \frac{1}{N} \sum_{\mathbf{k},\mathbf{k}'} \left(e^{-i\mathbf{k}\mathbf{r}} e^{i\mathbf{k}'(\mathbf{r}+\hat{n}_y)} e^{-i\beta\sigma_x} + e^{-i\mathbf{k}\mathbf{r}} e^{i\mathbf{k}'(\mathbf{r}+\hat{n}_x)} e^{-i\alpha\sigma_x} \right) c^{\dagger}_{\tau',\mathbf{k}'} c_{\tau,\mathbf{k}} + h.c. \\
&= -t \sum_{\mathbf{k}} \Psi^{\dagger}_k \left(e^{ik_y} e^{-i\sigma_x\beta} + e^{ik_x} e^{-\sigma_y\alpha} \right) \Psi_k \\
&= -t \sum_{\mathbf{k}} \Psi^{\dagger}_k \left[e^{ik_y} \left(\cos\beta - i\tfrac{1}{2}\sin\beta\sigma_x \right) + e^{ik_x} \left(\cos\alpha - i\tfrac{1}{2}\sin\alpha\sigma_y \right) \right] \Psi_k \\
&= -t \sum_{\mathbf{k}} \Psi^{\dagger}_k \left[(2\cos\beta\cos k_y + 2\cos\alpha\cos k_x)\mathbf{1} \right] \Psi_k \\
&\quad -t \sum_{\mathbf{k}} \Psi^{\dagger}_k \left[\sin k_y \sin\beta\sigma_x + \sin k_x \sin\alpha\sigma_y \right] \Psi_k \qquad (5.4)
\end{aligned}$$

The Hamiltonian is diagonalised in momentum space and the fermion gas becomes a collection of non-interacting quasi-particles with energies shown in Fig.5.5. Close to the "marginally" Abelian regime ($\Phi_\alpha, \Phi_\beta \approx \pi/2$), the energy gap closes at two independent points $\mathbf{k}_D$ called Dirac points. They can be calculated by putting the off-diagonal elements of the Hamiltonian (5.4) to zero. One finds

$$\begin{aligned}
\sin(k_y)\sin\beta = 0 &\implies k_x = n\pi, n \in \mathbb{Z} \\
\sin(k_x)\sin\alpha = 0 &\implies k_y = n\pi, n \in \mathbb{Z}.
\end{aligned}$$

And from this one can see that the four conical singularities in the spectrum are located at:

$$\mathbf{k}_{\mathrm{D}} \in \{(0,0), (\pi,0), (0,\pi), (\pi,\pi)\} \in \mathrm{BZ}, \qquad (5.5)$$

which correspond to massless relativistic excitations at half filling.

Dirac Hamiltonian

Let us expand the Hamiltonian around these points. For example if $\mathbf{k} = \mathbf{k}_D + \delta\mathbf{k} \equiv (k_{x,D}, k_{y,D}) + (\delta k_x, \delta k_y) = (n\pi, m\pi) + (\delta k_x, \delta k_y)$, then

$$\begin{aligned}
\cos(k_i) \simeq \cos(n\pi) - \sin(n\pi)\delta k_i + O(\delta^2) &= 1 + O(\delta^2) \\
\sin(k_i) \simeq \sin(n\pi) + \cos(n\pi)\delta k_i + O(\delta^2) &= \delta k_i + O(\delta^2)
\end{aligned}$$

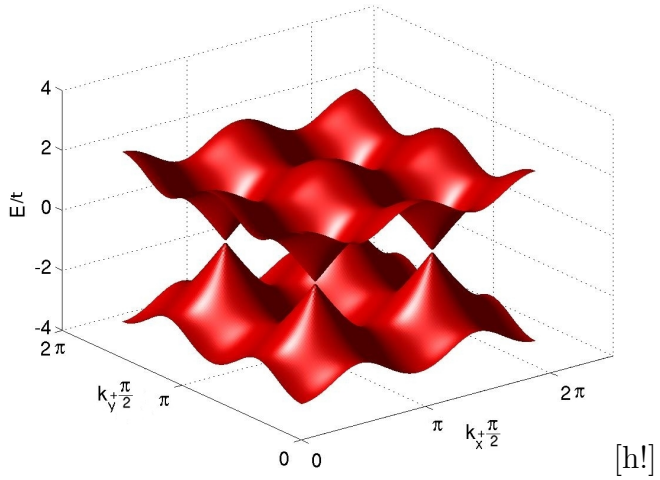

Figure 5.5: Energy bands close to the π-flux regime ($\alpha = \pi/2 + 0.1, \beta = \pi/2 - 0.1$), with vanishing Abelian flux $\Phi = 0$. The bands touch at the Dirac points inside the first Brillouin zone where the spectrum is linear in k.

In this point the expansion of the Hamiltonian gives:

$$\begin{aligned}
\mathcal{H} &= -\sum_{\mathbf{k}} \begin{pmatrix} 2\cos\beta + 2\cos\alpha & 0 \\ 0 & 2\cos\beta + 2\cos\alpha \end{pmatrix} \\
&+ -\sum_{\mathbf{k}} \begin{pmatrix} 0 & \sin\alpha\delta k_y \\ \sin\alpha\delta k_y & 0 \end{pmatrix} \\
&+ -\sum_{\mathbf{k}} \begin{pmatrix} 0 & -\mathrm{i}\sin\beta\delta k_x \\ \mathrm{i}\sin\beta\delta k_x & 0 \end{pmatrix}
\end{aligned}$$

Around the points $\mathbf{p} = \mathbf{k} - \mathbf{k}_{\mathrm{D}}$, the low-energy properties are accurately described by a Dirac Hamiltonian

$$H_{\mathrm{eff}} = -\sum_{\mathbf{p}} \Psi^{\dagger}_{\mathbf{p}} H_{\mathrm{D}} \Psi_{\mathbf{p}}, \qquad H_{\mathrm{D}} = c_x \alpha_x p_x + c_y \alpha_y p_y, \tag{5.6}$$

where $\Psi_{\mathbf{p}} = (c_{1\mathbf{p}}, c_{2\mathbf{p}})^t$ is the relativistic spinor, the Dirac matrices α_x, α_y fulfill $\{\alpha_j, \alpha_k\} = 2\delta_{jk}, \quad i, j, k = 1, 2, 3$ (e.g. around $\mathbf{k}_{\mathrm{D}} = (0, \pi)$, $\alpha_x = \sigma_y$ and $\alpha_y = \sigma_x$), and $c_x = 2\sin\alpha$, $c_y = 2\sin\beta$ represent the effective speeds of light in the x and y directiosn. We stress here that the control over the non-Abelian fluxes α, β offers the exotic opportunity to modify the structure of the underlying Minkowski space-time, reaching anisotropic situations where $c_x \neq c_y$. Hence, non-Abelian optical lattices provide a quantum optical analogue of relativistic QED, where the emerging fermions and the properties of the corresponding space-time rely on the non-Abelian features of the external fields. Furthermore, it is also possible to observe a transition between relativistic and non-relativistic dispersion relations as the energy is increased. This abrupt change of the quasi-particle nature is revealed by Van Hove singularities (VHS) in the density of states, as displayed in Figs. 4.10 and 4.9.

Van Hove singularities

In order to find the position of VHS we find the eigenvalues of the Hamiltonian:

$$\mathcal{H} = -t\sum_{\mathbf{k}} \left(\begin{array}{c|c} 2\cos\beta\cos k_y & \sin k_y \sin\beta \\ +2\cos\alpha\cos k_x & -i\sin k_x\sin\alpha \\ \hline c.c. & 2\cos\beta\cos k_y \\ & +2\cos\alpha\cos k_x \end{array}\right).$$

The eigenvalues read:

$$\begin{aligned} E_1 &= 2\cos\beta\cos k_y + 2\cos\alpha\cos k_x + \sqrt{\sin^2 k_y \sin^2\beta + \sin^2 k_x \sin^2\alpha} \\ E_2 &= 2\cos\beta\cos k_y + 2\cos\alpha\cos k_x - \sqrt{\sin^2 k_y \sin^2\beta + \sin^2 k_x \sin^2(\alpha)} \end{aligned}$$

Van Hove singularities are located in the maxima of the function E_1 which is:

$$\begin{aligned} E_1(\mathbf{k}_1) &= E_1(\alpha, 0) = 2(1 + \cos\beta) \\ E_1(\mathbf{k}_2) &= E_1(\alpha, \pi) = 2(1 - \cos\beta) \\ E_1(\mathbf{k}_3) &= E_1(0, \beta) = 2(1 + \cos\alpha) \\ E_1(\mathbf{k}_4) &= E_1(\pi, \beta) = 2(1 - \cos\alpha) \end{aligned} \tag{5.7}$$

5.2 Abelian and non-Abelian fields

To connect the non-Abelian features discussed above with the QHE, we introduce the Abelian flux Φ in the Dirac Hamiltonian (5.6). This time we will use the symmetric gauge $\mathbf{A} = \frac{B_0}{2}(-y, x)$. The vector potential couples to the momentum by $\mathbf{p} \to \mathbf{p} - \mathbf{A}$, and we obtain

$$H_{\mathrm{D}} = g_- \left(\sigma^+ a + \sigma^- a^\dagger\right) + g_+ \left(\sigma^+ a^\dagger + \sigma^- a\right), \tag{5.8}$$

where $\sigma^+ = |\chi_1\rangle\langle\chi_2|$, $\sigma^- = |\chi_2\rangle\langle\chi_1|$ are color-flip operators, $a^\dagger, a$ are bosonic operators

$$\begin{aligned} a_j &= \sqrt{\frac{\omega}{2}}(x_j + \frac{i}{\omega}p_j) \\ \omega &\equiv \frac{B_0}{2} = \frac{1}{l_B^2}, \quad j = x, y \\ a &\equiv \frac{a_x - \mathrm{i}a_y}{\sqrt{2}} \\ a^\dagger &\equiv \frac{a_x^\dagger + \mathrm{i}a_y^\dagger}{\sqrt{2}} \end{aligned}$$

and the parameters $g_+ \equiv \sqrt{\omega}(c_y + c_x)$, $\quad g_- \equiv \sqrt{\omega}(c_y - c_x)$. It is interesting to notice that the Hamiltonian (5.8) is analogous to a sum of Jaynes-Cummings and anti Jaynes-Cummings interactions well

known from quantum optics [1][83]. In the isotropic limit $g_- = 0$, the Hamiltonian consists of an anti-Jaynes-Cummings term only, that leads to the usual relativistic Landau levels, the same ones as in graphene. Conversely, in the non-isotropic regime $g_- \neq 0$, simultaneous combination of Jaynes-Cummings and anti-Jaynes-Cummings terms, produces a new type of Landau levels. These novel LL are obtained by means of a Bogoliubov squeezing transformation.

Bogoliubov transformation

The Hamiltonian takes simpler form when we note that the operators:

$$b \equiv \quad \frac{1}{\sqrt{g_+^2 - g_-^2}}(g_- a^\dagger + g_+ a), \quad b^\dagger \equiv \quad \frac{1}{\sqrt{g_+^2 - g_-^2}}(g_- a + g_+ a^\dagger) \tag{5.9}$$

have the same commutation relations as standard creation/annihilation operators:

$$[b, b^\dagger] = 1, \quad [b, b] = [b^\dagger, b^\dagger] = 0.$$

To transform the equation to this operators I use the Bogoliubov squeezing transformation $S(\zeta)$

$$S(\zeta) \equiv e^{\frac{\zeta}{2}(a^2 - (a^\dagger)^2)}. \tag{5.10}$$

The operators $a, a^\dagger$ transform according to the formulas:

$$\begin{aligned} S^\dagger(\zeta) a S(\zeta) &= a\cosh(|\zeta|) - a^\dagger e^{i\theta}\sinh(|\zeta|) \\ S^\dagger(\zeta) a^\dagger S(\zeta) &= a^\dagger\cosh(|\zeta|) - a e^{i\theta}\sinh(|\zeta|) \\ \zeta &= |\zeta| e^{i\theta} \end{aligned}$$

In the case we are considering x $\zeta \in \mathbb{R}$. In order to get the desired operators $b, b^\dagger$ as defined above we have to find corresponding value of ζ. This value is:

$$\frac{g_-}{g_+} = \tanh\zeta, \tag{5.11}$$

[1] introducing a mass term of the form $mc^2\sigma_z$ to the Hamiltonian (5.6) would be equivalent to detuning the Jaynes-Cummings interaction by $\delta = mc^2$.

so that the operator transforming the equation takes the form:

$$S(\zeta) = e^{\frac{1}{4}\ln\left(\frac{g_+ + g_-}{g_+ - g_-}\right)\left(a^2 + (a^\dagger)^2\right)}, \tag{5.12}$$

and the Hamiltonian simplifies after the transformation as follows:

$$S^\dagger(\zeta)\mathcal{H}_D S(\zeta) = (\sqrt{g_+^2 - g_-^2})\left(\sigma^+ b^\dagger + \sigma b\right) \equiv \mathcal{H}_D^S. \tag{5.13}$$

The Hilbert space is a sum of two dimensional subspaces invariant under the action of the Hamiltonian that can be now easily found.

$$\mathcal{H} = \bigoplus_{n=0}^{\inf} \mathcal{H}_n, \qquad \mathcal{H}_n \equiv \mathrm{Span}\{|\chi_\uparrow, n\rangle, |\chi_\downarrow n-1\rangle\} \tag{5.14}$$

$$\begin{aligned} H_n|n,\uparrow\rangle &= (\sqrt{g_+^2 + g_-^2})\sqrt{n}|n-1,\downarrow\rangle \\ H_n|n-1,\downarrow\rangle &= (\sqrt{g_+^2 + g_-^2})\sqrt{n}|n,\uparrow\rangle \end{aligned}$$

leading to the energy spectrum

$$E_{\mathrm{LLL}} = 0, \quad E_n^\pm = \pm\sqrt{(2B_0 c_x c_y)n}, \quad n = 1, 2... \tag{5.15}$$

and corresponding eigenstates

$$|\mathrm{LLL}\rangle = |\chi_2\rangle S^\dagger(\zeta)|\mathrm{vac}\rangle,$$

$$|E_n^\pm\rangle = \tfrac{1}{\sqrt{2}}|\chi_1\rangle S^\dagger(\zeta)|n-1\rangle \pm \tfrac{1}{\sqrt{2}}|\chi_2\rangle S^\dagger(\zeta)|n\rangle,$$

with $|n\rangle = (n!)^{-1/2}(a^\dagger)^n|\mathrm{vac}\rangle$ being the usual Fock states. Accordingly, the effect of non-Abelian fields is to squeeze the usual LL. In particular, the lowest Landau level (LLL) is a zero-energy mode characterised by a coloured squeezed vacuum, which is in clear contrast with its Abelian counterpart, the latter being simply the vacuum. Besides, this LLL presents half the degeneracy of the remaining excited states $n \geq 1$ [84], and leads to the so-called anomalous half-integer QHE

$$\sigma_{xy} = \pm\tfrac{g}{h}\left(\nu + \tfrac{1}{2}\right), \tag{5.16}$$

where the filling factor ν is defined as the integer part of $[E_F^2/2B_0c_xc_y]$, and g is the Dirac points degeneracy. Let us stress that the non-Abelian fluxes modify the Hall plateaus in a non-trivial manner as already emphasised through the numerical results. In particular, the Hall conductivity in Eq. (5.16) predicts the anomalous half-integer plateaus represented in Fig. 4.9(c), where the conical singularities are four-fold degenerate $g = 4$. Conversely, in the non-Abelian case shown in Fig. 4.9(d), the degeneracy is lifted to $g = 1$, and thus the size of the steps is modified in accordance.

Honeycomb lattice

Since the anomalous quantum Hall effect is known to exist in graphene even without non-Abelian field it is interesting to see how the latter modifies the spectrum and the transport properties. That analysis has been done by A. Bermudez et. al. [100]. If non-Abelian field is applied to that geometry, new Dirac points appear. Depending on the particular values of the potential parameters the number and position of the new points vary. For an illustration see fig. 5.6. Also the topological properties of the phases in the system change. The interplay between the field induced and geometry induced anomalies is yielding a complex behaviour of that system. For detailed description, the reader is referred to the reference [100].

5.3 Conclusions

We have shown that non-Abelian optical lattices offer an intriguing route to probe the striking properties of emerging Dirac fermions in anisotropic Minkowski space-times. In particular, the versatility offered by such experimental setups leads to the unique possibility of tuning the anisotropy of the underlying space-time.

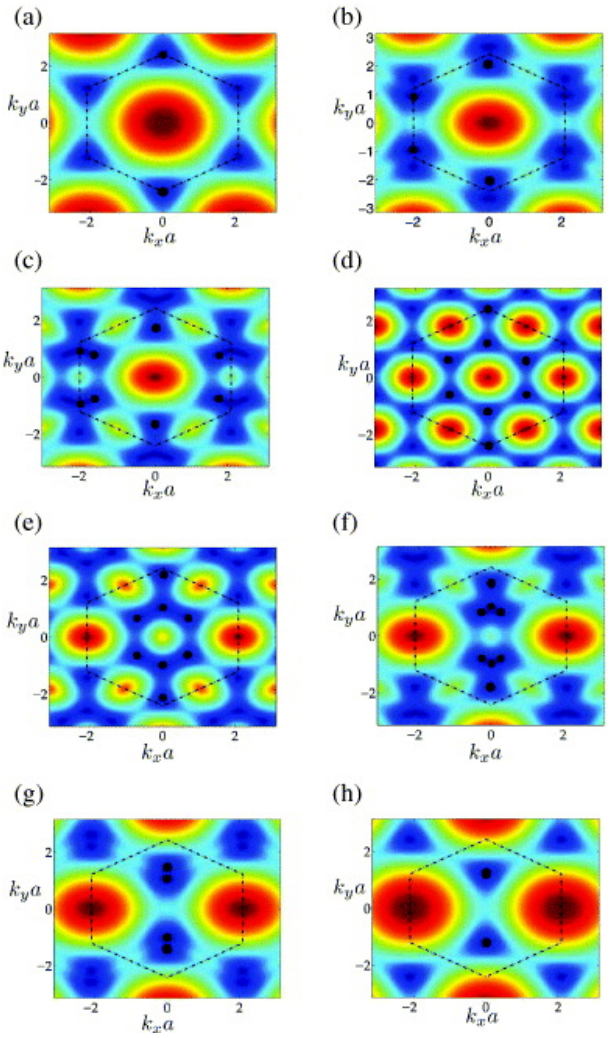

Figure 5.6: The Dirac points in the first Brillouin zone in the honeycomb lattice (marked with the dashed line) for different values of field fluxes through one lattice cell. Dirac points are marked with black dots. The gauge fluxes are the following: (a) $\alpha = 0 = \beta$, (b) $\alpha = 0.15\pi, \beta = 0$, (c) $\alpha = 0.30\pi, \beta = 0$, (d) $\alpha = 0.45\pi, \beta = 0$, (e) $\alpha = 0.60\pi, \beta = 0$, (f) $\alpha = 0.75\pi, \beta = 0$, (g) $\alpha = 0.90\pi, \beta = 0$ and (h) $\alpha = \pi, \beta = 0$. Figure from [100].

Chapter 6

Fermi superfluid in SU(2) fields

6.1 Introduction

So far in the previous chapters the effect of the Abelian and non-Abelian gauge fields has been presented only for the non-interacting systems. Since interactions are fundamental in order to access both the superfluid regime and the FQH physics, now we will consider the ultracold gas of atoms that weakly attract one another. The interactions will be treated in a mean-field approach, so that technically the effective Hamiltonian will describe single-particle physics. We will construct a model based on Bardeen, Cooper, and Schrieffer (BCS) theory in which the interaction term in the Hamiltonian implies the pairing between atoms of opposite momenta and spins. The BCS theory predicts formation of a superfluid state of the pairs in low enough temperatures.We will also study the appearance of exotic phases induced by the external gauge fields as well as the spin imbalance in the system. Those phases are recently gaining increasing attention both theoretically and experimentally, since they are known to contain anyons, quasi-particles which are neither bosons nor fermions, and are intrinsically robust and protected against decoherence and external perturbations. These excitations may have also non-Abelian statistics. Non-Abelian anyons have been proposed as the key ingredient for the realisation of a

topologically-protected quantum computer [87].

Despite the Landau theory of symmetry breaking constituting the fundamental tool to characterise the different phases of matter, the discovery of the Quantum Hall (QH) and Quantum Spin Hall (QSH) effects showed however, that some physical systems undergo transitions between distinguishable phases without breaking any local symmetry [85]. These transitions have a topological character, in the sense that the corresponding "order parameter" is not a local quantity, but rather an integer number describing the system as a whole. Systems with topological phases include various classes of topological insulators [86] and the famous the $\nu = 5/2$ Fractional Quantum Hall (FQH) state (Pfaffian state). The experimental realisation of the artificial gauge fields for neutral atoms opens the way to realising *all* possible classes of topological insulators in a single experimental setup [86, 94]. Artificial gauge fields for neutral atoms may be realised as already mentioned in the chapter 2 via the aid of, as examples, adiabatic control of superpositions of degenerate dark states, spatially varying Raman coupling, or Raman-induced transitions to auxiliary states in optical lattices. Recently Abelian fields have been successfully realised experimentally and non-Abelian fields may be available soon.

In this chapter we will study again a two-component fermionic gas on a 2D square lattice, with an external non-Abelian gauge field effectively yielding a spin-orbit (SO) coupling in the gas. We take a vector potential of the form $A = (\alpha\sigma_y, \beta\sigma_x)$, where σ_i are the Pauli matrices, and α, β are independently tuneable parameters. As shown in the chapter 5 in the absence of interactions, the excitations of this system include massless Dirac fermions, and the associated Dirac cones may be tuned to be asymmetric in the x and y directions. In presence of an additional Abelian field, the ground state forms the so called squeezed Laughlin state, and the system exhibits anomalous Integer QH physics (see chapter 4). In our case the internal degree of freedom will play the role of the spin in BCS pairing and the two components of the wavefunction will be denoted as $\uparrow, \downarrow$. The simplest case of superfluidity, that is s-wave pairing, the phase does not support any topological phases.

In the case of p-wave and other higher partial waves, the non-trivial topological order is possible. Here we consider s-wave pairing with non-Abelian gauge field and the "spin" imbalance. We will show that the resulting phases are topologically non-trivial. In presence of a strong external magnetic field the superfluid enters a topological phase characterised by anyonic excitations with non-Abelian statistics [90, 91]. The corresponding Hamiltonian is unitary equivalent to the one of a p-wave superfluid [90]. There is one important issue to be addressed. High values of the spin imbalance can destroy the superfluidity. The threshold above which this happens is called Chandrasekar-Clogston (CC) limit [92]. We will see that the value of imbalance needed to observe a phase transition towards a topological state is larger than the one predicted to yield pair breaking. We will investigate here this important and still unaddressed question: is a topological phase accessible at all in ultracold s-wave superfluids? As it is shown in the following, we find a positive answer to this question: the spin-orbit coupling makes a superfluid sufficiently stable to enter various topological phases. In the case of non-Abelian fields the superfluidity is more stable and the CC is shifted towards higher imbalances.

We will continue by presenting the full topological phase diagram, calculated as a function of the lattice filling and the strength of the spin-flipping couplings along the x and y directions. The phase diagram is characterised in terms of the corresponding Chern numbers (CN), which we obtain via a simple and efficient method. Topological phases may be discussed in terms of the symmetry classes introduced by Altland and Zirnabuer [93]. In our system Time-Reversal and Spin-Rotation invariances are destroyed by the Zeeman and SO terms, and as a consequence our Hamiltonian belongs to most general symmetry class D. The periodic classification of topological insulators [94, 86] predicts that the topological phases of this Hamiltonian in 2D are indexed in terms of an integer number. As we will see, phases with CN$=0, \pm 1, \pm 2$ are accessible with ultracold fermionic gases in presence of the strong SO coupling provided by a synthetic gauge field.

We study different classes of edge modes in this system, evidencing their strict relation with the Chern numbers. In analogy with the

QSH effect, we also find that the topological protection of the edge modes is destroyed when pairs of states with same spin appear on the same edge. Topological protection of these modes is therefore characterised in terms of the $\mathbb{Z}_2$ index given by the parity of CN.

6.2 Description of the system

We consider a spin-imbalanced mixture of two fermionic species with interspecies attractive interaction. Particles are free to move in a 2D square lattice in presence of an external non-Abelian field. Introducing $\mathbf{c}_{\mathrm{i}}^{\dagger} = (c_{\mathrm{i}\uparrow}^{\dagger}, c_{\mathrm{i}\downarrow}^{\dagger})$, the hopping contribution may be written as

$$\mathcal{H}_{\mathrm{KIN+SO}} = -\mathrm{t} \sum_{\mathrm{i}} \sum_{\hat{e}=\hat{x},\hat{y}} \left(\mathbf{c}_{\mathrm{i}+\hat{e}}^{\dagger} \gamma_{\mathrm{i}\to\mathrm{i}+\hat{e}} \mathbf{c}_{\mathrm{i}} + \mathrm{h.c.} \right) \tag{6.1}$$

The hopping terms are defined as:

$$\gamma_{\mathrm{i}\to\mathrm{i}+\hat{x}} = e^{-i\sigma_y \alpha} \qquad \gamma_{\mathrm{i}\to\mathrm{i}+\hat{y}} = e^{i\sigma_x \beta} \tag{6.2}$$

Using the identity $e^{i\mathcal{A}\sigma_j} = \mathbf{1}_{2x2} \cos\mathcal{A} + i\sigma_j \sin\mathcal{A}$, it is easy to see that the spin-conserving [spin-flipping] hopping terms in the x and y directions are proportional respectively to $\cos(\alpha)$ and $\cos(\beta)$ [$\sin(\alpha)$ and $\sin(\beta)$]. Adding the chemical potential, Zeeman and interaction terms, we obtain the complete Hamiltonian:

$$\begin{aligned} \mathcal{H} = \mathcal{H}_{\mathrm{KIN+SO}} + \sum_{\mathrm{i}} \Delta_{\mathrm{i}} \left[c_{\mathrm{i}\uparrow}^{\dagger} c_{\mathrm{i}\downarrow}^{\dagger} + c_{\mathrm{i}\downarrow} c_{\mathrm{i}\uparrow} \right] \\ - \sum_{\mathrm{i}} \left[(\mu + h) c_{\mathrm{i}\uparrow}^{\dagger} c_{\mathrm{i}\uparrow} + (\mu - h) c_{\mathrm{i}\downarrow}^{\dagger} c_{\mathrm{i}\downarrow} \right]. \end{aligned} \tag{6.3}$$

And more explicitly:

$$\begin{aligned}\mathcal{H} &= -\mathrm{t}\sum_{\mathrm{i}}\left[\left(c^{\dagger}_{\mathrm{i}+\hat{x},\uparrow}c_{\mathrm{i}\uparrow}+c^{\dagger}_{\mathrm{i}-\hat{x},\uparrow}c_{\mathrm{i}\uparrow}\right)\cos\alpha+\left(c^{\dagger}_{\mathrm{i}+\hat{y},\uparrow}c_{\mathrm{i}\uparrow}+c^{\dagger}_{\mathrm{i}-\hat{y},\uparrow}c_{\mathrm{i}\uparrow}\right)\cos\beta+(\text{same with}\downarrow\downarrow)\right]\\ &\quad -\mathrm{t}\sum_{\mathrm{i}}\left[\left(c^{\dagger}_{\mathrm{i}+\hat{x}\downarrow}c_{\mathrm{i}\uparrow}-c^{\dagger}_{\mathrm{i}-\hat{x}\downarrow}c_{\mathrm{i}\uparrow}\right)\sin\alpha+\mathrm{i}\left(c^{\dagger}_{\mathrm{i}+\hat{y}\downarrow}c_{\mathrm{i}\uparrow}-c^{\dagger}_{\mathrm{i}-\hat{y}\downarrow}c_{\mathrm{i}\uparrow}\right)\sin\beta+h.c.\right]\\ &\quad -\mu\sum_{\mathrm{i}}\left[c^{\dagger}_{\mathrm{i}\uparrow}c_{\mathrm{i}\uparrow}+c^{\dagger}_{\mathrm{i}\downarrow}c_{\mathrm{i}\downarrow}\right]\\ &\quad -h\sum_{\mathrm{i}}\left[c^{\dagger}_{\mathrm{i}\uparrow}c_{\mathrm{i}\uparrow}-c^{\dagger}_{\mathrm{i}\downarrow}c_{\mathrm{i}\downarrow}\right]\\ &\quad +\sum_{\mathrm{i}}\Delta_{\mathrm{i}}\left[c^{\dagger}_{\mathrm{i}\uparrow}c^{\dagger}_{\mathrm{i}\downarrow}+c_{\mathrm{i}\downarrow}c_{\mathrm{i}\uparrow}\right],\end{aligned} \tag{6.4}$$

. Here $V>0$ is the attraction strength, the BCS s-wave pairing $\Delta_{\mathrm{i}}=-V\langle c_{\mathrm{i}\downarrow}c_{\mathrm{i}\uparrow}\rangle$ has been taken real, and a constant term has been neglected. Due to the mean-field character of the BCS approximation, it is important to realize that the pairing strength Δ_{i} is not an external parameter which is tunable at will, but it is a quantity that has to be calculated self-consistently. This point will be analyzed in detail in the next Section.

In presence of periodic boundary conditions, the pairing gap may be taken as constant throughout the system ($\Delta_{\mathrm{i}}=\Delta$) and the Hamiltonian can be easily diagonalized [90]. We introduce $\Psi^{\dagger}_{\mathbf{k}}=(c^{\dagger}_{\mathbf{k},\uparrow},c^{\dagger}_{\mathbf{k},\downarrow},c_{-\mathbf{k},\uparrow},c_{-\mathbf{k},\downarrow})$ with $\mathbf{c}^{\dagger}_{\mathbf{k}}=V^{-1/2}\sum_{\mathrm{i}}e^{i\mathbf{k}\cdot\mathrm{i}}\mathbf{c}^{\dagger}_{\mathrm{i}}$, and obtain

$$\mathcal{H}=\frac{1}{2}\sum_{\mathbf{k}}\Psi^{\dagger}_{\mathbf{k}}\mathcal{H}_{\mathbf{k}}\Psi_{\mathbf{k}}, \tag{6.5}$$

$$\mathcal{H}_{\mathbf{k}}=\begin{pmatrix}\epsilon_{\mathbf{k}}-h\sigma_z+\mathbf{g_k}\cdot\boldsymbol{\sigma} & i\Delta\sigma_y\\ -i\Delta\sigma_y & -\epsilon_{\mathbf{k}}+h\sigma_z+\mathbf{g_k}\cdot\boldsymbol{\sigma}^{*}\end{pmatrix} \tag{6.6}$$

where $\boldsymbol{\sigma}=(\sigma_x,\sigma_y)$. The spin-conserving dispersion is given by

$$\epsilon_{\mathbf{k}}=-2\mathrm{t}(\cos\alpha\cos k_x+\cos\beta\cos k_y)-\mu, \tag{6.7}$$

while the spin-flipping term arising from SO coupling reads

$$\mathbf{g}^{\dagger}_{\mathbf{k}}=2t\left(\sin\beta\sin k_y,-\sin\alpha\sin k_x\right). \tag{6.8}$$

The eigenvalues of this Hamiltonian are

$$\lambda_{\mathbf{k}}^2 = \epsilon_{\mathbf{k}}^2 + h^2 + |\mathbf{g}_{\mathbf{k}}|^2 + \Delta^2 \pm 2\sqrt{h^2(\epsilon_{\mathbf{k}}^2 + \Delta^2) + \epsilon_{\mathbf{k}}^2 |\mathbf{g}_{\mathbf{k}}|^2}. \quad (6.9)$$

In presence of pairing ($\Delta \neq 0$), the spectrum is generically gapped, but the gap may close at the four distinguishable momenta which yield $\mathbf{g}_{\mathbf{k}0} = 0$, i.e., $\mathbf{k}_0 \in \{(0,0),(0,\pi),(\pi,0),(\pi,\pi)\}$. The four values of the spin-imbalance at which the gap closes are given by

$$h_{\mathbf{k}_0} = \sqrt{\epsilon_{\mathbf{k}_0}^2 + \Delta^2}. \quad (6.10)$$

Transitions between phases with different topological properties may only happen at gap-closing points. Since the balanced superfluid ($h = 0$) is known to be topologically trivial, the latter condition states that to access a topological phase one has to consider imbalances satisfying the condition $h > \min_{\mathbf{k}_0}(h_{\mathbf{k}_0})$.

6.3 Self-consistent calculation of the pairing gap

It has been recently pointed out [90, 91, 95] that topologically nontrivial phases should appear in fermionic s-wave superfluids in presence of both SO coupling and spin-imbalance. In these works, the pairing gap was introduced as an external parameter tunable at will. This assumption should be taken with care at large spin-imbalance, since it is well known that superfluidity breaks down when the Zeeman energy (proportional to h) becomes large as compared to Δ_0, the pairing gap at $h = 0$ and $T = 0$. There, the free energy of the paired state becomes larger than the one of the normal ($\Delta = 0$) state, and the system presents a first order phase transition from superfluid to normal. In absence of SO coupling ($\alpha = \beta = 0$) and in the continuum, the critical value is analytic and given by the so called Chandrasekar-Clogston (CC) limit, $h_{\mathrm{CC}} = \Delta_0/\sqrt{2}$ [92]. It may be seen from eq. (6.10) that $h_{\mathbf{k}_0} > h_{CC}$ for every $\mathbf{k}_0$, a condition that excludes the possibility of having topological phases for fermionic s-wave superfluids in the absence of SO coupling.

The self-consistent calculation of the pairing gap Δ proceeds via the minimization of the free energy

$$F = \frac{N\Delta^2}{V} + \sum_{\mathbf{k}} \left[\epsilon_{\mathbf{k}} - \frac{k_{\mathrm{B}}T}{2} \sum_{i=1}^{4} \ln\left(1 + \mathrm{e}^{-\lambda_{\mathbf{k},i}/k_{\mathrm{B}}T}\right) \right]. \qquad (6.11)$$

Here $\lambda_{\mathbf{k},i}$ $(i = 1, \ldots, 4)$ are the four solutions of eq. (6.9), and N is the number of lattice sites. In the absence of SO coupling ($\alpha = \beta = 0$) and in the continuum limit, by solving eq. (6.11) we find that Δ drops abruptly to zero at $h = h_{\mathrm{CC}}$ in agreement with the CC limit. The results of this calculation in presence of SO on a lattice are shown in fig. 6.1, where we plot the magnitude of Δ as a function of the spin imbalance h and the attraction strength V. As one cranks up the SO coupling, the sharp phase transition gets smoothened [96], and we find we find that values of $\Delta \gtrsim t$ are easily reachable in the regions where $h > \min_{\mathbf{k}_0}(h_{\mathbf{k}_0})$. Largest gaps are obtained when the spin-conserving and spin-flipping tunneling energies have comparable magnitudes, i.e., for $|\tan(\alpha)| \sim |\tan(\beta)| \sim 1$. As we will see in the following section, all phases with $|\mathrm{CN}| \leq 2$ may be reached at $h \gtrsim \min_{\mathbf{k}_0}(h_{\mathbf{k}_0})$ for particular values of α, β, and μ. In fig. 6.1, this imbalance yields respectively (from top to bottom) CN=1,-1,-2. The superfluid is instead always unstable due to pairing breakdown at imbalances much larger than $\min_{\mathbf{k}_0}(h_{\mathbf{k}_0})$.

6.4 Topological phase diagram

Our Hamiltonian has built-in particle-hole symmetry, i.e. its eigenvalues come in $\pm$ pairs. The topological state of this system may then be characterized in terms of the bulk Chern number (CN) of the upper band of the spectrum. The latter is a $\mathbb{Z}$ topological invariant which may change only when the spectral gap between two bands closes. In addition, the sum of CNs associated to an isolate set of bands is conserved before and after the band touching. We calculate the upper band's CN following the elegant method proposed by Bellissard in ref. [97]. Let's assume that the gap closes at point $\mathbf{k}_0$ as h crosses the critical value $h_{\mathbf{k}_0}$. The Hamiltonian $\mathcal{H}$ has then two eigenvectors $|\psi_0^{(1)}\rangle, |\psi_0^{(2)}\rangle$ with vanishing eigenvalue.

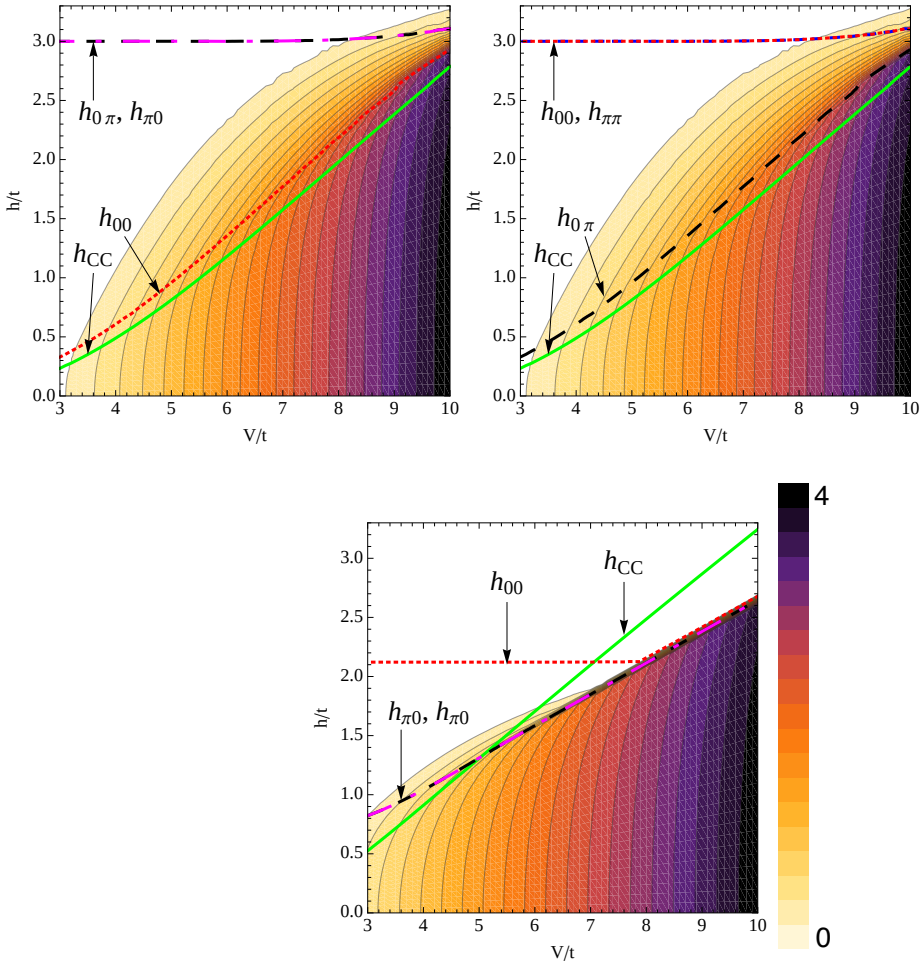

Figure 6.1: Plots of $|\Delta|/t$ as a function of imbalance h and attraction strength V. The lines represent respectively the CC limit $h_{\rm CC}$ (continuous), and the topological boundaries h_{00} (dotted), $h_{0\pi}$ (wide dashed), $h_{\pi 0}$ (dot-dashed) and $h_{\pi\pi}$ (fine dashed). Here we have chosen $(\alpha, \beta, \mu) = (\pi/4, \pi/4, -3t)$ (left), $(\pi/4, 3\pi/4, -3t)$ (right), and $(\pi/4, \pi/4, -\sqrt{2}t/2)$ (bottom).

In the neighborhood of $(\mathbf{k}_0, h_{\mathbf{k}_0})$, we may approximate the Hamiltonian with an effective 2×2 matrix obtained by projecting $\mathcal{H}$ on $|\psi_0^{(1)}\rangle, |\psi_0^{(2)}\rangle$. Using the Pauli matrices $\vec{\sigma} = (\sigma_x, \sigma_y, \sigma_z)$, the effective Hamiltonian may be written as

$$\mathcal{H}_{\text{eff}}(\mathbf{k}, h) = E(\mathbf{k}, h) + \vec{\sigma} \cdot \vec{f}(\mathbf{k}, h). \tag{6.12}$$

If the spectrum features a linear Dirac cone at $(\mathbf{k}_0, h_{\mathbf{k}_0})$, the Jacobian matrix $J_{\vec{f}}$ has a non-zero determinant at this point. In this case, as h increases above $h_{\mathbf{k}_0}$, the change in Chern number of the upper band is given by the sign of the determinant itself. This quantity is called the Berry index of the gap-closing point. More generally, if at a given value $\tilde{h}$ the spectrum features multiple Dirac cones centered in $\mathbf{k}_0^{(1)}, \mathbf{k}_0^{(2)}, \ldots$, the change in Chern number at $h = \tilde{h}$ is given by the sum of the Berry indices at all the touching points,

$$\Delta\text{CN}(\tilde{h}) = \sum_{\text{i}} \text{sign}\{\det[J_{\vec{f}}(\tilde{h}, \mathbf{k}_0^{(i)})]\}. \tag{6.13}$$

From the latter formula, it is clear that each Dirac cone changes the Chern number of a band by ± 1. If the determinant of the Jacobian at a given gap-closing point vanishes, the Chern number of a band changes there instead by 0, or ± 2 [97]. The latter case is however rather pathological. In the present context, it is verified only when either α or β equal integer multiples of $\pi/2$.

In order to investigate the topological character of various phases, we show in fig. 6.2 the curves corresponding to the four critical imbalances $h_{\mathbf{k}_0}$ defined in eq. (6.10). The curves are plotted as a function of β for fixed $\alpha = \pi/4$, and for four increasing values of the chemical potential μ (from left to right). We consider only negative chemical potentials, since the Hamiltonian has built-in particle-hole symmetry, and reversing the sign of μ produces symmetric phases to the ones found here. At small imbalances an s-wave superfluid is topologically trivial for any μ, and CN=0. Each time the imbalance h crosses one of the critical curves $h_{\mathbf{k}_0}$, the gap between the bands closes at the corresponding momentum $\mathbf{k}_0$, and a topological phase transition occurs. At low lattice fillings, we find phases characterized by Chern numbers CN=-1,0,1. For higher lattice filling there appear phases with Chern numbers as large as ± 2. As we

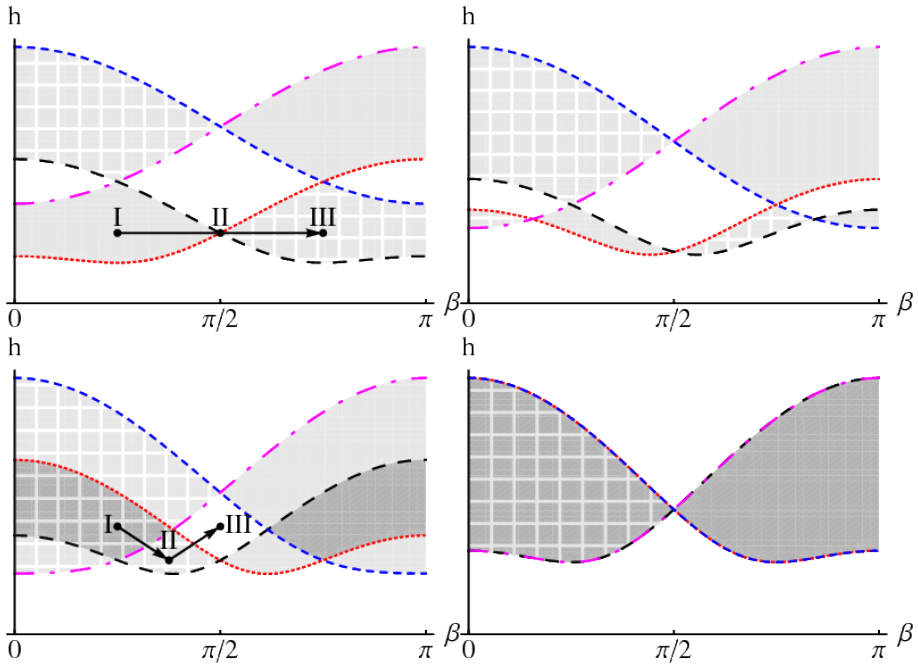

Figure 6.2: Topological phase diagram as a function of β at fixed $\alpha = \pi/4$ and $\Delta = t$. From left to right, $\mu/(\sqrt{2}t) = -2$ (a),-1.25 (b),-0.5 (c), 0 (d). The lines depict the critical imbalances h_{00} (dotted), $h_{0\pi}$ (wide dashed), $h_{\pi 0}$ (dot-dashed), $h_{\pi\pi}$ (fine dashed). The phases are indexed by the Chern numbers calculated from eq. (6.13): CN=0 (white), |CN|=1 (light gray), |CN|=2 (dark gray), and the meshed phases are the ones with negative CN. The labeled dots in the first and third plots mark the imbalances plotted respectively in figs. 6.3 and 6.4.

will see in the following section, where we will discuss edge states, the phases with CN=-1,1 are topologically protected and distinguishable, while the phases with CN=-2,0,2 are not protected. The topological protection of the system is therefore characterized by the $\mathbb{Z}_2$ number given by $\mathrm{mod}_2(\mathrm{CN})$, in analogy with the theory of the Quantum Spin Hall effect [98]. At half-filling, $\mu = 0$, the phase diagram is composed of regions with CN=-2,0,2, and is therefore not topological for any α, β, and h.

As we have seen before, not all regions of the phase diagram plotted in fig. 6.2 are accessible due to pair-breaking. Nonetheless, phases with equal CN are topologically equivalent, and we have shown that phases with all CNs (-2,-1,0,1,2) may be realized with sufficiently large $\Delta(\sim t)$ when $h \gtrsim \min_{\mathbf{k}_0}(|h_{\mathbf{k}_0}|)$.

6.5 Spectrum on a cylinder

A characteristic feature of topological phases is the presence of intra-gap modes localized on open boundaries of the system. To investigate this aspect, we calculate the spectrum of the Hamiltonian (6.3) on a cylinder, i.e., respectively with open and periodic boundary conditions along the x and y directions. Due to the broken translational symmetry along the x-direction, we diagonalize the Hamiltonian by performing a Fourier transformation along the y-direction only, by introducing $c_i = c_{m,n} = 1/\sqrt{L_y}\sum_{k_y} e^{-ik_y n} c_m(k_y)$. The Hamiltonian may then be written as

$$\mathcal{H} = \frac{t}{2}\sum_{k_y} \psi^\dagger_{k_y} \mathcal{H}_{k_y} \psi_{k_y}, \tag{6.14}$$

with $\Psi^\dagger_{k_y} = (c^\dagger_{k_y,\uparrow}, c^\dagger_{k_y,\downarrow}, c_{-k_y,\uparrow}, c_{-k_y,\downarrow})$ and $c^\dagger_{k_y,\sigma} = (c^\dagger_{x_1,k_y,\sigma}, c^\dagger_{x_2,k_y,\sigma}, \ldots, c^\dagger_{x_{L_x},k_y,\sigma})$. The matrix $\mathcal{H}_{k_y}$ has dimension $(4L_x * 4L_x)$ (where a factor of 2 comes from spins, and another from PH symmetry), and reads

$$\mathcal{H}_{k_y} = \begin{pmatrix} A & B & 0 & E \\ B^T & D & -E & 0 \\ 0 & -E & -A & B^T \\ E & 0 & B & -D \end{pmatrix} \tag{6.15}$$

with

$$A = -(2\cos\beta\cos k_y + \mu + h)D_0 - \cos\alpha(D_\uparrow + D_\downarrow) \quad (6.16)$$
$$B = 2\sin\beta\sin k_y D_0 - \sin\alpha(D_\uparrow - D_\downarrow) \quad (6.17)$$
$$D = -(2\cos\beta\cos k_y + \mu - h)D_0 - \cos\alpha(D_\uparrow + D_\downarrow) \quad (6.18)$$
$$E = -\Delta D_0 \quad (6.19)$$

and $D_0, D_\uparrow, D_\downarrow$ are respectively the $(L_x * L_x)$ matrices with ones along the diagonal starting from element (1,1), (1,2), (2,1), and zeros elsewhere.
In figs. 6.3 and 6.4 we show the spectrum of $\mathcal{H}_{x,k_y}$ as a function of k_y for various combinations of μ, β, and h. The spectrum on a torus would be generally gapped, but when open boundary conditions are taken into account isolated states appear inside the gap. The eigenvectors corresponding to these isolated eigenstates are linear superpositions of $\uparrow$ and $\downarrow$ spin components, exponentially localized on either of the boundaries, as may be seen in fig. 6.5. These are therefore termed "edge states". Edge modes in this context have first been discussed in ref. [90] for the specific case $\alpha = \beta = \pi/4$.

Given the reflection symmetry of the spectrum with respect to the sign of k_y, these states always appear in $\pm\tilde{k}$ pairs. Edge excitations may cross at zero energy with a linear dispersion at $k_y = 0$ or π, similarly to lattice Dirac fermions. Their origin is topological, and these zero-energy crossings may appear or disappear only at the critical points $h = h_{\mathbf{k}_0}$ where the bulk spectra of the upper and lower bands touch in zero, see e.g. fig. 6.3(II). Since the fully-balanced ($h = 0$) and the fully-polarized ($h \gg t$) states are not topological and do not support any edge modes, on a lattice we find that edge states are present only for imbalances satisfying $\min_{\mathbf{k}_0}(h_{\mathbf{k}_0}) < h < \max_{\mathbf{k}_0}(h_{\mathbf{k}_0})$.

When a single pair of states is present, see e.g. figs. 6.3a and 6.3c, the two counter-propagating edge modes with $\pm\tilde{k}$ are localized on opposite boundaries. Since on a given boundary there is no state available for backward spin-conserving scattering, these states are topologically protected. These conditions are realized when $\mathrm{mod}_2(\mathrm{CN})=1$. When instead the parity of CN is 0, as depicted in fig. 6.4, the system contains either zero or two pairs of edge states.

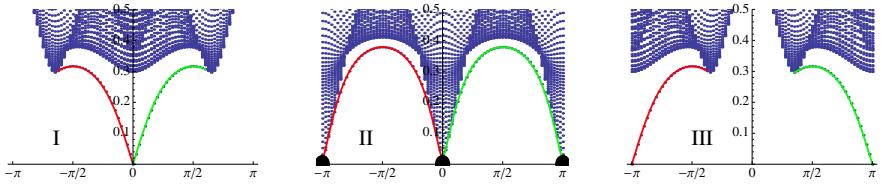

Figure 6.3: Spectrum on a cylinder, plotted as a function of k_y for the three combinations of β and h marked by the labeled dots in fig. 6.2a. The lines mark the edge states, and the thick dots mark the position of the gap-closing points. The CN of the upper band is 1 (-1) in the left (right) image, while the central image depicts a topological critical point. The chemical potential is $\mu/(\sqrt{2}t) = -2$, and the energy on the vertical axis is in units of t.

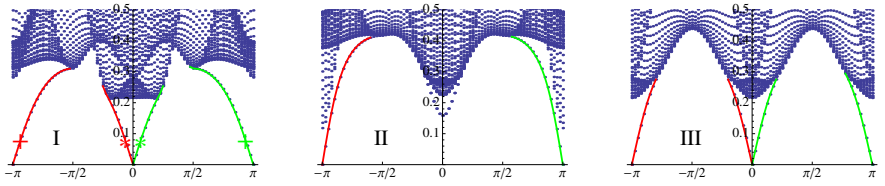

Figure 6.4: Same as fig. 6.3, but here $\mu/(\sqrt{2}t) = -0.5$ and the plots correspond to the values of β and h marked by the labeled dots in fig. 6.2c. The symbols + and * identify the eigenstates plotted in fig. 6.5. From left to right, the CN of the upper band is respectively -2,-1, and 0.

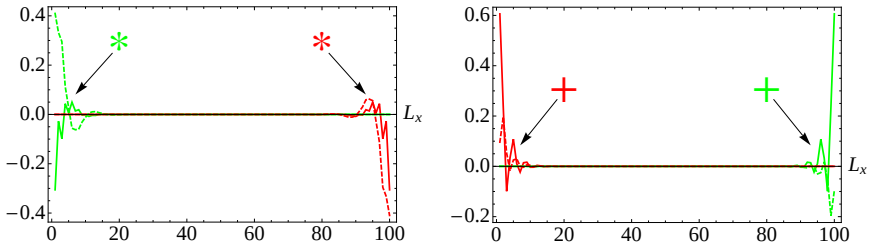

Figure 6.5: Edge modes on a cylinder: continuous (dashed) lines depict the amplitude of the spin ↑ (↓) component of the wavefunction with α, β, μ and h as in fig. 6.4(I). The momenta of the edge states are given by the corresponding symbols in fig. 6.4(I). There are two counterpropagating modes with identical spin state localized on the same edge. In analogy with the QSH effect, this yields the destruction of the topological protection of the states, since a weak perturbation may induce backscattering from one mode to the other.

At sufficiently low-energy, the eigenvectors at a given energy are characterized by symmetric quasi-momenta $k_y = \pm\tilde{k}, \pm(\pi - \tilde{k})$. As may be seen in fig. 6.5, the counter-propagating edge states with $k_y = \tilde{k}$ and $k_y = -\pi + \tilde{k}$ are both localized on the same edge. When $\mathrm{mod}_2(\mathrm{CN})=0$, we see that either edge modes can perform spin-conserving backscattering, or that there are no edge modes at all. A phase with even parity of the CN does not contain therefore any topologically-protected states.
It is interesting to note that fig. 6.4(III) depicts a physical state with two pairs of edge states but vanishing CN. To the best of our knowledge, this case has not been discussed so far in the context of cold atomic gases. Edge states in ultracold gases may be observed along the lines proposed in ref. [99]. It should also be remembered that the core of a vortex is topologically equivalent to an edge which has been closed on itself. The topologically-protected edge modes described above are therefore equivalent to the Majorana fermions known to exist, e.g., in the core of vortices of p-wave superfluids.

6.6 Conclusions

We have studied here interacting ultracold fermions in presence of non-Abelian gauge fields. We have demonstrated that spin-imbalance can lead to a variety of intriguing topological phases. We characterized these phases by the associated Chern numbers, we presented the full phase diagram, and we discussed the link existing between edge states and Chern numbers. Furthermore, we have shown via a self-consistent calculation which of the phases can be realized experimentally, and which are non-physical due to pairing breakdown. In light of the recent ground-breaking experimental realizations of synthetic Abelian [35, 25, 37] fields in ultracold gases, and given the prospective to realize non-Abelian fields soon, the fascinating physics discussed.

Chapter 7

Towards fractional quantum Hall effect

As discussed in the chapter 4, the anomalous QHE is essentially a single-particle phenomenon that relies on the peculiar properties of the Landau levels. The whole new class of phenomena occurs when the correlations between the particles are strong and the system must be considered in the many body picture. After the first observation of the fractional quantisation of the Hall resistivity which came as a big surprise and was rewarded by the Nobel Prize [101, 102] it soon became clear that this phenomenon can not be explained in the simple one-particle physics framework. R.B. Laughlin has proposed a function that proved to describe properly the ground of 2D gas of electrons in the magnetic field of magnitude B_0 perpendicular to the surface of the electrons motion as state of the FQHE phase [28]. The so called Laughlin function reads:

$$\Psi_L(z_1,..,z_N,\bar{z}_1,..,\bar{z}_N) = \prod_{i,j}(z_i - z_j)^m e^{-\frac{\sum i|z_i|^2}{4l_B^2}}. \qquad (7.1)$$

Here $l_B = \sqrt{\frac{1}{B_0}}$, and the variables $z_i, \bar{z}_i$ are equal respectively $x_i + iy_i$ and $x_i - iy_i$ and N is the number of particles. Using the same argument as in chapter 4 when calculating the degeneracy of the Landau levels, one can immediately see that the parameter m is related to the filling factor ν. The maximal allowed angular momentum is in the case of the Laughlin function (7.1) equal to Nm where N is

the number of particles in the system. The limitation of the system size imposes the limit on it and in turn, on N. If $m = 1$ which is the case of IQHE, the filling of the states is also 1, which means that for each magnetic flux penetrating the system, there is one electron. When for example $m = 3$ the filling $\nu = \frac{1}{3}$ and there are three flux quanta per electron. If we create an excitation in the system, which is a hole in position z_0, the wave function will have a form:

$$\Psi_{excited}(z_0; z_1, .., z_N) = \prod_i (z_i - z_0)\Psi_L(z_1, .., z_N). \qquad (7.2)$$

Physically this corresponds to inserting one flux quantum of strength Φ_0 to the system which creates a zero of the wavefunction. In order to transform the system back to its ground state but with $N \longrightarrow N + 1$, one would need to include three such zeros. Following the original argument of Laughlin, one can use the analogy with one component plasma (OCP), the building block that characterises the peculiar properties of quasiparticles in the fractional QHE [80]. In this picture, the Laughlin function is a classical partition function and one can see the system as consisting of quasiparticles of charge $\frac{1}{m}$ which in this case means $\frac{1}{3}$ interacting with a charged background so that the net charge of the system is zero. Such quasi-particles not only have a fractional charge, but also their quantum statistics vary from the standard bosonic or fermionic one. Depending on a particular case and the number m, interchanging of two of them effects in a phase factor $e^{2\pi m}$ of the wave function. In fact fermions and bosons are only special cases with $m = 1, 2$ for which the phase reduces to ± 1 factor. Because of this peculiar property, these quasi-particles are called *any*ons in order to stress that they are neither bosons nor fermions. So far only the anyons of charge $\frac{1}{3}$ and $\frac{1}{5}$ have been observed directly [104, 105], [106].

A big effort have been being done recently to find and properly describe non-Abelian anyons. They are believed to be a key ingredient needed for the topological quantum computation that is robust against decoherence. A candidate for such non-Abelian particle is an excitation of the FQHE state with $\nu = \frac{2}{5}$ [107, 108]. A completely convincing experimental proof of its non-Abelianity is,

however, still missing. The quantum ultracold atomic simulators are a natural context to study FQHE and anyonic excitations since they allow for creation of high magnetic fields, are nearly impurity-free and offer a high degree of control over the system. One purpose for studying non-Abelian gauge field is to investigate if under its action the anyonic excitations are more likely to be also non-Abelian. The creation of non-Abelian gauge potential does not translate immediately to non-Abelian anyons. It deforms the spectrum and as it was shown in previous chapters, other interesting phenomena occur.

Squeezed Laughlin function for non-Abelian fields

In the case of the non-Abelian gauge field in the system as considered in chapter 5 the Landau levels have been squeezed. If we write down the many-particle wavefunction we obtain an exotic Laughlin-like state:

$$\phi^m_{\mathrm{LLL}}(x,y) = \left(\sqrt{\tfrac{c_y}{c_x}}x - \mathrm{i}\sqrt{\tfrac{c_x}{c_y}}y\right)^m \mathrm{e}^{-\left(\frac{x^2}{2\tau_x^2}+\frac{y^2}{2\tau_y^2}\right)}. \tag{7.3}$$

Here $\tau_x = l_{\mathrm{B}}\sqrt{2c_x/c_y}$, $\tau_y = l_{\mathrm{B}}\sqrt{2c_y/c_x}$, describe the anisotropic extent of the wavefunction in units of the magnetic length l_{B}. The loss of rotational invariance caused by the non-Abelian induced anisotropy $c_x \neq c_y$, leads to the squeezing of the vortex levels (Figs. 7.1(a)-(d)). Filling these squeezed degenerate states (7.3) according to Fermi statistics, we obtain the Laughlin wavefunction

$$\Psi[z] = \prod_{j<k}(uz_{jk} - v\bar{z}_{jk})\mathrm{e}^{-\sum_j f(u,v)|z_j|^2 - g(u,v)(z_j^2+\bar{z}_j^2)}, \tag{7.4}$$

where $u = \cosh\zeta$, $v = \sinh\zeta$, $f(u,v) = \frac{1}{4}(u^2+v^2)$ and $g(u,v) = \frac{1}{4}uv$ depend on the anisotropy through the squeezing parameter ζ, and $z_{jk} = z_j - z_k$ represents the complex two-fermion distance. Here the squeezing parameter ζ is the same as introduced already in chapter 5: $\tanh\zeta = \frac{g_-}{g_+}$, with $g_\pm = \sqrt{\omega}(c_y \pm c_x)$ depending on the two speeds of "light" in x and y directions. These velocities depend on the parameters α and β and are given by $c_x = 2\sin\alpha, c_y = 2\sin\beta$. In the Abelian limit $\zeta = 0$, one recovers the standard integer

Laughlin wavefunction $\Psi[z] = \prod_{j<k} F(z_j, z_k) \mathrm{e}^{-\sum_j |z_j|^2/4l_\mathrm{B}^2}$, where $F(z_j, z_k) = z_j - z_k$ belongs to the space of holomorphic functions (Bargman-Fock space [103]). Strikingly, in the non-Abelian scenario $\zeta \neq 0$, the wavefunction (7.4) does not belong to such space due to the interference between holomorphic $F(z)$ and antiholomorphic $F(\bar{z})$ components, and thus represents an instance of a non-chiral QHE. As shown below, this new anomaly modifies the classical analogy with the one-component plasma (OCP). The Laughlin state can be interpreted as the partition function of a OCP $|\Psi[z]|^2 \propto Z_\mathrm{c} = \int \prod_j dz_j d\bar{z}_j \mathrm{e}^{-U_\mathrm{c}/kT}$ with $kT = 1/2$, a classical gas of particles interacting with a charged background through the potential

$$U_\mathrm{c} = \sum_j \left[\left(-\sum_k \log |u z_{jk} - v \bar{z}_{jk}| \right) + f(u,v)|z_j|^2 - g(u,v)(z_j^2 + \bar{z}_j^2) \right]. \tag{7.5}$$

The last term corresponds to the charged background jellium of the charge density $\rho_\mathrm{j} = -\frac{1}{4\pi l_\mathrm{B}^2}(\frac{c_x}{c_y} + \frac{c_y}{c_x})$, whereas the first describes a collection of positively charged particles $q = 1$ surrounded by a charge cloud $\delta\rho(z)$, with $z = |z|\mathrm{e}^{-\mathrm{i}\theta}$, and

$$\delta\rho(|z|, \theta) = \frac{\tanh\zeta}{|z|^2} \frac{(1 + \tanh^2\zeta)\cos 2\theta - 4\tanh\zeta}{(1 + \tanh^2\zeta) - 4\tanh\zeta \cos 2\theta}. \tag{7.6}$$

Notice how the surrounding charge cloud is absent $\delta\rho(z) = 0$ in the Abelian limit $\zeta = 0$, and we recover the usual OCP analogy. Conversely, for non-Abelian regimes, the collection of interacting positively charged particles becomes locally surrounded by an anisotropic charge cloud $\rho = \sum_j q\delta(z - z_j) + \delta\rho(z_j)$ with $\int d^2z \delta\rho(z) = 0$. In accordance, the paradigmatic plasma analogy is altered due to the squeezed nature of the LLL, a fact that may find profound consequences in the fractional QHE.

Recently a continuous version of the two-dimensional atomic gas in the presence of both the Abelian and non-Abelian vector potential $\mathbf{A} = (\alpha\sigma_x - \frac{B}{2}y, \alpha\sigma_y + \frac{B}{2}x)$ has been studied by M. Burello and A. Trombettoni [109]. They show that if the non-Abelian coupling

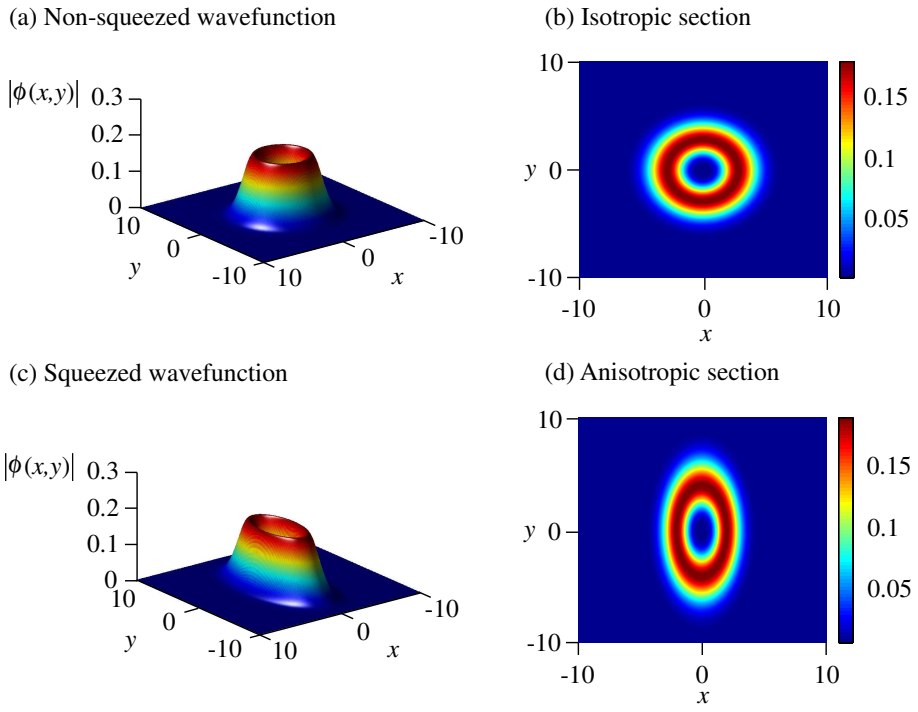

Figure 7.1: Vortex-like single-particle wavefunctions of the LLL $\phi^m_{\mathrm{LLL}}(x, y)$ for $m = 4$. (a),(b) Isotropic limit $c_x = c_y$. (c),(d) Anisotropic regime $c_y = 2c_x$. Distances are measured in units of the magnetic length l_{B}.

α is strong enough, namely $\frac{\alpha^2}{B} \geq (2n+1)$ the n-th Landau level crosses the $(n+1)$-th. Above these values the order of the Landau levels is changed accordingly. The eigenvalues of the Hamiltonian in that case are

$$E_n = 2Bn + \alpha^2 \pm \sqrt{B^2 + 8\alpha^2 Bn} \tag{7.7}$$

Interestingly enough, in the case of the degeneracy, i.e. $\frac{\alpha^2}{B} = (2n+1)$, when the superpositions of different Landau levels are allowed in the ground state, the latter one includes the non-Abelian excitations. As presented in ref. [109] the possible ground states of the system, depending on the filling factor, include Pfaffian-like states [110].

7.1 Analytical treatment of FQHE

In the following sections we will consider a two-dimensional gas of atoms in an external gauge field. First we will focus on the Abelian case in order to understand the basic properties of the FQHE. Next, we will consider the case of non-Abelian gauge field and the squeezed Laughlin function in the limit of small squeezing. The final aim is to find an expression for the interaction matrix V in that case and diagonalise the Hamiltonian with exact diagonalisation method. We will give an analytical expression for the matrix elements.

Properties of FQHE in Abelian field

In order to understand the basic properties of the FQHE and the Laughlin function, let us go back to the Landau level picture of the spectrum. The Hamiltonian for non-interacting charged particle moving in 2D and in a homogeneous magnetic field perpendicular to the surface is given by:

$$H = \sum_i \frac{1}{2}\left(p_{x_i}^2 - A_{x_i}\right)^2 + \frac{1}{2}\left(p_{y_i}^2 - A_{y_i}\right)^2, \tag{7.8}$$

where the summation runs over all particles in the system and we take for simplicity the mass of the particle $M = 1$. If we choose

the symmetric gauge for the vector potential: $A = \frac{B}{2}(-x, y, 0)$ the Hamiltonian can be rewritten in the terms of four independent operators $\mathcal{D}, \mathcal{D}^\dagger, d, d^\dagger$ out of which two are in fact absent in the Hamiltonian as a consequence of the Landau levels degeneracy in respect to angular momentum:

$$H = \sum_i \mathcal{D}_i^\dagger \mathcal{D}_i, \tag{7.9}$$

with

$$\begin{aligned} \mathcal{D} &\equiv \frac{a_{x_i} + i a_{y_i}}{\sqrt{2}} \\ \mathcal{D}^\dagger &\equiv \frac{a_{x_i}^\dagger - i a_{y_i}^\dagger}{\sqrt{2}} \\ d_i &\equiv \frac{a_{x_i} - i a_{y_i}}{\sqrt{2}} \\ d_i^\dagger &\equiv \frac{a_{x_i}^\dagger + i a_{y_i}^\dagger}{\sqrt{2}}. \end{aligned}$$

Where the operators $a, a^\dagger$ are regular Cartesian operators fulfilling the bosonic commutation relations:

$$a_{x_i} \equiv \frac{x_i - i p_{x_i}}{\sqrt{2}} \tag{7.10}$$

$$a_{x_i}^\dagger \equiv \frac{x_i + i p_{x_i}}{\sqrt{2}} \tag{7.11}$$

These operators fulfil commutation relations like harmonic oscillator:

$$[\mathcal{D}_i, \mathcal{D}_j] = 0 = [d_i, d_j] \text{ and } [\mathcal{D}_i, \mathcal{D}_j^\dagger] = \delta_{ij} = [d_i, d_j^\dagger].$$

The operators $\mathcal{D}, \mathcal{D}^\dagger$ move the particles between the Landau levels, while the operators $d, d^\dagger$ are related to the angular momentum projection L_z:

$$L_z = d^\dagger d - \mathcal{D}^\dagger \mathcal{D}. \tag{7.12}$$

For the lowest Landau level LLL the operator $d^\dagger d$ measures the angular momentum of the state. This is even more clear when

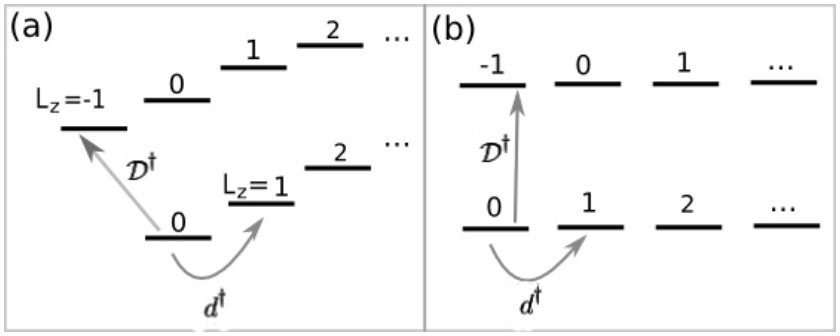

Figure 7.2: The Landau levels and the action of the $\mathcal{D}^\dagger, d^\dagger$ operators. a) the nearly degenerate levels for a fast rotating harmonic trap, b) Landau levels.

we recall that the LL structure of energy spectrum can be also produced by a rotating harmonic oscillator (see chapter 2). In that picture $\mathcal{D}^\dagger$ creates a left-handed quantum and $d^\dagger$ the right-handed one (see fig. 7.2). Let us now introduce some useful notation and give explicit formulas for several lowest eigenstates of the system:

$$\begin{aligned} |0\rangle &\equiv vacuum \\ |n,m\rangle &\equiv \frac{1}{\sqrt{\pi n! m!}} (d^\dagger)^m (\mathcal{D}^\dagger)^n |0\rangle \end{aligned}$$

The number n labels the Landau levels and the number m is related to the angular momentum l: $l = n - m$. In the first quantisation notation for $z \equiv x + iy$:

$$\begin{aligned} \langle z,\bar{z}|0\rangle &\equiv \frac{1}{\lambda\sqrt{\pi}} e^{-\frac{|z|^2}{2\lambda^2}} \\ \langle z,\bar{z}|0,m\rangle &= \frac{1}{\lambda\sqrt{\pi m!}} z^m e^{-\frac{|z|^2}{2\lambda^2}} \\ \langle z,\bar{z}|n,0\rangle &= \frac{1}{\lambda\sqrt{\pi n!}} \bar{z}^n e^{-\frac{|z|^2}{2\lambda^2}} \\ \langle z,\bar{z}|1,m\rangle &= \frac{1}{\lambda\sqrt{\pi m!}} [\bar{z} z^m - m z^{m-1}] e^{-\frac{|z|^2}{2\lambda^2}} \\ \langle z,\bar{z}|2,m\rangle &= \frac{1}{\lambda\sqrt{\pi m! 2!}} [\bar{z}^2 z^m - 2m\bar{z} z^{m-1} + m(m-1) z^{m-2}] e^{-\frac{|z|^2}{2\lambda^2}} \end{aligned}$$

Later also the notation: $\Lambda_{n,m}(z,\bar{z}) = \langle z,\bar{z}|n,m\rangle$ will be used.

7.2 Single particle state for small squeezing

We consider the single-particle eigenstates of the effective Hamiltonian for two-dimensional atomic gas in non-Abelian gauge field given by the vector potential $\mathbf{A} = (\alpha\sigma_x, \beta\sigma_y)$, as described in the previous chapter 5. The parameters α, β differ by a small value, so that the squeezing is small. In this way the system is non-Abelian and still having the Dirac-like spectrum. Each of single particle wave functions has a form:

$$\begin{aligned}\langle z,\bar{z}|0,m\rangle^{sq} &\equiv \frac{1}{\lambda\sqrt{\pi m!}}\frac{\left[z+\epsilon\bar{z}\right]^m}{\sqrt{1+\epsilon^2}}e^{-\frac{(z+\epsilon\bar{z})(\bar{z}+\epsilon z)}{1+\epsilon^2 2\lambda^2}} \\ &\approx \frac{1}{\lambda\sqrt{\pi m!}}\left[z^m + m\epsilon\bar{z}z^{m-1} - \tfrac{1}{2}\epsilon z^{m+2} - \tfrac{1}{2}\epsilon\bar{z}^2 z^m\right]e^{-\frac{|z|^2}{2\lambda^2}},\end{aligned}$$

where *sq* stands for squeezed state. Writing it down in the Landau levels language:

$$\langle z,\bar{z}|0,n\rangle^{sq} = \Lambda_{0,m} - \epsilon\Big(\Lambda_{2,m} - \tfrac{1}{2}\sqrt{m(m-1)}\Lambda_{0,m-2} + \tfrac{1}{2}\sqrt{(m+1)(m+2)}\Lambda_{0,m+2}\Big) \tag{7.13}$$

Expansion in the small parameter ϵ is very convenient because calculations in the basis of non-squeezed states are much simpler. Interestingly enough, the expansion contains not only the LLL, but also the second one (2LL).

Choice of the many-body basis

As the first step to calculate the interaction matrix between many-body states we write the many-particle states in the second quantisation notation. The basis are N-body Fock states of particles in non-squeezed Landau Levels.

The states are enumerated as follows: First, all of the particles from the LLL in order of increasing angular momentum, next we

take the 1LL also with increasing angular momentum and so on. The choice of the ordering does not influence the final result. For the second quantisation notation the order described above will be used.

$$|\Psi_\nu\rangle = (a_1^\dagger)^{\nu_1}(a_2^\dagger)^{\nu_2}(a_3^\dagger)^{\nu_3}...|0\rangle, \qquad \nu_i \in \{0,1\} \quad \text{for fermions.} \tag{7.14}$$

Hamiltonian

The expression for the Hamiltonian of interactions in the basis of Fock states has form:

$$\begin{aligned} h_{\mu\nu} &= \langle\Psi_\mu| \sum_{ijpq} V_{ijpg} a_i^\dagger a_j^\dagger a_p a_q |\Psi_\nu\rangle \\ &= \sum_{ijpq} V_{ijpg} \langle 0| \left[\prod_i \left(a_i^\dagger\right)^{\mu_i}\right]^\dagger |a_i^\dagger a_j^\dagger a_p a_q| \prod_i \left(a_i^\dagger\right)^{\nu_i} |0\rangle \\ &\equiv \sum_{ijpq} V_{ijpg} \sigma_{ijpg}^{\mu\nu} \end{aligned} \tag{7.15}$$

Permutating the inside annihilation (creation) operators to the right (left) to the states $|0\rangle$ ($\langle 0|$) will give the sign of the expression. We will come back to this problem in the subsection *Antisimmetrization*.

Dipolar interactions

In the following we assume that the system is polarised, so that the wavefunction has only one component. This simplifies the calculations, but excludes the contact interactions. We assume dipolar interactions between atoms and denote the dipolar moments of a particle i by $\mathbf{m}_i$. The interaction potential has the form:

$$V(\mathbf{r}_i, \mathbf{r}_j) = \frac{\mathbf{m_i} \cdot \mathbf{m_j} - 3(\hat{\mathbf{n}}_{ij} \cdot \mathbf{m_i})(\hat{\mathbf{n}}_{ij} \cdot \mathbf{m_j})}{|\mathbf{r}_i - \mathbf{r}_j|^3}. \tag{7.16}$$

Here $\hat{\mathbf{n}}_{ij}$ is a versor in the direction of the distance between the particle i and j. In the simplest case when all of the dipoles are perpendicular to the plane and parallel to each other, the term: $3(\hat{\mathbf{n}}_{ij}\cdot\mathbf{m_1})(\hat{\mathbf{n}}_{ij}\cdot\mathbf{m_2})$ is absent. We will from now consider that case. The potential simplifies to:

$$V(\mathbf{r},\mathbf{r}') = \frac{d^2}{|\mathbf{r}-\mathbf{r}'|^3}, \tag{7.17}$$

Where d is the strength of the dipolar momenta of the atoms. For simplicity we will take $d = 1$ in the following. Using the notation introduced above we can calculate the matrix elements of the interaction potential with the formula:

$$V_{ijpq} = \int \Lambda_i^*(z_1,\bar{z}_1)\Lambda_j^*(z_2,\bar{z}_2)\, V\,(z_1,\bar{z}_1,z_2,\bar{z}_2)\Lambda_p(z_1,\bar{z}_1)\Lambda_q(z_2,\bar{z}_2)d^2z_1 d^2z_2. \tag{7.18}$$

In above equation the functions Λ_i have only one index, that corresponds to two quantum numbers as before: $\Lambda_i \equiv \Lambda_{k_i,m_i}$.

7.3 Interaction matrix elements calculation

Expansion of single particle states

The eigenstates of the full Hamiltonian are squeezed Landau states. The squeezing mixes the Landau levels so the ground state will consist of the lowest Landau level and some correction of the higher ones. The most convenient way to treat this system is to decompose the squeezed states in the non-squeezed ones, as already mentioned:

$$\langle z,\bar{z}|0,m\rangle^{sq} =$$
$$\Lambda_{0,m} - \epsilon\Big(\Lambda_{2,m} - \tfrac{1}{2}\sqrt{m(m-1)}\Lambda_{0,m-2} + \tfrac{1}{2}\sqrt{(m+1)(m+2)}\Lambda_{0,m+2}\Big).$$

We will also decompose the non-squeezed Landau levels Λ in even simpler parts in order to make the calculation of the interaction matrix easy. There is, however, important note to be done at this point: we are considering particles that are fermions, so the wave

functions have to be antisymmetric. The internal degree of freedom is taken to be polarised so the antisymmetric part must be in the coordinate function: $\phi^{n,n';m,m'}(z_1,z_2) = \langle z_1;z_2|n,m;n',m'\rangle - \langle z_1;z_2|n',m';n,m\rangle$ Nevertheless, first we will use non-antisymmetrized states as the basis. This choice of basis is very convenient for calculations. The functions, however, should not be interpreted as wave functions of the atoms. In the end the antisymmetrization problem will be addressed and we will give the real values of coefficients of interaction energy matrix between real physical states.

Any state $\Lambda_i \equiv \Lambda_{n_i,m_i}$ belonging to any Landau Level can be written in a form:

$$\begin{aligned}\Lambda_{n_i,m_i} &= \frac{1}{\lambda\sqrt{\pi n_i! m_i!}} \sum_{n=0,m=0}^{\infty} A^{n_i,m_i}_{n,m}\, \bar{z}^n z^m e^{-\frac{|z|^2}{2\lambda^2}} \\ &\equiv \mathcal{N}_{n_i,m_i} \sum_{n=0,m=0}^{\infty} A^{n_i,m_i}_{n,m} \phi_{n,m}(z,\bar{z}) \qquad (7.19)\end{aligned}$$

Where two symbols are introduced:

$$\begin{aligned}\mathcal{N}_{n_i,m_i} &\equiv \frac{1}{\lambda\sqrt{\pi n_i! m_i!}} \\ \phi_{n,m}(z,\bar{z}) &\equiv \bar{z}^n z^m e^{-\frac{|z|^2}{2\lambda^2}}\end{aligned}$$

For example:

$$\begin{aligned}A^{0,m_i}_{n,m} &= \delta_{n,0}\delta_{m,m_i} \\ A^{n_i,0}_{n,m} &= \delta_{n,n_i}\delta_{m,0} \\ A^{1,m_i}_{n,m} &= \delta_{n,1}\delta_{m,m_i} + m_i\delta_{n,0}\delta_{m,m_i-1} \\ A^{2,m_i}_{n,m} &= \delta_{n,2}\delta_{m,m_i} - 2m_i\delta_{n,1}\delta_{m,m_i-1} + m_i(m_i-1)\delta_{n,0}\delta_{m,m_i-2}\end{aligned}$$

In fact the formula (7.19) is very general and the only coefficient needed for our considerations are the ones listed above, since the lowest squeezed Landau level is composed of the states from LLL and the 2LL. The functions $\phi_{k,m}(z,\bar{z})$ are the simplest building

blocks of all functions and they will be used to calculate the interaction coefficients. One can rewrite the general form of the matrix elements:

$$\begin{aligned} V_{ijpq} &\equiv \langle \Lambda_i \Lambda_j \; V \; \Lambda_p \Lambda_q \rangle \\ &= \mathcal{N}_i \mathcal{N}_j \mathcal{N}_p \mathcal{N}_q \sum_{n,m} \sum_{n',m'} \sum_{n'',m''} \sum_{n''',m'''} \\ &\quad \left(A^{n_i,m_i}_{n,m} \right)^* \left(A^{n_j,m_j}_{n',m'} \right)^* A^{n_p,m_p}_{n'',m''} A^{n_q,m_q}_{n''',m'''} \; \mathcal{I}^{n,m;n',m'}_{n'',m'';n''',m'''}, \end{aligned}$$

where

$$\mathcal{N}_i \equiv \frac{1}{\lambda \sqrt{\pi n_i! m_i!}}$$

$$\mathcal{I}^{n,m;n',m'}_{n'',m'';n''',m'''} \equiv \int \phi^*_{n,m}(z_1, \bar{z}_1) \phi^*_{n',m'}(z_2, \bar{z}_2) V(z_1, \bar{z}_1, z_2, \bar{z}_2) \phi_{n'',m''}(z_1, \bar{z}_1) \phi_{n''',m'''}(z_2, \bar{z}_2). \tag{7.20}$$

Change of the basis

In order to calculate the integral $\mathcal{I}^{n,m;n',m'}_{s,l;s',l'}$ one more transformation is convenient.

The change of the basis from

$$|n, m; n', m'\rangle \equiv \phi_{n,m}(z_1, \bar{z}_1) \phi_{n',m'}(z_2, \bar{z}_2)$$

to

$$|s, l; s'l'\rangle^{+-} \equiv \phi_{s,l}(z_+, \bar{z}_+) \phi_{s',l'}(z_-, \bar{z}_-)$$

$$z_+ \equiv \tfrac{z_1 + z_2}{\sqrt{2}}, \quad z_- \equiv \tfrac{z_2 - z_1}{\sqrt{2}}$$

The new basis states are denoted by: $|s, l; s'l'\rangle^{+-}$ and the transfer matrix to the new basis is given by coefficients $\mathcal{C}^{k,m,k',m'}_{s,l;s'l'}$:

$$|s, l; s'l'\rangle^{+-} = \sum_{m,l} \sum_{m',l'} \mathcal{C}^{n,m,n',m'}_{s,l;s'l'} |s, l; s', l'\rangle \tag{7.21}$$

$$\mathcal{C}^{n,m,n',m'}_{s,l;s'l'} \equiv \langle n, m; n', m' | s, l; s'l' \rangle \tag{7.22}$$

After some calculations one gets:

$$\begin{aligned}
\mathcal{C}^{n,m,n',m'}_{s,l;s'l'} &= \lambda^4\sqrt{2}^{-(l+l'+s+s')}\pi^2\sum_{v=0}^{s}\sum_{w=0}^{s'}\binom{s}{v}\binom{s'}{w}(-1)^w\times \qquad (7.23)\\
&\sum_{p=\nu}^{\mu}\binom{l}{p}\binom{l'}{M'-n'-p}(-1)^{M'-n'-p}M!M'!\delta_{m+m'-n-n',l+l'-s-s'}\\
M &= m+s+s'-v-w\\
M' &= m'+v+w\\
\nu &= \max\{0,m'-n'-l'\}\\
\mu &= \min\{m'-n',l'\}
\end{aligned}$$

The reverse transformation is given by a transposed matrix: $C^T = {}^{+-}\langle s,l;s'l'|n,m;n',m'\rangle$ because all of the coefficients are real.

7.3.1 The matrix elements of the interaction operator

The final expression for the matrix element V_{ijpq} can be now written down as:

$$\begin{aligned}
V_{ijpq} &= \mathcal{N}_i\frac{1}{\lambda\sqrt{\pi n_j!m_j!}}\frac{1}{\lambda\sqrt{\pi n_p!m_p!}}\frac{1}{\lambda\sqrt{\pi n_q!m_q!}}\sum_{n,m,n'm'}\sum_{n'',m'',n''',m'''}\\
&\left(A^{n_i,m_i}_{n,m}\right)^*\left(A^{n_j,m_j}_{n',m'}\right)^*A^{n_p,m_p}_{n'',m''}A^{n_q,m_q}_{n''',m'''}\sum_{l,s,l',s'}\sum_{l'',s'',l''',s'''}C^{n,m;n',m'}_{s,l;s'l'}C^{n'',m'';n''',m'''}_{s'',l'';s''',l'''}\\
&\int\left(\frac{\bar{z_+}}{\lambda}\right)^l\left(\frac{z_+}{\lambda}\right)^s\left(\frac{\bar{z_-}}{\lambda}\right)^{l'}\left(\frac{z_-}{\lambda}\right)^{s'}V(|z_-|)\left(\frac{\bar{z_+}}{\lambda}\right)^{s''}\left(\frac{z_+}{\lambda}\right)^{l''}\left(\frac{\bar{z_-}}{\lambda}\right)^{s'''}\left(\frac{z_-}{\lambda}\right)^{l'''}\\
&\times\delta_{m+m'-n-n',l+l'-s-s'}\delta_{m''+m'''-n''-n''',l''+l'''-s''-s'''}\mathrm{e}^{-\frac{\left(|z_+|^2+|z_-|^2\right)}{\lambda^2}}d^2z_1d^2z_2 \qquad (7.24)
\end{aligned}$$

This form is convenient to calculate, because the potential V only depends on z_-. In order to close the calculation, we come back to the antisymmetrization problem, which amounts to determine $\mathcal{P}$.

Antisymmetrization

A N-particle state can be written as:

$$\Psi_{1..N} = \prod_{i=1..N} (a_i)^\dagger |0\rangle \tag{7.25}$$

where we use the enumeration of the particles as described in the beginning of this section. In this notation any two-body interaction can be written as:

$$\hat{V} = \sum_{ijmn} V_{ijmn} (a_i)^\dagger (a_j)^\dagger a_m a_n \tag{7.26}$$

Calculating the interaction between the states, terms like:

$$\langle \Psi_{1..N} | \hat{V} | \Psi'_{1..N} \rangle \tag{7.27}$$

will have to be evaluated. This will contain the terms like:

$$a_m a_n \prod_{i=1..N} (a_i)^\dagger |0\rangle$$

Where $a_m a_n$ come from the potential expression. Now, we permutate the a's to the right toward $|0\rangle$ where they annihilate the state. Using the anti-commutation relations we can get nonzero contribution only in the case where the both of the annihilation operators come across complementary creation operator. After the first operator meets its hermitian conjugate we are left with only one operator, whose permutation to the right gives now a factor (-1) for each permutation until it meets its own conjugate. In the products of the operators we introduced an order which is

$$... < a_{i-1} < a_i < a_{i+1} < ...$$

and

$$... < a^\dagger_{i-1} < a^\dagger_i < a^\dagger_{i+1} < ...$$

And we can define a "distance" between two particles in the N-particle state as a number of particles "between" the two counting according to the order. In other words it is the number of creation operators between the two operators creating the pair.

$$\Delta^{i-j} = \#\text{ of creation operators between } a_i^\dagger \text{ and } a_j^\dagger$$

in the product

$$\Psi_{1..N} = \prod_{i=1..N} (a_i)^\dagger |0\rangle$$

And so the sign $\mathcal{P}$ of matrix element V_{ijpq} will be:

$$\mathcal{P}(V_{ijpq}) = (-1)^{\Delta^{i-j}+\Delta^{p-q}} \tag{7.28}$$

The above calculation is a basis for exact diagonalisation of the interacting system and so to analysing the fractional quantum Hall effect which is a very challenging topic. Here we have considered the dipole interactions, but the formula (7.24) can be easily evaluated for any central potential. Recent results from ref. [109] by M. Burello and A. Trombettoni show that the FQHE in non-Abelian gauge field support non-Abelian anyons and so considering the squeezed spectrum could be an interesting continuation of their study.

Chapter 8

Conclusions

In this thesis the behaviour of two-dimensional system of atoms in both Abelian and non-Abelian gauge field has been investigated. In the chapters 1 and 2 we present an introductory material, suitable for all readers, also those unfamiliar with the topics presented later. The new results are presented in the next chapters.

First, the basic properties of a non-interacting atomic gas in a square optical lattice and its spectrum have been studied. We have compared the classical Hofstadter-Butterfly spectrum in the case of a constant magnetic field with analogous system with various types of Abelian and non-Abelian gauge fields. In the first case characteristic large energy gaps form a fractal shaped pattern, after which it is called a "butterfly". It was known that in some cases of other fields the large gaps are destroyed and the spectrum has, the so called, "moth" form. From this comparison we have drawn the conclusion, that the non-Abelian character of the field does not necessary lead to the moth-spectrum. It is rather the constant or non-constant character of the field that decides whether the gaps are destroyed or not. Taking this finding into account we have found the whole family of non-Abelian butterfly-like spectra for the field given by the vector potential $\mathbf{A} = B(0, y, 0) + (\alpha\sigma_x, \beta\sigma_y, 0)$.

The large gaps in the spectrum are important for IQHE to take place. The plateaus in the Hall conductivity can only be present when Fermi energy of the system lies in the energy gap. For this reason the new butterfly-like spectra were natural candidates for finding IQHE. In order to find the conductivity as a function of

the field strength the method of Chern numbers was used. We found the conductivities and completed the spectrum plot to the full phase diagram, where all conductivities are shown. From this analysis it was evident that for some values of the parameters α and β i.e. the strengths of the non-Abelian gauge fields, the Hall effect takes an anomalous form, very similar to the one known from the graphene. In our case, however, the control over α and β gives more flexibility. We have also found that similarly to the graphene case, the so called, Dirac points are present in the spectrum. Around these points the dispersion relation is linear and atoms behave like massless particles moving with a modified speed of light. In our case, unlike in graphene, the speed of light can be changed by the change of the field parameters. By choosing $\alpha \neq \beta$ one can create an anisotropic case, in which the speed of light is different for the x and y directions. This offers possibility of simulating anisotropic Minkowski space-time and with tunable anisotropy with the use of ultracold atoms.

As a first step towards understanding of the interacting systems of atoms in non-Abelian gauge fields a BCS mean-field approach has been used. We have studied again the square lattice case in the presence of the gauge field $\mathbf{A} = (\alpha\sigma_x, \beta\sigma_y, 0)$ considering a system with an imbalance between the population of two different types of atoms. The "spin" imbalance drives a phase transition between topologically trivial and non-trivial phases. We have addressed two important questions - first, whether the phases have a topological order and if yes, how to characterise them, and second, whether these topological phases are possible to reach in a real experiment. In other words: Do the assumptions needed for the validity of BCS theory hold in the conditions needed to reach the topologically non-trivial phases? The full phase diagram for different values of α and β was given, and the phases were characterised with the use of Chern numbers and edge modes. We have also answered the second question positively. The "spin" imbalance needed to reach the topological phases is higher than, the so called, CC- limit for which it is known that BCS theory is not valid anymore in the standard case. Nevertheless it has been shown that the non-Abelian field stabilises the superfluid phase beyond this limit. All types of topological phases predicted in our model are possible to reach in the

experiment. This again gives an unprecedented possibility of simulating all types of topological insulators in one single experimental setup and controlling the phase transitions with the tuning of α and β.

In the last chapter of the thesis a step towards understanding of the interacting system and FQHE has been done. First, based on the results from the previous chapters, a prediction of the squeezed Landau levels and squeezed Laughlin function was given for the case of the anisotropic Dirac points in the spectrum. Next, a case of the interaction for the small squeezing is investigated. The preliminary results presented in that chapter can be used to perform exact diagonalisation. The squeezed Landau levels were expanded in the basis of non-squeezed states and finally, an analytical formula for the interaction potential matrix elements was given.

As discussed in the first two chapters, ultracold atomic systems are a good candidate for the quantum simulators. The creation of synthetic non-Abelian fields in a laboratory is still a challenge, but a very fast progress in this field is being done and there are several very promising proposals. The results reported in this thesis show that it is possible to simulate a wide range of phenomena using synthetic fields in these ultracold atomic systems.

Bibliography

[1] D. J. Wineland and W. M. Itano Phys. Today **40** 34 (1987).

[2] C. Wieman and S. Chu, Eds., J. Opt. Soc. Am. B **6**, 2020 (1989).

[3] C. Cohen-Tannoudji, and W. D. Phillips, Phys. Today **43**, 33 (1990).

[4] A. E. Leanhardt, T. A. Pasquini, M. Saba, A. Schirotzek, Y. Shin, D. Kielpinski, D. E. Pritchard, and W. Ketterle, Science, **301** 5639 (2003).

[5] M. H. Anderson, J. R. Ensher, M. R. Matthews, C. E. Wieman, and E. A. Cornell, Science, **269** (1995).

[6] A. Einstein,*Quantum theory of monatomic ideal gases*, Sitzungsberichte der Preussichen Akademie der Wissenschaften Physikalisch-Mathematische Klasse, **261** (1924).

[7] K.B. Davis, M.-O. Mewes, M.R. Andrews, N.J. van Druten, D.S. Durfee, D.M. Kurn, and W. Ketterle, Phys. Rev. Lett. **75**, 3969 (1995).

[8] I. Bloch, J. Dalibard, and W. Zwerger, Rev. Mod. Phys., **80** 885 (2008).

[9] S. Giorgini, L. P. Pitaevskii, and S. Stringari, Rev. Mod. Phys. **80**, 1215 (2008).

[10] E. Tiesinga, A. J. Moerdijk, B. J. Verhaar, and H. T. C. Stoof, Phys. Rev. A **46**, R1167 (1992); E. Tiesinga, B. J. Verhaar, and H. T. C. Stoof, Phys. Rev. A. **47**, 4114 (1993).

[11] Ph. Courteille, R. S. Freeland, D. J. Heinzen, F. A. van Abeelen, and B. J. Verhaar, PRL. **81**, 69 (1998).

[12] J. M. Kosterlitz and D. J. Thouless, J. Phys. C **6**, 1181 (1973).

[13] M. Greiner, C.A. Regal, D.S. Jin, Nature (London) **426**, 537 (2003).

[14] I. Bloch, Nature Phys. **1**, 23 (2005).

[15] R. Grimm, M. Weidemüller, and Yu. B. Ovchinnikov, Adv. At. Mol. Opt. Phys. **42**, 95 (2000).

[16] P. S. Jessen and I. H. Deutsch, Molec. and Opt. Phys. **37**, (1996).

[17] D. Jaksch,C. Bruder, J. I. Cirac, C. W. Gardiner, and P. Zoller, Phys. Rev. Lett. **81**, 3108 (1998).

[18] R.P. Feynman, Int. J. Theor. Phys. **21**, 467 (1982).

[19] C.R. Clarc, T.S. Metodi, S.D. Gasster, and K.R. Brown, Phys. Rev. A **79**, 062314 (2009).

[20] Y. A. Bychkov and Rashba, Solid State Phys. **17** , 6039 (1984).

[21] G. Dresselhaus, Phys. Rev. **100**, 580 (1955).

[22] M. R. Matthews, B. P. Anderson, P. C. Haljan, D. S. Hall, C. E. Wieman, and E. A. Cornell, Phys. Rev. Lett. **83**, 2498 (1999).

[23] J. R. Abo-Shaeer, C. Raman, J. M. Vogels, and W. Ketterle, Science, **292**, 476 (2001).

[24] K. W. Madison, F. Chevy, W. Wohlleben, and J. Dalibard, Phys. Rev. Lett. **84**, 806 (2000).

[25] Y.-J. Lin, R. L. Compton, K. Jimenez-Garcia, J. V. Porto, I. B Spielman, Nature **462**, 628 (2009).

[26] N. K. Wilkin, J. M. F. Gunn, R. A. Smith, Phys. Rev. Lett. **80**, 2265 (1998)

[27] N. K. Wilkin, J. M. F. Gunn, R. A. Smith, Phys. Rev. Lett. **84**, 2265 (2000)

[28] R. B. Laughlin, Phys. Rev. Lett. **50**, 1935 (1983).

[29] R. E. Prange and S. M. Girvin, *The Quantum Hall Effect*, (Springer Verlag, Berlin 1990).

[30] M. V. Berry 1984, Proc. Roy. Soc. London A **45** 392.

[31] C. Cohen-Tannoudji, J. Dupont-Roc, and G. Grynberg, *Atom-Photon Interactions*,(Wiley, New York 1992)

[32] G. Juzeliūnas and P. Öhberg, Phys. Rev. Lett. **93**, 033602 (2004).

[33] G. Juzeliūnas, J. Ruseckas, P. Öhberg, and M. Fleischhauer, Phys. Rev. A **73**, 025602 (2006).

[34] K. J. Günter, M. Cheneau, T. Yefsah, S. P. Rath, and J. Dalibard, Phys. Rev. A **79**, 011604 (2009).

[35] Y. J. Lin, R. L. Compton, A. R. Perry ,W. D. Phillips, J. V. Porto, and I. B. Spielman, Phys.Rev.Lett. **102,** 130401 (2009)

[36] F. Wilczek and A. Zee, Phys. Rev. Lett. **52**, 2111 (1984).

[37] N. Gemelke, E. Sarajlic, and S. Chu, arXiv:1007.2677

[38] D. Jaksch and P. Zoller, New J. Phys. **5**, Art. 56 (2003)

[39] F. Gerbier, J. Dalibard arxiv:0910.4606

[40] J. Dalibard, F. Gerbier, G. Juzeliūnas, P. Öhberg, arXiv:1008.5378

[41] R. Dum and M. Olshanii, Phys. Rev. Lett. **76**, 1788 (1996).

[42] A. Klein and D. Jaksch, Europhys. Lett. **85**, 13001 (2009)

[43] V. Pietilä, and M. Möttönen, Phys. Rev. Lett. **102**, 080403 (2009).

[44] E. Arimondo,*Progress in Optics, vol 35*(ed. E. Wolf, Elsvier, 1996).

[45] D. Hofstadter, Phys. Rev. B **14**, 2239 (1976).

[46] P.G. Harper, Proc. Phys. Soc. Lond. A **68**, 874 (1955).

[47] F. A. Butler and E. Brown, Phys. Rev. **166**, 630 (1968).

[48] K. Osterloh, M. Baig, L. Santos, P. Zoller and M. Lewenstein, Phys. Rev. Lett. **95**, 010403 (2005).

[49] N. Goldman, P. Gaspard, Europhys. Lett. **78**, 60001 (2007).

[50] Y. Hatsugai, T. Fukui, and H. Aoki, Phys. Rev. B **74**, 205414 (2006).

[51] I.I. Satija, D. C. Dakin, J. Y. Vaishnav and C. W. Clark, Phys. Rev. A **77**, 043410 (2008).

[52] N. Goldman and P. Gaspard, Europhys. Lett. **78**, 60001 (2007).

[53] M. A. Paalanen, D. C. Tsui, and A. C. Gossard, Phys. Rev. B **25**, 5566 (1982)

[54] D. J. Thouless, M. Kohmoto, M. P. Nightingale, and M. den Nijs, Phys. Rev. Lett. **49**, 405 (1982).

[55] M. Nakahara, *Geometry, Topology and Physics*, 2nd edition (Institute of Physics, Bristol, 2003).

[56] T. Fukui, Y. Hatsugai, and H. Suzuki, J. Phys. Soc. Jap. **74**, 1674 (2005).

[57] D. Osadchy and J. Avron, J. Math. Phys. **42**, 5665 (2001).

[58] X. G. Wen and Q. Niu, Phys. Rev. B **41**, 9377 (1990).

[59] M. Hafezi, A. S. Sørensen, E. Demler, and M. D. Lukin, Phys. Rev. A **76**, 023613 (2007).

[60] D. J. Thouless, M. Kohmoto, M. P. Nightingale, M. den Nijs, Phys. Rev. Letters **49**, 405-408 (1982).

[61] N. Goldman and P. Gaspard, Phys. Rev. B **77**, 024302 (2008).

[62] R. B. Laughlin, Phys. Rev. B **23**, 5632 (1981).

[63] B. Simon, Phys. Rev. Lett. **51**, 2167 (1983).

[64] D. Osadchy and J. Avron, J. Math. Phys. **42**, 5665 (2001).

[65] N. Goldman, *Quantum transport in lattices subjected to external gauge fields*,(VDM Verlag Dr. Mü ller, Saarbrucken 2009).

[66] K.S. Novoselov, A. K. Geim, S. V. Morozov, D. Jiang, M. I. Katsnelson, I. V. Grigorieva, S. V. Dubonos, and A. A. Firsov, , Nature **438**, 197 (2005).

[67] G. W. Semenoff, Phys. Rev. Lett. **53,** 2449 (1984).

[68] A. H. Castro Neto , F. Guinea , N. M. R. Peres , K. S. Novoselov, and A. K. Geim, Rev. Mod. Phys. **81**, 109 (2009).

[69] Y.B. Zhang , Y.W. Tan, H.L. Stormer, and P. Kim, Nature **438**, 201 (2005).

[70] S. -L. Zhu, B. Wang, and L. -M. Duan, Phys. Rev. Lett. **98**, 260402 (2007).

[71] X. G. Wen, *Quantum Field Theory of Many-body Systems*, (Oxford Univ. Press, Oxford, 2004).

[72] L.-K. Lim, C. M. Smith, and A. Hemmerich, Phys. Rev. Lett. **100**, 130402 (2008).

[73] J.-M. Hou, W.-X. Yang, and X.-J. Liu, Phys. Rev. A **79**, 043621 (2009).

[74] J. Ruseckas, G. Juzeliūnas, P. Öhberg, and M. Fleischhauer, Phys. Rev. Lett. **95,** 010404 (2005).

[75] G. Juzeliūnas, J. Ruseckas, A. Jacob, L. Santos, and P. Öhberg, Phys. Rev. Lett. **100,** 200405 (2008).

[76] G. Juzeliūnas, J. Ruseckas, M. Lindberg, L. Santos, and P. Öhberg, Phys. Rev. A **77,** 011802(R) (2008).

[77] I. I. Satija, D. C. Dakin, and C. W. Clark, Phys. Rev. Lett. **97,** 216401 (2006).

[78] I. Bloch, J. Dalibard, and W. Zwerger, Rev. Mod. Phys. **80,** 885 (2008).

[79] N. Goldman, A. Kubasiak, P. Gaspard, and M. Lewenstein, Phys. Rev. A. **79,** 023624 (2009).

[80] M. Stone, *Quantum Hall Effect*, (World Scientific, London, 1992).

[81] R. O. Umucalilar, H. Zhai, and M. Ö. Oktel, Phys. Rev. Lett. **100,** 070402 (2008).

[82] M. Kohmoto, Ann. Phys. **160**, 343 (1985).

[83] E. T. Jaynes and F. W. Cummings, Proc. IEEE **51,** 89 (1963).

[84] V. P. Gusynin and S. G. Sharapov, Phys. Rev. Lett **95,** 146801 (2005).

[85] Wen X. G. and Niu Q., Phys. Rev. B **41,** 9377 (1990); Wen X. G., Phys. Rev. B **65,** 165113 (2002);

[86] Hasan M. Z. and Kane C. L., arXiv:1002.3895v1.

[87] Kitaev A., Ann. Phys. **321,** 2 (2006).

[88] Read N. and Green D., Phys. Rev. B **61,** 10267 (2000).

[89] Massignan P., Sanpera A. and Lewenstein M., Phys. Rev. A **81,** 031607(R) (2010).

[90] M. Sato, Y. Takahashi, and S. Fujimoto, Phys. Rev. Lett. **103,** 020401 (2009).

[91] D. Sau Jay, R. M. Lutchyn, S. Tewari, and S. Das Sarma, Phys. Rev. Lett. **104,** 040502 (2010).

[92] Clogston A. M., Phys. Rev. Lett. **9,** 226 (1962); B. S. Chandrasekhar, Appl. Phys. Lett. **1,** 7 (1962).

[93] A. Altland and M. R. Zirnbauer, Phys. Rev. B **55,** 1142 (1997).

[94] A. P. Schnyder, S. Ryu, A. Furusaki, and A. W. W. Ludwig, Phys. Rev. B **78,** 195125 (2008)

[95] M. Sato and S. Fujimoto,, Phys. Rev. B **79,** 094504 (2009). D. Sau Jay, S. Tewari, R. Lutchyn, T. Stanescu and S. Das Sarma, arXiv:1006.2829v1. M. Sato, Y. Takahashi, and S. Fujimoto, arXiv:1006.4487.

[96] P. A. Frigeri, D. F. Agterberg, A. Koga, and M. Sigrist, Phys. Rev. Lett. **92,** 097001 (2004)

[97] J. Bellissard, arXiv:cond-mat/9504030.

[98] C. L. Kane and E. J. Mele, Phys. Rev. Lett. **95,** 146802 (2005).

[99] N. Goldman, I. Satija, P. Nikolic, A. Bermudez, M. A. Martin-Delgado, M. Lewenstein, and I. B. Spielman, arXiv:1002.0219

[100] A. Bermudez, N. Goldman, A. Kubasiak, M. Lewenstein, M.A. Martin-Delgado, New J. Phys. **12**, 033041 (2010).

[101] D.C. Tsui, H.L. Stormer, A.C. Gossard, Phys. Rev. Lett. **48** 1559 (1982).

[102] H.L. Stormer, Rev. Mod. Phys. **71** 875 (1999).

[103] S. M. Girvin and T. Jach, Phys. Rev. B **29,** 5617 (1984).

[104] R. de-Picciotto, M. Reznikov, M. Heiblum, V. Umansky, G. Bunin, D. Mahalu, Nature **389** 162 (1997).

[105] L. Saminadayar, D. C. Glattli, Y. Jin, and B. Etienne, Phys. Rev. Lett. **79**, 2526 (1997).

[106] M. Reznikov, R. de Picciotto, T. G. Griffiths, M. Heiblum, V. Umansky, Nature **399**, 238 (1999).

[107] M. Dolev, M. Heiblum, V. Umansky, Ady Stern, and D. Mahalu, Nature **452**, 829 (2008).

[108] I P. Radu, J. B. Miller, C. M. Marcus, M. A. Kastner, L. N. Pfeiffer, and K. W. West, Science **320**, 899 (2008).

[109] M. Burello and A. Trombettoni, Phys. Rev. Lett. **105**,125304 (2010).

[110] G. Moore and N. Read, Nucl. Phys. B **360**, 362 (1991).